



DeepL

Subscribe to DeepL Pro to translate larger documents.
Visit www.DeepL.com/pro for more information.

Research on avionics wireless LAN relay communication method

A Dissertation Submitted for the Degree of Master

Candidate: Wu Junjie

Supervisor: Prof. Li Qiao

School of Electronic and Information Engineering
Beihang University, Beijing, China

abstract

The integrated network of avionics systems is the centre for in-flight data exchange, and the cable size, power consumption and maintenance costs of traditional wired networks cannot be ignored. The integrated network of avionics systems is the centre for in-flight data exchange, and the cable size, power consumption and maintenance costs of traditional wired networks cannot be ignored. Wireless Avionics intra-communication (WAIC) technology can replace the wired interconnection between some devices in the aircraft with wireless, which can reduce the fuel consumption caused by the original cables and their reinforcement components and improve the in-flight environment. In this paper, the IEEE 802.11 protocol is adapted for avionics intra- aircraft high-rate communication scenarios, and the effective use of WAIC technology can be improved. In this paper, the IEEE 802.11 protocol is adapted for avionics intra- aircraft high-rate communication scenarios, and the effective capacity model is introduced to analyze the queuing delay at the transmitter side and solve the power IEEE 802.11 protocol is adapted for avionics intra- aircraft high-rate communication scenarios, and the effective capacity model is introduced to analyze the queuing delay at the transmitter side and solve the power allocation problem of the relay cooperation communication system under the total power constraint.

The main research content and innovative work of this paper include the following parts.

1. In this paper, the WAIC applicability simulation and analysis of IEEE 802.11 physical layer communication technology are carried out. The dimension characterization of the line replaceable units and modules was carried out concerning the ASAAC standard. The ray-tracing algorithm is used to model the channel, and the root-mean-square delay spread of the multipath channel is used for the simulation. The ray-tracing algorithm is used to model the channel, and the root-mean-square delay spread of the multipath channel is about 8ns, which is a quasi-static channel. Setting the significance level to 1% by the K-S test, it is possible to determine the significance level of the multipath channel. 1% by the K-S test, it is determined that the Rice distribution is suitable for the channel fading of the avionics compartment channel. The performance of different physical layer signal processing technologies was

evaluated. different physical layer signal processing technologies was evaluated, and the tolerable bit error rate was set as 10^{-6} . The signal-to-noise ratio of The signal-to-noise ratio of different modulation orders was recorded as the interval reference of rate adaptive control.

2. By introducing the effective capacity model, the queuing delay of the signal at the transmitter is analyzed. The formulas of delay violation probability for flat fading and frequency selective fading channels are derived. The formulas of delay violation probability for flat fading and frequency selective fading channels are derived. For a WAIC system with a communication bandwidth of 20MHz, an average signal-to noise ratio of the receiving end of 10dB, a transmission data frame length of 2ms, and a constant arrival rate of 55Mbit/s, the delay violation probability constraint value is set to 10^{-4} . Simulation results show that the upper bound of queuing delay at the transmitter is 15ms.

3. Considering that the outage capacity of a single-link transmission communication system may approach 0 under QoS requirements, this paper introduces a single relay node, analyses Amplify-and-Forward and Decode-and-forward modes, and introduces diversity gain into the system. The simulation results show that when the QoS exponent approaches infinity, the system can obtain a non-zero QoS exponent. show that when the QoS exponent approaches infinity, the system can obtain a non-zero zero-outage capacity under the cooperation of the relay node, which can meet the requirements of effectiveness and reliability of avionics communication. DF usually performs better than AF when the distance between the DF usually performs better than AF when the distance between the relay node and the transmitter is close to that between the relay node and the receiver.

Key words: wireless LAN, WAIC, effective capacity, cooperation communication

CONTENTS

Chapter I. Introduction.....	1
1.1 Sources and Significance of the Study	1
1.2 Current status of domestic and international research	2
1.2.1 Wireless avionics in-flight communications.....	2
1.2.2 Effective Capacity Modelling.....	4
1.2.3 Relay collaborative communications	5
1.3 Main contents of the paper.....	8
1.3.1 Research	8
1.3.2 Thesis chapter organisation.....	9
Chapter 2 Avionics Wireless LAN Communication Performance Assurance Mechanism Study	11
2.1 IEEE 802.11 Protocol Technical Analysis	11
2.1.1 IEEE 802.11 Protocol Overview	11
2.1.2 IEEE 802.11 Physical Layer Technology Analysis.....	13
2.2 Technical Applicability of IEEE 802.11 for WAIC Applications	19
2.2.1 Transmitter CSI Acquisition Mechanism.....	19
2.2.2 Beamforming.....	22
2.2.3 Transmit Rate Adaptive	24
2.3 IEEE 802.11 Applicability in WAIC Technology Simulation	25
2.3.1 Simulation Analysis of Beamforming Technology	25
2.3.2 Simulation Analysis of Rate Adaptive Techniques	27
2.4 Chapter Summary.....	29
Chapter 3 Avionics Wireless Communications Effective Capacity Study.....	30
3.1 Avionics wireless channel modelling.....	30
3.1.1 Ray Tracing Algorithms	30
3.1.2 Simulation and Analysis of Avionics Cabin Wireless Channels	32
3.1.3 Simulation and analysis of wireless channels in avionics bay	35
3.2 Analysis of effective capacity-based upper bounds on queuing delay	38

3.2.1 Theoretical Models of Effective Capacity and Effective Bandwidth	38
3.2.2 Effective capacity analysis of frequency selective channels	40
3.2.3 Effective bandwidth analysis of arrival traffic with exponentially distributed data frame lengths.....	42
3.3 Simulation analysis of transmitter-side buffer queue queuing.....	43
3.3.1 Channel distribution fitting analysis	43
3.3.2 Queuing Emulation Parameter Settings	46
3.3.3 Queuing Simulation and Theoretical Analysis	47
3.4 Chapter Summary.....	50
 Chapter 4: Research on Coded Forwarding Relay Technology for Avionics Wireless LANs	51
4.1 Relay Collaborative Communication Transmission Mode Selection ..	51
4.1.1 Amplify-and-forward relay communication protocol.....	53
4.1.2 Coded Forwarding Relay Communication Protocol	54
4.2 Study of node power allocation problem based on effective capacity model	55
4.2.1 AF node power allocation method study	55
4.2.2 Study of DF node power allocation methods	58
4.2.3 DF Node Power Allocation Method Improvement Strategy Analysis.....	60
4.3 Simulation validation of code-forwarding technique based on effective capacity model.....	62
4.3.1 Relay communication simulation parameter settings	62
4.3.2 Analysis of simulation results for relay communication	63
4.4 Chapter Summary.....	66
 Chapter 5 Avionics Wireless LAN Simulation Evaluation Study	67
5.1 MATLAB-based Avionics Wireless LAN Communication Simulation.....	67
5.1.1 Wireless LAN simulation parameter settings.....	67
5.1.2 Analysis of wireless LAN simulation results.....	68
5.2 Analysis of real-world measurements based on a software radio platform	72

5.2.1 Software Radio Platform Parameter Settings.....	72
5.2.2 Confined environment communication empirical analysis.....	74
5.2.3 Empirical Analysis of Rate Adaptive Algorithms.....	76
5.3 Chapter Summary.....	78
Summary and Outlook.....	79
References.....	81
Appendix	87
A. Derivation of the effective capacity formula	87
Academic achievements during the master's degree programme	89
Acknowledgements.....	90

Bibliography

Figure 1 WAIC System Classification	3
Figure 2 802.11 physical layer signal processing process.....	13
Figure 3 Data Scrambler	14
Figure 4 Subcarrier allocation	16
Figure 5 CP Processing.....	16
Figure 6 2x2 MIMO Schematics	17
Figure 7 802.11ax single-user physical data frame structure.....	19
Fig. 8 Beamforming flow.....	24
Figure 9 Flow of detection at the transmitter and beamforming at the receiver.	
26	
Fig. 10 Comparison of MCS3 quantised beamforming PER performance with different bits.....	26
Fig. 11 Comparison of MCS5 quantised beamforming PER performance with different bits.....	27
Fig. 12 BER and PER with different MCS settings	28
Fig. 13 Simulation results of adaptive rate algorithm	28
Figure 14 SBR Receiving Schematic.....	31
Figure 15 Boeing 737-200 cabin channel simulation.....	33
Figure 16 Boeing 737-200 cabin channel PDPs.....	34
Fig. 17 RMS delay extensions calculated from 500 cabin simulations.....	35
Figure 18 Avionics module model.....	36
Figure 19 View of A777-200 avionics bay	36
Fig. 20 Avionics bay ray tracing simulation results.....	37
Fig. 21 PDP of the equipment bay channel obtained in one of the simulations.	
37	
Figure 22 Launch-side buffer queue queuing model	39
Fig. 23 Fitting results of channel distribution of avionics equipment bay	44
Fig. 24 Normalised effective capacity at different average SNRs	45

Fig. 25 Scene 1 queuing simulation and theoretical calculation results	47
Fig. 26 Scene 2 queuing simulation and theoretical calculation results.....	48
Fig. 27 Scene 3 queuing simulation and theoretical calculation results.....	48
Figure 28 Effective Capacity vs. Effective Bandwidth Curve	49

Figure 29 Scene 4 Queuing Simulation and Theoretical Calculation Results.	50
Figure 30 Schematic diagram of the trunking collaborative communications system	52
Figure 31 Schematic diagram of trunk collaboration in a WAIC network	62
Fig. 32 Normalised effective capacity of AF node power allocation method with direct communication links.....	63
Fig. 33 DF node power allocation method β_3 Normalised effective capacity with direct communication links	64
Fig. 34 Three different DF node power allocation methods vs. effective capacity of the direct-fire link as $\theta \rightarrow 0$	64
Figure 35 Comparison of Effective Capacity Values for DF and AF	65
Fig. 36 MATLAB simulation flowchart	68
Figure 37 Avionics bay ray tracing algorithm results	69
Fig. 38 3D plot of delay power spectrum with departure and arrival angles .	69
Fig. 39 Received signal information when simulating transmission of packet 1	70
Figure 40 Constellation diagram of packet 1 with MCS 4	70
Figure 41 Power spectra of transmitted and received signals.....	71
Figure 42 Statistics obtained by simulating 100 packets.	71
Fig. 43 Schematic diagram of the signal processing process in PC mode of the Y320 card.....	73
Figure 44 Physical diagram of the software radio	74
Figure 45 System Parameter Settings and Measured Data	74
Fig. 46 Constellation diagram of the received signal waveform in the time domain and after channel equalisation in the data domain	75
Fig. 47 Received signal power spectral density and channel estimation results	
75	
Fig. 48 Coarse and fine synchronisation time domain signal waveforms.....	75
Figure 49 IEEE802.11ax Receiver PHY Demo Simulation Interface.....	76
Fig. 50 Flow of rate adaptation algorithm.....	77

Fig. 51 Results of the adaptive algorithm for the measured rate of the original strategy	77
Fig. 52 Improved strategy measured rate adaptive algorithm results	78

Schedule catalogue

Table 1 IEEE 802.11 Protocol Families	12
Table 2 IEEE 802.11n, ac and ax comparison.....	12
Table 3 802.11ax MCS Table.....	15
Table 4 Signal-to-noise ratio with PER reduced to 10^{-2}	27
Table 5 LRM modelling dimensional information.....	35
Table 6 Equipment bay ray tracing statistics.....	37
Table 7 K-S test results for channel distribution with $\alpha = 1\%$	44
Table 8 WAIC WLAN Simulation Parameters.....	67
Table 9 Y320 transmitter RF front-end operating parameter settings	72
Table 10 Y320 Receiver RF Front End Operating Parameter Settings.....	73

English Abbreviations Comparison Table

abbreviations	full name	Chinese Interpretation
WAIC	Wireless Avionics intra-communication	Wireless avionics in-flight communications
ASAAC	Allied Standard Avionics Architecture Council	Joint Standards Avionics Architecture Board
LRU	Line Replaceable Unit	Route Replaceable Units
LRM	Line replaceable Module	Route Interchangeable Modules
DF	Decode and Forward	decode and forward
AVSI	Aerospace Vehicle System Institute	Institute of Aerospace Vehicle Systems
IMA	Integrated Modular Avionics	Integrated modular avionics system
RA	Radio Altimeter	radio altimeter
ITU	International Telecommunication Union	ITU
WSN	Wireless Sensor Network	Wireless Sensor Networks
WATM	Wireless Asynchronous Transfer Mode	Wireless Asynchronous Transmission Mode
AP	Access Point	access points
EC	Effective Capacity	effective capacity
CSI	Channel State Information	channel state information
AF	Amplify and Forward	amplify and forward
MIMO	Multi-Input Multi-output	Multiple inputs and multiple outputs
SINR	Signal Interference Noise Ratio	signal-to-noise ratio
MMSE	Minimum mean-squared error	minimum mean square error
DCF	Distributed Coordination Function	Distributed coordination function
BER	Bit Error Rate	bit error rate (BER)
FCC	Federal Communications Commission	Federal Communications Commission (FCC)

abbreviations	full name	Chinese Interpretation
GI	Guard Interval	guard interval
FEC	Forward Error Correction	Forward error correction
LDPC	Low-density Parity-check	Low-density parity check
MCS	Modulation and coding scheme	modulation coding strategy
SC	sub-carrier	subcarrier
DC	Direct Current	direct current (D.C.)
ICI	Inter-carrier interference	intercarrier interference
RU	Resource Unit	resource block
IFFT	Inverse Fast Fourier Transform	inverse Fourier transform (physics)
ISI	Inter-Symbol Interference	intersymbol interference
CP	Cyclic Prefix	cyclic prefix (linguistics)
SNR	Signal to Noise Ratio	signal-to-noise ratio
STBC	Space-Time Block Coding	space-time grouping code
L-STF	Legacy-short training field	Traditional short training domain
L-LTF	Legacy-long training field	Traditional long training domain
L-SIG	Legacy-Signal field	Traditional signalling domain
HE	High Efficiency	high efficiency
AGC	Automatic Gain Control	Automatic Gain Control
CSD	Cyclic Delay Diversity	circular shift subset (math.)
SISO	Single Input Single Output	single-issue and single-receipt
SIMO	Single Input Multiple Output	single-shot, multiple-receiver (SAMR)
ZF	Zero Forcing	(computing) zero (physics)
STA	Station	wireless terminal
SVD	Singular Value Decomposition	singular value decomposition

		(math.)
AWGN	Additive White Gaussian Noise	Gaussian white noise
TDD	Time Division Duplexing	time division duplex
ARF	Automatic Rate Fallback	auto-rate regression
ACK	Acknowledge	recognise
abbreviations	full name	Chinese Interpretation
PER	Packet Error Rate	miss packet rate
UWB	Ultra Wide Band	ultra-broadband
LOS	Line of sight	visible range
SBR	Shooting and Bouncing Rays Method	emission tomography
RMS	Root Mean Square	root mean square (math.)
SNC	Stochastic Network Calculus	stochastic network algorithm
LDP	Large Derivation Principle	Large Offset Principle
PDF	Probability Density Function	probability density function
CDF	Cumulative distribution function	cumulative distribution function
OSI	Open System Interconnect	Open system interconnection
MRC	Maximal Ratio Combining	maximum ratio merger
KKT	Karush-Kuhn-Tucker	Karush Koon Tucker
SDR	Software Defined Radio	software radio
PC	Personal Computer	PC
DMA	Direct Memory Access	direct memory access

Chapter I. Introduction

1.1 Sources and significance of the study

This topic is derived from the research section of the Wireless Avionics intra-communication (WAIC) advance study related to the adaptation of wireless LAN technology applicability.

Avionics systems have evolved from discrete, to joint, to integrated, to advanced integrated, and are still moving towards better real-time performance and higher reliability.^[1] As one of the main support technologies of avionics system, airborne network communication is one of the main support technologies. As one of the main supporting technologies of avionics system, airborne network communication technology has also made a lot of progress. Airborne network connects many kinds of communication equipments and transmits data according to a fixed way and rate, which has the characteristics of high reliability. With the continuous development of avionics systems, the amount of data that needs to be transmitted by airborne networks is getting larger and larger. The existing wired network architectures, such as MIL-STD-1553, AFDX, and TTE, require a large number of cables to be laid out inside the aircraft. Texas A&M University Aerospace Vehicle Systems Institute

(According to a study by the Aerospace Vehicle System Institute (AVSI), an A380-880 aircraft is equipped with 100,000 cables of 470km in length, weighing 5,700kg, and requires an additional 30% of the weight of the retainer for the cables, which increases the overall weight to 7,410kg. As the number of cables increases, the total load and fuel storage capacity of the aircraft is affected, and its range and flight performance are reduced. In recent years, the adoption of many advanced technologies such as microsensors and Integrated Modular Avionics (IMA) architecture has placed higher demands on system bandwidth and network bus topology. In order to reduce the weight of the airframe, lower the installation and maintenance costs, and improve the safety and reliability of flight, the use of wireless communication to replace part of the wired communication is

one of the future directions for the development of in-flight communication in aircraft.^[2] .

This study is based on the applicability of commercial shelf protocol IEEE 802.11. Firstly, we analyse and compare the QoS performance of different physical layer signal processing technologies, such as error bit rate and throughput. For the special characteristics of the avionics cabin, such as multi-metal parts and confined environment, the physical model of multipath channel is modelled and the fading characteristics of the channel are analysed. Based on the above fading distribution, the effective bandwidth and effective capacity models are introduced to derive the delay violation probability equations for flat fading and frequency-selective fading channels, and to compare and analyse the performance of queuing delay in the buffer queue of the transmitter under different arrival rates. For a single relay system with a direct shot link, the relaying method of amplified forwarding and coded forwarding is used to model the effective capacity maximisation problem under the restriction of the total system transmit power remaining unchanged, to optimally allocate the transmit power of each node of the communication system, to optimise the overall performance of the system, and to analyse the effectiveness and reliability performance of the relay communication system.

1.2 Current status of research at home and abroad

1.2.1 Wireless avionics in-flight communications

Avionics systems place high demands on the effectiveness and reliability of communication systems. For a long time, data transmission in avionics systems has been based on wired networks such as MIL-STD-1553, ARINC-429, and ARINC-664 (AFDX), but the use of wired networks is accompanied by many problems. The complex network structure contains a large number of devices and cables, which requires a great deal of manpower and resources to maintain them. Communication cables between equipment on many air vehicles are used for long periods of time and are not replaced until the next major overhaul, and the repair process requires the removal of the entire communication equipment to complete. The ageing of the cables may cause link failures or even discharge fires, resulting in irreparable damage that affects operational efficiency and flight safety.

With the rapid advances in wireless communications technology, the idea of using wireless communications to replace some of the wired communications within an aircraft has gained a lot of attention from manufacturers. The proliferation of wireless avionics in-flight communications has led to a number of emerging standards for migrating regulatory and safety-related applications from wired networks to next-generation wireless networks.^[3] for migrating regulatory and safety-related applications from wired networks to next-generation wireless communication networks. The use of WAIC technology reduces total cable weight, lowers maintenance costs, and improves overall aircraft efficiency. The WAIC system communicates wirelessly using a specific range of frequencies, which are allocated to the avionics system in order to avoid interfering with other wireless communication systems. The WAIC system is used to communicate wirelessly over a range of frequencies, which are allocated to the avionics system to avoid interference with other wireless communication systems. Inside the aircraft, various devices are connected to each other through wireless interfaces and send and receive signals through a distributed antenna system.

These devices include avionics, sensors, actuators, control panels, etc. The WAIC will be used for tasks related to safe, reliable, and efficient aircraft operations, such as health monitoring of the aircraft structure, sensing, control, voice, video, and fieldbus communications, etc.^[4]. On the other hand, due to the random fading propagation characteristics of wireless communications, it is a difficult task to implement the QoS assurance features of wired networks over wireless networks. In addition to this, WAIC also needs to consider the interference problem of Radio Altimeter (RA) on data communication.

The safety and economy of WAIC is seen by the industry as a new challenge in the development of avionics. The 2010 World Radiocommunication Conference (WRC-10) adopted report M.2197, which introduced the current status of WAIC system applications expected by the international commercial aviation industry, and the 2013 WRC-13 adopted report M.2283, which discussed the application characteristics of the WAIC system and the estimation of the spectrum demand, and report M.2318, which was released in November 2014, indicated that

The 4.2~4.4GHz band is the only option below 15.7GHz to satisfy the WRC-15 agenda requirements. 2015 WRC released the standard M.2285, which formally identifies 4.2~4.4GHz as the communication band for WAIC.^[5] WAIC

Researchers have considered choosing among various commercial off-the-shelf (COTS) wireless protocols to meet the real-time and reliability requirements of avionics systems. Recommendation M.2283 published by the International Telecommunication Union (ITU)^[6] Considering 802.15.4 (Zigbee) as the

The WAIC system uses 802.11a/g as the communication protocol for Wireless Sensor Network (WSN) and 802.11a/g as the high rate transmission protocol. As shown in Fig. 1, the WAIC system classifies the communication scenarios into four categories according to the communication rate and antenna position: internal high speed application (high inside, HI), internal low speed application (low inside, LI) external high speed application (HI), and external high speed application (HI).

(The proposal proposes a series of solutions for low-speed scenarios with a single link rate of less than 10kbit/s, based on IEEE 802.15.4; for low-speed scenarios with a single link rate ranging from 12.5kbit/s to 12.5kbit/s, based on IEEE 802.15.4. The proposal puts forward a series of solutions: for low-speed scenarios where the single link rate is less than 10kbit/s, IEEE 802.15.4 is used as the basis for applicability modification; for high-speed scenarios where the range of the single link rate is from 12.5kbit/s to 1.6Mbit/s, and the peak rate can be up to 4.8Mbit/s, IEEE 802.11 is used as the basis for communication protocol development. communication protocol development based on IEEE 802.11.

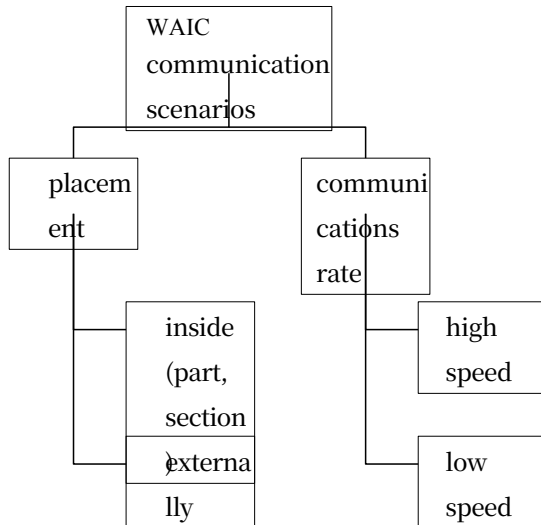


Figure 1 WAIC System Classification

In terms of wireless protocol selection, the literature [7] has included 802.15.3 (UWB) 802.11a, 802.11n, ECMA 368 (Wi-Media) 802.15.4 (Zigbee), and 802.16 (Wi-Max) are compared in WAIC systems considering transmission time, coding efficiency, coverage, received power, and some QoS metrics such as throughput, energy loss, and bit error rate. The simulation results show that the data transmission time is more likely

to be affected by the protocol transmission rate than the data load size and the data header percentage. In terms of coding efficiency, Zigbee is more suitable for small data transmission, and UWB, Wi-Max and Wi-Fi perform better as the data size increases. The analysis shows that 802.11n and ECMA-368 are more suitable for HI/HO systems, while Zigbee is better suited for LI/LO scenarios. Literature [8] evaluates the feasibility of LTE/5G technology to support high rate data communication over WAIC. Measurements in an unmanned simulated cabin and external environment showed that at least one of the communication technologies can meet the high rate transmission requirements in scenarios without RA interference. While in scenarios with RA signal interference, more robust strategies should be considered to improve the robustness of the communication network.

In terms of wireless communication system architecture, literature [9] proposes a communication scheme that combines wired and wireless, Wireless Asynchronous Transfer Mode (WATM) WATM uses AFDX or TTE as the wired part, and without changing the original network structure, the access point (Access Point (AP)

The WATM is interconnected with the wireless devices at the AFDX/TTE. Typically WATM on the AFDX/TTE architecture is an extension of the existing wired network and does not require any modifications to the traditional network backbone. The processing of all data associated with WATM, ATM, and terminals is isolated by adapters. The adapter completes the conversion and link between wired and wireless communications by processing the wired data frames, together with the header and footer of the wireless protocol. Literature [10] proposes an access point deployment scheme where multiple APs need to be installed to reduce the necessary transmission power in order to reduce the interference to the avionics devices by the airborne mobile communication devices deployed in the cabin. Due to the tunnel shape of the cabin channel, multiple APs are connected via optical fibre to provide transmission diversity. In this article, an optimal deployment scheme is proposed, and the transmission characteristics of the wireless signals between the user and the APs are calculated by finite-difference simulation method. Compared with the single AP communication scheme, it not only reduces the interference but also increases the communication capacity.

Compared with the traditional wired network, WAIC reduces the weight of the aircraft equipment, reduces the design complexity, and can provide better economic effect and flight efficiency. However, in the face of the unpredictable wireless environment, how to design and develop appropriate communication protocols to meet the requirements of reliability and effectiveness of communication is still a major challenge for the future development of avionics systems.

1.2.2 effective capacity model (ECM)

The traditional Shannon capacity theory only focuses on the channel state of the physical layer air interface when describing the maximum transmission rate that can be supported by a wireless communication system, and does not involve the analysis of transmission delay in the upper layer. In contrast, the Effective Capacity (EC) proposed by Wu Dapeng et al [11] introduces the delay QoS requirement at the data link layer, which has been

increasingly adopted by the research of delay-sensitive communication technologies in recent years. Effective capacity as a physical layer-data link layer cross-layer signal transmission model, the significance of which is to reflect the maximum transmission rate that can be supported by the transmitter side of the wireless system under the given buffer queuing delay QoS constraints, and when the QoS exponent tends to 0, the effective capacity converges to the Shannon capacity, and when it tends to infinity, the effective capacity converges to the zero-interruption capacity.

In dyad with the notion of effective bandwidth^[12] , the effective capacity model shows the minimum service rate needed to guarantee a given original traffic queuing delay requirement; conversely, the effective capacity model can also be used to find the maximum source rate that can be handled by a channel with a desired delay constraint. There are several main applications of effective capacity:

- (1) Effective capacity modelling based on exhaustive queue analysis is used to characterise the relationship between raw rate and service rate, taking into account both link layer and physical layer parameters. This characterisation enables pre-validation of the system, e.g. the implementation of effective access control^[13] ;
- (2) With the notion of effective capacity, QoS configuration and effective bandwidth allocation over a radio link can be achieved in the form of a closed-form solution while satisfying certain delay probability guarantee constraints^[11] (a);
- (3) Effective capacity is the dual concept of effective bandwidth^[14-15] , which explains the maximum constant arrival rate of the wireless channel while satisfying the delayed interruption probability constraints^[16] . This feature can be utilised for certain applications with specific QoS requirements.

Procedures to realise the requirements;

(4) The QoS performance of various classical algorithms can be investigated with the help of effective capacity, such as water injection and channel inversion methods. The performance of adaptive modulation and coding schemes for various protocols can be tested using the effective capacity as a metric parameter

^[17];

(5) Using the effective capacity model, the adaptive resource allocation for a particular QoS-aware connection can be analysed in the form of a closed-form solution, which can help optimise system performance by exploring the path towards better system performance;

(6) Providing QoS guarantees that support various service flows requires efficient scheduling algorithms. The concept of effective capacity enables the design of delay-constrained efficient scheduling methods^[18].

Based on the different stochastic characteristics of channel fading in different environments, literature [19] gives the analytical expression of the effective capacity of the general fading channel model for various scenarios in which the channel state information (CSI) is acquired in different states at the transmitter and receiver. Literature [20] investigates the performance of the effective capacity model in the IEEE 802.11 protocol. The effective capacity model is evaluated based on empirical data from a large number of wireless network scenarios by varying parameters such as communication performance range, channel coding and modulation scheme, and nodes competing for shared channel resources, etc. The packet delays in the wireless link can be directly measured in the built simulation platform, and the effective capacity provides an accuracy ranging from 0.0074% to 9.09% when compared with the existing empirical data. Accuracy. The simulation analyses that when the effective bandwidth requirement exceeds the threshold of the effective capacity, QoS violation occurs and the probability of packet delay events increases.

In summary, based on the effective capacity and effective bandwidth models, it is possible to analyse the upper bound of queuing delay in the

queue at the transmitter side. By adopting certain flow control algorithms, QoS can be optimised and analysed at the physical layer level to meet the reliability requirements of the communication system.

1.2.3 Trunking collaborative communications

When only direct shot links are present in a single-user communication scenario, based on the effective capacity model analysis, the higher the QoS requirement, the zero-interruption capacity of the system decreases continuously and tends to 0 as the QoS parameter increases^[21] This is not in line with the principle of avionics communication. This does not meet the requirements of effectiveness and reliability of aviation electronic communication. When the relay is introduced in the communication system to forward the original signal, a certain diversity gain can be introduced in the receiving single, and the literature [22] analyses and compares after simulation, the zero interruption capacity of the communication system does not converge to 0 with the increase of QoS parameter, which meets the actual requirements of avionics communication.

Relay communication can expand the signal coverage, and its introduction of diversity gain can effectively improve the channel fading effect caused by multipath transmission, the commonly used relay methods are Amplify and Forward (AF) and Decode and Forward (DF), etc., and collaborative communication using relay protocols has gained the attention of researchers. Literature [23] studied three collaborative diversity protocols: fixed relaying, selective relaying and incremental relaying, and pointed out that relaying collaborative communication

Relay can effectively enhance the performance of the communication system and reduce the probability of interruption. However, the bandwidth required for half-duplex relay communication under the premise of fixed rate is twice as much as that of direct link transmission, and it is more necessary to consider issues such as power control and hardware cost in practice. With the continuous development of multi-antenna Multi-Input Multi-output (MIMO) technology, relay nodes can also be combined with beamforming, space-time coding, and other techniques to further improve the system performance. Currently there are several main schemes to improve the relay collaboration:

(1) Relay collaboration programme based on beamforming technology

Relay nodes increase the degree of freedom of the communication system, and the effective improvement of the system performance can be achieved through the mutual collaborative communication between different relay nodes. Zijian Wang, Shanghai Jiaotong University^[24] Consider a two-hop MIMO wireless multi-relay network, where both source and destination nodes are equipped with multiple antennas and communicate through multiple half-duplex AF relay terminals with multiple antennas. Since it is difficult to obtain perfect channel state information in real multiple and networks, the imperfect CSI of all channels is considered in the article. focusing on maximising the Signal Interference Noise Ratio (SINR) of the destination node, a new robust linear beamforming method is proposed based on the QR decomposer of the destination node, which performs continuous interference cancellation. Using the law of large numbers, the asymptotic rate of imperfect CSI is obtained, based on which the proposed relay beamforming coefficients are optimised. Simulation results show that the asymptotic rate matches the traversal rate well, which is better than the traditional beamforming scheme.

C. Li, Southeast University^[25] A beamforming scheme combining source and relay nodes is proposed for a MIMO system with distributed single antenna relay. The optimisation problem of beamforming is first

formulated by taking the lower limit of the signal-to-noise ratio at the destination node as the objective function. The joint beamforming problem is then divided into two sub-optimisation problems corresponding to beamforming at the source and relay nodes. The first sub-problem corresponds to the quadratic concave minimisation problem, which is solved linearly by an iterative algorithm. The second problem corresponds to the Rayleigh-Ritz ratio problem, which is solved by a closed-form generalised singular value decomposition method. In the article, the solutions of the two subproblems are united and a global iterative algorithm is designed to implement a beamforming scheme with joint source and relay nodes. Simulation results show that the system communication capacity under this scheme is better than some existing relay schemes.

Junxu Su, Nanjing University of Aeronautics and Astronautics^[26] A precoding algorithm based on the Minimum mean-squared error (MMSE) criterion is proposed for MIMO relay systems in multiple scenarios, considering the communication system with BER as an optimisation objective under the condition of incomplete CSI in which the channel has estimation error and feedback delay. Literature [27] decomposed the complex non-convex problem of solving the matrices of the transmitter, relay node, and receiver into three independent sub-optimization problems, the transmitter is a single antenna configuration, the precoding matrix of the transmitter is determined firstly, the convex optimization problem of solving the relay matrix is transformed into a semipositivistic programming problem, and the processing matrix at the receiver is solved by linear search algorithms, and finally, the optimal solution of the node matrix is obtained by using joint iteration method, which can significantly improve the performance of the precoding algorithm. The optimal solution is obtained by a joint iterative method, which can significantly improve the system's false bit rate performance.

(2) Relay collaboration programme based on scheduling improvements

Literature [28] addresses energy-constrained wireless networks. A reasonable collaborative transmission protocol and cross-layer collaboration protocol are proposed for energy consumption, spectral efficiency and spatial frequency reuse performance by jointly considering three aspects: power control, relay selection and protocol overhead. Aiming at the problem of short lifetime of energy-constrained networks, the article proposes an energy-oriented collaborative MAC protocol for minimising the total transmission power. Based on the limitation of the error bit rate, the article analyses the transmission power of direct transmission links and collaborative links, and allocates the power to the source and relay nodes with the goal of minimising the total transmission power between the source and relay nodes. The article gives the collaborative MAC timing and flow for total transmit power minimisation by extending and adding the IEEE 802.11 Distributed Coordination Function (DCF) control frame. Compared with similar MAC protocols, the energy saving effect of this collaborative MAC protocol is more significant when the network has higher Bit Error Rate (BER) requirement. In order to improve the reachability rate, the article also proposes a superposition coding-based collaborative transmission protocol that improves the processing of relay nodes' gratuitous forwarding in the traditional three-node model, and integrates the signals of the relays with the signals of the source nodes using superposition coding. By adjusting the transmission power of relay nodes, the communication coverage area of collaborative transmission is limited to the communication coverage area of direct transmission links, and the relay selection area for transmission without collaborative interference is given; the selection method of the best relay is improved, and source nodes are included in the set of candidate relays to participate in the competition for the best relay, and on the basis of joint optimization of the relay selection area and the transmission power, the system's single-link transmission interruption is analysed probability and the interruption probability under the restriction of relay selection region. The simulation results show that the protocol can effectively increase

the number of concurrent links in the collaborative network, improve the spatial frequency reuse rate and network throughput, and reduce the interruption probability of transmission.

Literature [29] studies buffer-assisted relay transmission techniques, which are classified into two applications according to the different number of relay nodes: relay selection technique for the multi-relay node model and link selection technique for the single-relay node model. For the multi-relay system, the relay for receiving and forwarding messages can only be the same; for the single-relay system, the relay receives messages and forwards messages alternately. The article considers that by combining the buffer technology with the traditional half-duplex relay, a certain storage buffer space is given to the relay, so that the relay has more freedom while sending and receiving information, and the multi-relay communication can choose different relay nodes to complete the information sending and receiving work according to the same time slot with different channel conditions; the single relay can decide whether to receive or send the information according to the channel conditions, which eliminates the inherent limitations of the traditional relay transmission technology. Single relay can decide whether to receive or send information according to the channel condition, eliminating the inherent limitations of traditional relay transmission technology.

(3) Optimisation method for relay communications with application of effective capacity models

In order to introduce delay constraints, researchers have combined relay collaborative communication with effective capacity to propose the problem of maximising the communication rate of the system under delay probability guarantee. Literature [30] proposes a collaborative communication model in which the source node first sends the information to the relay node, which then forwards it to the destination node by DF, without considering the direct path. Each relay node is assigned to get a time slice and the individual time slices are orthogonal to each other. The article will effectively tolerate

The optimisation problem of capacity is transformed into a convex optimisation problem of time-slice allocation, and two allocation methods, optimal and sub-optimal solutions, are proposed. Through simulation, it is concluded that when the delay constraints are looser, the relay node with the best average channel state needs to be selected to maximise the effective capacity; whereas, when the delay constraints are stricter, sufficiently large numbers of relays need to be selected to minimise the probability of interruption.

Literature [22] considers communication scenarios that include direct paths, and proposes a physical layer by introducing an effective capacity model

-A cross-layer resource allocation method for the data link layer. The power allocation strategies of two relaying protocols, AF and DF, are studied and analysed to maximise the effective capacity under power constraints. Since both AF and DF relaying transmit in half-duplex mode, which uses only half of the system degrees of freedom, it is possible that the direct path performs better than relaying when the delay constraint is looser. More efficient relaying protocols such as bi-directional relaying can also be considered to improve the system performance. There are also effective capacity based multi-hop relaying^[31] and buffer-assisted relaying^[32] and buffer-assisted relaying based on effective capacity. These researches obtain better performance by changing the relay structure and signal regeneration method.

In summary, under the constraints of limited resources such as time, frequency as well as power, there are more methods to be explored on how to better allocate the resources, combine them with other communication technologies, optimise the effective capacity in the context of relay collaborative communication, and maximise the communication rate of the system under the constraints of delay probability.

1.3 Main content of the paper

1.3.1 Research

This study mainly contains the following four chapters, forming a more complete set of wireless avionics in-flight communication technology research and simulation verification programme.

1. Research on Avionics Wireless Local Area Network Communication Performance Assurance Mechanisms

Based on the applicable techniques of IEEE 802.11 protocol, simulation and analysis are carried out in WAIC high rate communication scenario (HI), including the selection of physical layer modulation coding strategies, feedback of channel state information and adaptive modulation techniques.

2. Research on effective capacity of avionics wireless communication

A ray-tracing algorithm is used for deterministic channel modelling for special confined space communication scenarios such as avionics compartments. The relative positions of the transmitter and the receiver are set to change, and random characteristics are introduced to analyse the fading distribution model of the multipath channel and derive the uniform expression of the effective capacity. Based on the effective capacity and effective bandwidth model, the upper bound of queuing delay of the buffer queue at the transmitter is analysed under different transmitter arrival rate and channel state conditions.

3. Research on Coding and Forwarding Relaying Technology for Avionics Wireless LAN

Based on the effective capacity model, considering the single-user single-link communication scenario with the existence of a direct path, the relay nodes are introduced for collaborative communication, comparing the two different relay communication modes, amplify-and-forward and code-and-forward, and analysing the QoS performance and throughput of the whole communication system.

4. Evaluation study of avionics wireless local area network simulation

On the basis of MATLAB toolbox simulation platform, the end-to-end communication model of WAIC based on IEEE 802.11 protocol is established for simulation analysis, and the communication test in confined environment and the real measurement analysis of adaptive rate control algorithm are carried out on the software radio platform.

1.3.2 Organisation of thesis chapters

This paper aims at the research of avionics wireless local area network relay communication method, based on commercial shelf technology IEEE

802.11 protocol is analysed for applicability. By modelling the avionics bay multipath channel model, fitting the channel fading distribution, deriving the analytical expression of the effective capacity under the specific channel model, and simulating and analysing the signal queuing delay at the transmitting end. By solving the power allocation optimisation problem in code-forward relay collaborative communication under total power constraints, the effectiveness and reliability requirements of avionics communication are met.

There are five chapters in this paper and the chapters are organised as follows:

Chapter 1 Introduction. This chapter introduces the source of the topic, the significance of the research and the current status of research at home and abroad, and summarises the current wireless avionics intra-aircraft communication (WAIC) requirements for the communication rate and communication system. It also briefly introduces the QoS requirements and the development direction of WAIC.

The second chapter of avionics wireless LAN communication performance guarantee mechanism research. Based on IEEE 802.11 protocol, it introduces a complete set of signal processing techniques used in the physical layer from sending to receiving, evaluates the QoS performance of different modulation and demodulation modes in the physical layer for the special communication scenarios of avionics, and analyses the CSI

acquisition mechanism and adaptive rate control algorithm at the receiving end. Specific research content includes:

- (1) Introduction to IEEE 802.11 Protocol Physical Layer Technology and WAIC Applicability Analysis;
- (2) Analysis of the mechanism for obtaining channel state information at the transmitter side;
- (3) Analysis of transmitter-side rate adaptation techniques.

Chapter 3: A study of effective capacity for avionics wireless communications. Effective capacity is a stochastic network algorithmic model based on the principle of large offset, which is dyadic to the concept of effective bandwidth. The multipath channel model of avionics cabin channel is established by ray tracing algorithm, and the fading distribution of avionics cabin channel is obtained by statistical analysis through multiple simulations, and then the analytical expression of effective capacity is derived. The transmitter-side delay violation probability performance of flat fading and frequency-selective fading channels is analysed by queuing simulation. The specific research includes:

- (1) Avionics wireless channel modelling and fading fitting;
- (2) Derivation of formulae for effective capacity based on specific fading distributions;
- (3) Upper bound analysis of transmitter-side queuing delay based on the effective capacity model.

Chapter 4: A study of code-forward relaying techniques for avionics wireless LANs. Introduce diversity gain into the communication system by using relay nodes to send copies of the original signals. Optimise the effective capacity of the system when the QoS requirement of the communication system is high, analyse and compare the effective capacity model maximisation problem under different relaying modes, solve the optimal power allocation method, and analyse the effective capacity performance of the relay collaboration system. The specific research includes:

- (1) Scenarios where a direct path exists: consider AF single-relay communication with a single antenna;
- (2) Scenarios in which a direct radius exists: consider DF single-relay communication with a single antenna.
- (3) Compare the performance of AF and DF strategies for optimising effective capacity.

Chapter 5 Simulation and Evaluation Study of Avionics Wireless LAN.

Building a complete set of IEEE based on MATLAB

802.11 physical layer simulation to analyse the QoS performance of physical layer technology under multipath channel in avionics equipment cabin. Based on the software radio platform, data measurement is carried out to analyse the performance of the adaptive rate control technology in the actual communication environment, which provides a certain reference for the follow-up research of WAIC. Specific research content includes:

- (1) MATLAB-based simulation analysis of IEEE 802.11 physical layer communication technology;
- (2) Analysis of real-world measurements of communications in confined environments based on a software radio platform;
- (3) An empirical analysis of an adaptive rate control algorithm based on a software radio platform.

Chapter 2: Research on Avionics Wireless LAN Communication Performance Assurance Mechanisms

The study of WLAN communication performance guarantee mechanisms needs to be carried out under specific communication regimes. For the high-speed communication scenario in WAIC, ITU recommends the use of commercial shelf protocols that have been studied for a long time and have more mature technology for applicability modification. This project will be based on the IEEE 802.11 protocol for applicability modification, analyse the impact of different modulation and demodulation, coding and decoding, and diversity multiplexing technologies on the communication performance, and select the most appropriate communication strategy to meet the effectiveness and reliability of avionics communication needs.

The transmitter obtains the channel state information and adopts different transmit strategies, and the receiver can obtain higher communication rate and SNR to optimise the performance of the communication system. The use of adaptive rate control technology, which dynamically adjusts the modulation order of the transmit signal based on different SNRs, is also an effective method to approach the limit of Shannon's capacity theory.

2.1 IEEE 802.11 Protocol Technical Analysis

2.1.1 IEEE 802.11 Protocol Overview

In the past decades, with the massive growth in the number of IEEE 802.11 terminals, wireless LANs have also been widely used, and technologies such as radio wave communications and radar have been greatly developed in both military and civilian applications. In 1985, the U.S. Federal Communications Commission (FCC) designated the industrial, scientific, and medical (ISM) frequency bands for commercial applications of spread spectrum, and opened three frequency bands of 900MHz, 2.4GHz and 5.8GHz. Since then, wireless LANs have developed rapidly and many new products and architectures for

LAN communications have emerged.

In 1990, the IEEE 802.11 committee was formally established. After two round robin votes, in September 1997, the first version of the 802.11 protocol (i.e. IEEE 802.11-1997) was officially adopted and published on 10 December, marking the first milestone in the development of Wi-Fi technology. The first version of the protocol specified two modes of communication, FM and direct-sequence spread spectrum, and supported limited rates. In 1999, the Wi-Fi Alliance was formally established, and in the same year, the IEEE promulgated the 802.11b protocol, which added HR/DSSS modes to the physical layer and introduced CCK encoding. A year later, the 802.11a version was also officially adopted. Unlike the previous technology, 802.11a introduced a new physical layer technology, Orthogonal Frequency Division Multiplexing (OFDM).

(Orthogonal Frequency Division Multiplexing (OFDM) OFDM technology offers higher spectrum utilisation than spread spectrum technology. In 2003, the second milestone in the development of Wi-Fi was the adoption of the 802.11g protocol, which moved the technology used by 802.11a in the 5GHz band to the 2.4GHz band, with some protocol compatibility design. In 2009, the third milestone in the development of Wi-Fi, the 802.11n protocol was adopted. Compared with the previous protocols, 802.11n introduces the multi-antenna technology of MIMO, which transmits data in parallel through multiple antennas to effectively improve

In 2014, the fourth milestone of Wi-Fi, 802.11ac technology, was officially passed. In 2014, the fourth milestone of Wi-Fi 802.11ac technology was formally adopted, through the introduction of MU-MIMO technology, an access point (AP) can communicate with multiple users at the same time through multiple antennas, expanding the application scenarios of Wi-Fi, and more in line with the actual needs of user communication. At the same time, 802.11ac also increases the modulation order and channel bandwidth, which further enhances the transmission rate of the system. 2019, the 802.11ax protocol is officially released, and in this version of the protocol, Orthogonal Frequency Division Multiple Access (OFDMA) technology is introduced, which is comparable to 5G mobile communication technology. In this version of protocol, OFDMA technology is introduced, which is more flexible in spectrum resource allocation and more widely used in communication scenarios compared with 5G mobile communication technology. Table 1 is a comparative analysis of different protocols in the 802.11 protocol family, from which it can be seen that, with the continuous improvement and upgrading of the protocol, the transmission rate is getting higher and higher, the performance of the equipment is getting better and better, and the application scenarios are getting more and more extensive, and the compatibility between the protocols is also better, and it can be applied to the field of avionics communication better.

Table 1 IEEE 802.11 Protocol Families

vintage s	protocols	speed	Operating band (GHz)	modulation technology	wireless transmission method
1997	802.11	1-2Mbps	2.4	DSSS and FHSS	SISO
1999	802.11a	6-54 Mbps	5	OFDM	SISO
1999	802.11b	1,2,5.5,11Mbps	2.4	HR-DSSS	SISO
2003	802.11g	6-54 Mbps	2.4	OFDM	SISO
2009	802.11n	Up to 600Mbps	2.4 and 5	OFDM	MIMO
2013	802.11ac	Up to 6.9Gbps	5	OFDM	MU-MIMO
2019	802.11ax	Up to 9.6Gbps	2.4 and 5	OFDMA	MU-MIMO

More subcarriers, higher coding ratios, shorter Guard Interval (GI) larger channel bandwidths, and more spatial streams are the trends in 802.11 technology, and an effective means to increase device throughput and improve system performance. Table 2 shows the comparison between 802.11n, ac, and ax, which shows that wireless LAN communication technology is progressing as the protocol family continues to evolve.

Table 2 IEEE 802.11n, ac and ax comparison

	802.11n (Wi-Fi 4)	802.11ac (Wi-Fi 5)	802.11ax (Wi-Fi 6)
Communication band (GHz)	2.4 and 5	5	2.4, 5 and 6
Channel bandwidth (MHz)	20, 40	20, 40, 60, 80, 160	20, 40, 60, 80, 160
Subcarrier spacing (Khz)	312.5	312.5	78.125
OFDM symbol length (μs)	3.2	3.2	12.8
Protection interval (μs)	0.4 or 0.8	0.4 or 0.8	0.8 or 1.6 or 3.2

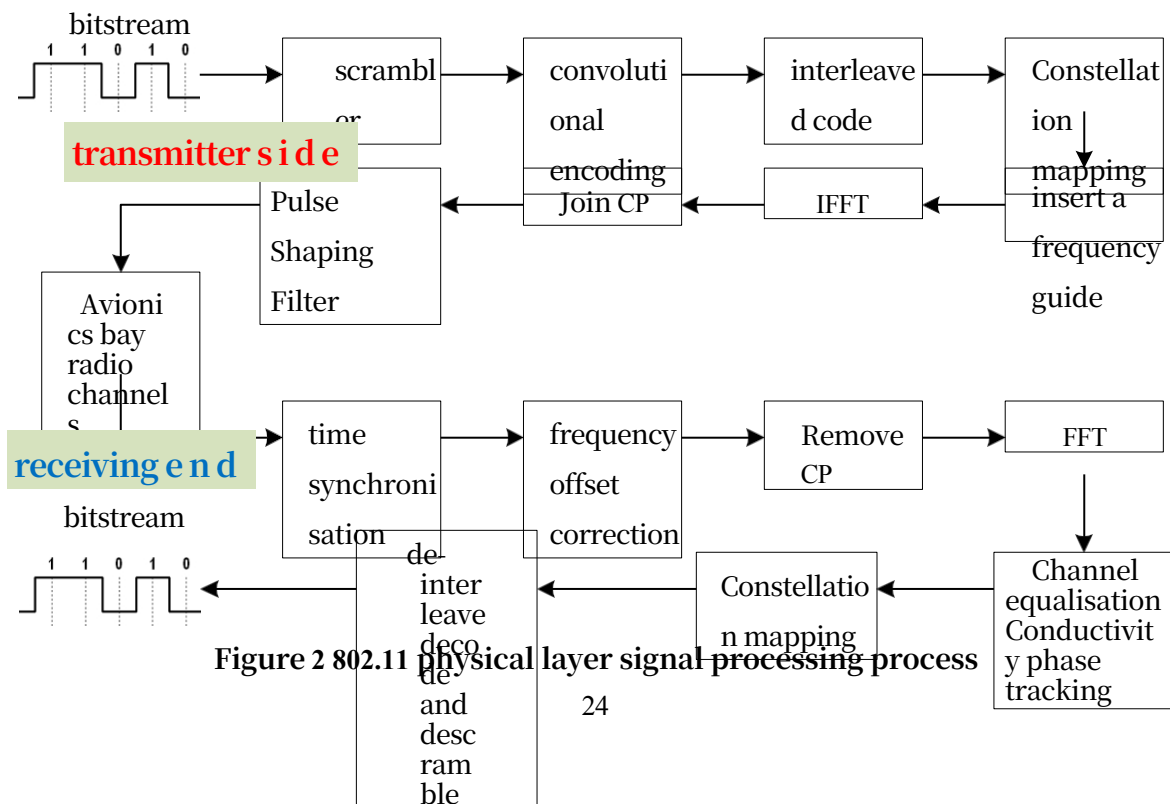
Table 2 IEEE 802.11n, ac and ax comparison (continued)

	802.11n (Wi-Fi 4)	802.11ac (Wi-Fi 5)	802.11ax (Wi-Fi 6)
modulation method	BPSK, QPSK, 16QAM, 64QAM	BPSK, QPSK, 16QAM, 64QAM, 256QAM	BPSK, QPSK, 16QAM, 64QAM, 256QAM, 1024QAM
MU-MIMO support	clogged	down train (i.e. away from the capital)	Upside and downside
Whether to support OFDMA	clogged	clogged	Upside and downside

Existing studies on WAIC are based on 802.11n and previous protocols. Considering the continuous development of the 802.11 protocol family and the interoperability and compatibility of technologies between protocol versions, this project will use 802.11ax protocol as the basis for a series of pre-study and simulation analyses of the physical layer.

2.1.2 IEEE 802.11 Physical Layer Technology Analysis

WLAN communication consists of a complete set of communication regimes from the transmitter to the receiver. ITU-R proposes a WAIC scenario where only one device is transmitting a signal at the same time.^[6] Based on the above assumptions, the impact of 802.11 physical layer technology on QoS is investigated. Figure 2 shows the complete process of the signal from the transmitter through the channel to the receiver for processing.



The bit stream arriving at the upper layer goes through the processes of source coding, channel coding, constellation mapping and OFDM modulation to form a complete transmission symbol, and then arrives at the RF front-end through pulse-forming filtering. After passing through the multipath channel, the signal waveform is affected to a certain extent, and undergoes a series of operations such as time synchronisation, frequency deviation correction, channel equalisation, etc. at the receiving end to complete the whole process of physical layer signal processing. The following will introduce and analyse the processing carried out in each part, respectively.

The effectiveness and reliability of WAIC's communication system requirements are met through rational selection.

(1) source coding and channel coding

802.11ax specifies that when the bit stream reaches the transmitter, the source is first coded using scrambling. Scrambling is a method of coding that alters the statistical characteristics of a digital signal by scrambling the signal without adding redundant bits, and the scrambled signal has Gaussian statistical characteristics similar to white noise. The sequence of information with the transmission service information and additional bits needs to pass through a frame synchronisation scrambler of length 127. As shown in Fig. 3, the main function of this scrambler is to make sure that an individual bit transmission error will result in only one individual bit error after descrambling at the receiving end^[33], which means that there is no possibility that the received signal will not have successive errors. The same scrambling sequence is required at the transmitter and receiver throughout the transmission of the signal, and the scrambler is always initialised to a non-zero state. The generating polynomial of the scrambler is as follows:

$$S(x) = x^7 + x^4 + 1 \quad (2.1)$$

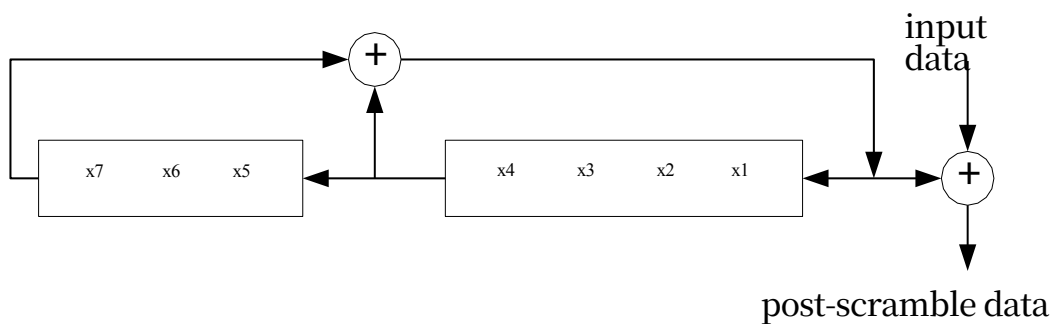


Figure 3 Data Scrambler

When scrambling is finished, the sequence is sequentially forward error correction (FEC) coded, the bits are used to form the code elements, and then interleaved coding is used to modulate the data and map it to the corresponding subcarrier plane. In this process, both FEC coding and interleaving coding are channel coding. 802.11ax protocol specifies that the

error correction codes that can be used are convolutional codes and low-density parity-check (LDPC) codes. Among them, convolutional codes are coded by the redundancy provided by the interleaving of information, and then different coding ratios are formed by punched (punctured) operation, which is suitable for channels where BERs do not occur continuously. The LDPC code is a class of packet error correction codes with sparse check matrix, which is suitable for almost all channels, and its performance can be close to Shannon's limit, and can provide higher coding gain compared to convolutional codes, but the coding complexity is higher, and the demand for hardware resources is also larger.

(2) OFDM modulation

The encoded data is mapped into constellations by selecting the appropriate modulation order, and then modulated into different subcarriers by OFDM to form an OFDM Symbol. Table 3 shows the modulation coding strategy (Modulation) specified by 802.11ax.

and coding scheme (MCS) 0~11 represent different combinations of modulation order and code rate (ratio of useful bits to total transmitted bits), respectively. The different bits of data are mapped to the constellation diagram by Gray code and multiplied by the corresponding coefficients for power normalisation.

Table 3 802.11ax MCS Table

MCS	Carrying bit number	modulation method	bitrate
0	1	BPSK	1/2
1	2	QPSK	1/2
2			3/4
3	4	16QAM	1/2
4			3/4
5			2/3
6	6	64QAM	3/4
7			5/6
8	8	256QAM	3/4
9			5/6
10	10	1024QAM	3/4
11			5/6

Each constellation point corresponds to a data subcarrier (sub-carrier, SC) and when the subcarrier interval is fixed, the

Different bandwidths correspond to different numbers of carriers.

802.11ax specifies a subcarrier spacing of $\Delta f = 78.125$ Hz, which is

A quarter of 802.11ac, when the bandwidth is fixed, more subcarriers are more sensitive to the frequency selectivity of the channel and the amount of data that can be transmitted increases accordingly. The frequency-guided subcarriers are sandwiched between the data subcarriers to compensate for phase rotation at the receive end and also to provide a rough estimate of the channel response. For example, with a bandwidth $B = 20$ MHz, there are 256 subcarriers, whereas there are only 234 subcarriers that actually carry the data, a difference of 22, which are used as the guarantor.

The protection intervals, including the protection intervals between the null

carrier, the DC carrier and the resource sub-block, are shown in Fig. 4. The different subcarrier labels are indicated by -128~127, and the guided frequency subcarriers are {-116, -102, -90, -76, -62, -48, -36, -22}.

-10, +10, +22, +36, +48, +62, +76, +90, +102, +116}, and the carrier labelled 0 is the DC

(Direct Current (DC) carriers. The six carriers on the left and the five carriers on the right are used as empty carriers, the same as in 802.11a, to suppress out-of-band radiation and reduce inter-carrier interference (ICI). Due to the OFDMA feature introduced in 802.11ax, the large bandwidth is further divided into small resource blocks.

(Resource Unit, RU) there is also a protection interval of 1 subcarrier between each resource block.

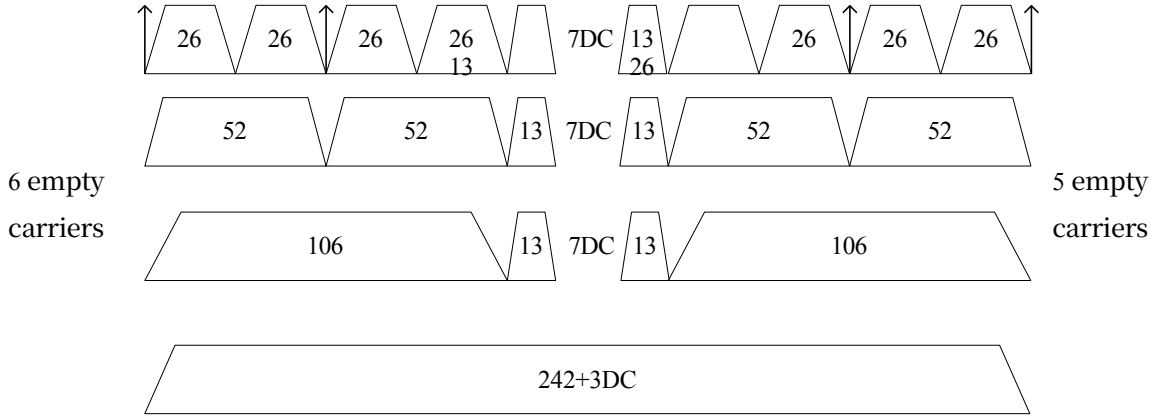


Figure 4 Subcarrier allocation

When the constellation point is mapped to the subcarrier, OFDM modulation is completed by Inverse Fast Fourier Transform (IFFT), at which time the signal is transformed to the time domain, and the Fourier Transform is performed at the receiver side by performing the (Fast Fourier Transform (FFT)) operation can demodulate the data. Compared with traditional modulation techniques, OFDM can provide better performance and gain, can somewhat overcome the channel frequency selectivity caused by multipath channels, reduce Inter-Symbol Interference (ISI) improve spectrum utilisation, and bring the transmission rate closer to the Shannon limit.

(3) Protected Interval and Cyclic Prefix

The orthogonality between OFDM subcarriers ensures that the signals are independent and uncorrelated throughout the symbol period, but it also results in OFDM modulated signals that are sensitive to frequency shifts caused by transmitter oscillators or Doppler phenomena, and the delay extension of the multipath also destroys the orthogonality of the subcarriers over the complete period resulting in ISI vs. ICI. The inclusion of a guard interval mitigates the effects of the multipath effect and maintains orthogonality of the subcarriers when the length of the guard interval is greater than the maximum delay of the multipath channel. If the guard interval length is less than the maximum multipath delay extension, the tail of the previous OFDM symbol will affect the head of the next OFDM symbol, resulting in ISI or ICI.

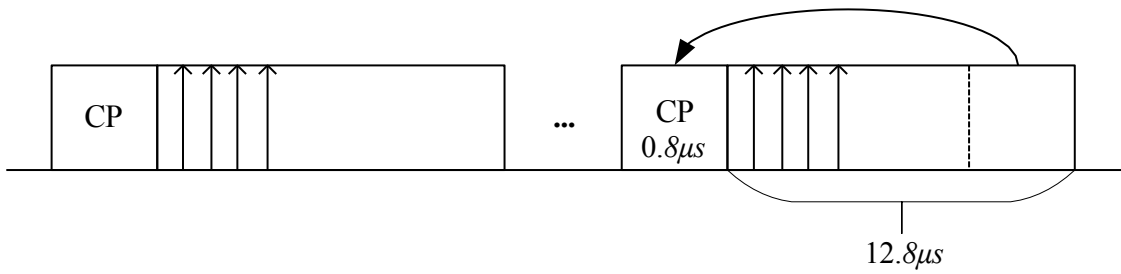


Figure 5 CP Processing

Cyclic Prefix (CP) is a way to protect the interval, which is formed by copying the signals from the end of the OFDM symbol to the header. As shown in Figure 5, there are three lengths of cyclic prefixes specified in 802.11ax, which are $0.8 \mu s$,

$1.6 \mu s$ and $3.2 \mu s$, which is *different* from 802.11ac and the previous regulations of $0.4 \mu s$ and $0.8 \mu s$, mainly due to the fact that the sampling rate remains unchanged, and the reduction of the subcarrier spacing leads to an increase of the symbol length, which requires an increase of the CP length to ensure the effectiveness of the protection interval. The addition of the CP ensures that OFDM symbols maintain their linear characteristics after passing through the channel, due to the fact that FFTs of the The circular convolution property, which allows the signal to be viewed as a circle, regardless of where it starts, to obtain a complete of the signal, there is only a difference in phase that does not affect the result of the integration.

(4) Multiplexing of multiple antennas with space-time packet coding

Starting from 802.11n, multi-antenna technology has been introduced in Wi-Fi, where multiple antennas are used at the transmitter and receiver to send and receive signals and improve the communication performance of the system. The MIMO technology takes advantage of the multipath effect, whereby the transmitted signals arrive at the receiver at different angles and at different times when they are reflected off walls, ceilings, and some objects.^[34] MIMO technology utilises the multipath effect. Fig. 6 shows a simple

2×2 MIMO system, MIMO can provide a large gain without increasing the transmit power and bandwidth.

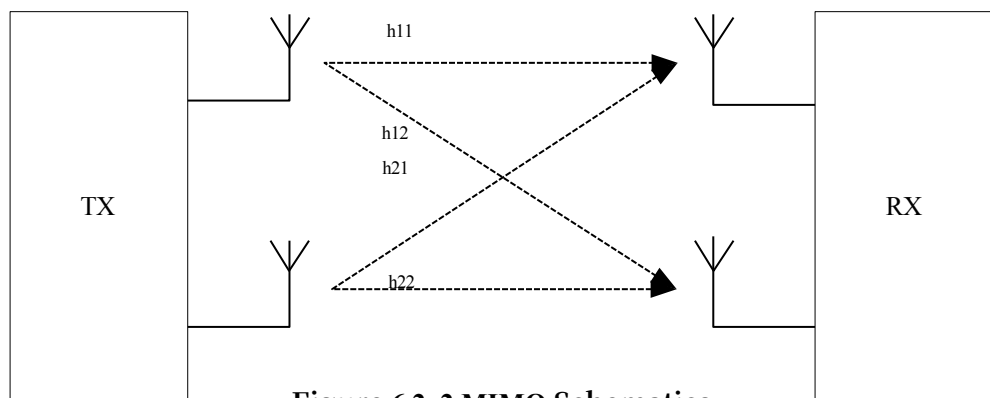


Figure 6 2x2 MIMO Schematics

Based on multiple antennas transmitting and receiving, diversity or

multiplexing strategy can be used flexibly according to different communication scenarios. Diversity technique is to send the same signal with multiple antennas, the signals transmitted by different antennas go through different channels, the correlation of the signals is weakened when receiving, which can be regarded as a copy of the same signal after different processing, and the diversity gain is obtained by choosing the appropriate merging technique. While multiplexing is to divide the high rate signal into multiple antennas transmitting at lower rates for transmission, which can be differentiated at the receiving end due to different spatial characteristics. At high Signal to Noise Ratio (SNR), the multiplexing technique works well to increase the system capacity. The number of spatial streams is limited below the number of antenna lines at the transmitter or receiver end, and the spacing between antennas is also required to ensure the independence between the transmitted signals, which is usually set to one-half wavelength size (2.7cm in the 5GHz band) Equation (2.2) is the expression for the received signal on the kth subcarrier.

$$\mathbf{R}(k) = \mathbf{H}(k)\mathbf{S}(k) + \mathbf{N}(k) \quad (2.2)$$

where $\mathbf{H}(k)$ is the channel matrix

$$\mathbf{H}(k) = \begin{bmatrix} h_{11} & \cdots & h_{1M}(k) \\ \vdots & \ddots & \vdots \\ h_{N1}(k) & \cdots & h_{NM}(k) \end{bmatrix} \quad (2.3)$$

The elements $h_{ij}(k)$ of the matrix represent the channel gain and phase of the k th subcarrier, $\mathbf{R}(k)$ is the received signal, $\mathbf{S}(k)$ is the transmitted signal, and $\mathbf{N}(k)$ is the Gaussian white noise. The **H matrix is** estimated by the leading (preamble) sequence of the physical frame and equalised to the symbols following it to finally obtain the transmitted data. In order to solve for the channel matrix \mathbf{H} , it is necessary to ensure that the $r(H) = M$, i.e., $\mathbf{H}(k)$ needs to contain M mutually independent row vectors^[35]. This requires that the transmitter and receiver

With a very rich scatterer, the signal can take many different paths to reach the receiver.

Space-Time Block Coding (STBC) improves the reliability of data transmission by transmitting multiple copies of a digitally processed signal through multiple antennas and receiving the signal at the receiving end and combining them. Transmitted signals often pass through complex environments with phenomena such as scattering, reflection and refraction, and are also subject to thermal noise at the receiving end. This means that some copies of the received data may be better than other signals, and such redundant data allows the receiving end to correctly decode the transmitted data on the basis of one or more less correlated copies. The main purpose of STBC is to use optimal receive merging methods in order to extract as much source information as possible from the multiple copies received. The 802.11 protocol specifies the use of the Alamouti strategy for STBC implementation, which in a two-antenna transmitting system can achieve full diversity gain with low complexity. For two input signals x_1 and x_2 in the time domain, a 2×1

The Alamouti space-time packet coding is done in a configuration where one antenna at the transmitter side transmits the two signals in their original order, and the other antenna with space-time coding transmits the mathematically processed copies of the signals $\otimes x^*$ and x^* - where the operation symbol * is used.

represents the conjugate operation, which is calculated as shown below, with inputs at the transmitter at two moments:

$$y = \begin{bmatrix} x_1 \\ x_2 \end{bmatrix}, \quad \begin{bmatrix} x_1 \\ x_2 \end{bmatrix} = \begin{bmatrix} x_1 \\ x_2^* \end{bmatrix} \quad (2.4)$$

The signal at the receiving end is shown in equation (2.5), where n_1 and n_2 are the Gaussian white noise at the receiving end at two moments, respectively.

$$\begin{aligned} r &= [h_{11} \quad h_{12}] \cdot \begin{bmatrix} x_1 \\ x_2^* \end{bmatrix} + n_1 \\ r &= [h_{21} \quad h_{22}] \cdot \begin{bmatrix} x_2 \\ x_1^* \end{bmatrix} + n_2 \end{aligned} \quad (2.5)$$

The receiver only needs to perform a linear transformation to recover the transmitted data. Compared with other space-time coding methods, although the diversity gain obtained by Alamouti is not obvious, its low complexity has a great advantage in hardware implementation, and it can also be flexibly combined with other transmission techniques to obtain better performance in practical multi-antenna transmission scenarios.

2.2 Technical applicability of IEEE 802.11 for WAIC applications

The ITU-R report suggests that the IEEE 802.11 protocol can be used for communication in high speed communication scenarios, and it is necessary to select the modulation order selection, diversity multiplexing and beamforming techniques stipulated in the protocol, etc. The WAIC's wireless communication band is 4.2~4.4GHz, with a total of 200MHz bandwidth spectrum resources, which is well suited to the 20, 40, 80 and 160MHz communication bandwidth stipulated in the 802.11. However, because this part of the band is in line with the ISDN bandwidth, it is not suitable for the communication of the ISDN bandwidth. However, since there is no overlap between this part of the band and the WLAN communication band specified in the ISM band, it is necessary to adjust the RF front-end and change the carrier frequency. The interior of avionics equipment compartment is also characterised by many metal devices and fewer moving objects, etc. The rms delay extension of avionics compartment channel is small, which may keep the channel gain characteristics unchanged for a long period of time, and it is a class of quasi-stationary channel. Therefore, it is necessary to simulate the physical layer to evaluate the performance of different technologies and selectively adopt them.

2.2.1 Transmitter CSI Acquisition Mechanism

The 802.11 data frame consists of a preamble and a data portion, where the preamble consists of the legacy preamble for protocol compatibility and the preamble defined by the different protocols, as shown in Figure 7, which shows the structure of the Single User (SU) physical data frame defined in 802.11ax. The L-STF (Legacy-short training field) L-LTF (Legacy-long



training field) and L-SIG (Legacy-Signal field) are the legacy preamble, while HE-STF and HE-LTF are the 802.11ax High Efficiency (HE) preamble. Efficiency (HE) preamble part.

... PE

Figure 7 802.11ax single-user physical data frame structure

The legacy portion of the data frame can be recognised by devices running pre-802.11ax protocols to achieve compatibility, where L-STF is mainly used for header detection and automatic gain control (AGC) coarse timing synchronisation and coarse frequency bias estimation in the time domain, while L-LTF is mainly used for fine timing synchronisation and fine frequency bias estimation, and L-SIG records some service fields of the data frame for device recognition. L-SIG records some service fields of the data frame for device identification.

The HE preamble part can only be recognised by devices running the 802.11ax protocol, which also contains the definition data frame

type of service field and long and short training sequences. the MIMO signals are transmitted using a circular shift diversity

(The purpose of Cyclic Delay Diversity (CSD) is to add different delay copies of the same signal transmitted by multiple antennas, and after experiencing different channel fading, the diversity gain can be obtained at the receiving end by adopting certain merging techniques. This leads to the fact that it is difficult to adjust the AGC to a suitable value in the process of MIMO signal reception by only using the L-STF. The main function of HE-STF is to improve the AGC in the MIMO reception process, which is a complementary function to L-STF. The function of HE-LTF is to estimate the MIMO channel at the receiving end, and its number is related to the number of airtime streams to be transmitted at the transmitting end, which is the N_{STS} . The number of HE-LTFs is related to the number of NSTSs to be transmitted at the transmitter side. 1 HE-LTF is included when $N_{STS} = 1$, and 2 HE-LTFs are included when $N_{STS} = 2$;

Contains 4 HE-LTFs when $N_{STS} = 3, 4$.

Based on the HE-LTF field, the receiver can estimate the channel for each subcarrier separately. Let $\hat{H}^i(k)$ be the channel estimate on the k th subcarrier frequency point, the i -th transmit antenna, and the j -th airtime stream. Then, on all N_{SC} subcarriers

The estimation of the

channel can be expressed as follows:

$$\hat{H}^i = \left[\left[\hat{H}^i(1), \dots, \hat{H}^i(k), \dots, \hat{H}^i(N_{SC}) \right] \right] \quad (2.6)$$

\hat{H}^i

For the channel matrix $\hat{H}^i(k)$ on the k th subcarrier, N_{RX} is the number of antennas at the receiving end and there are

$$\hat{H}^i(k) = \begin{bmatrix} \hat{i}_{11}(k) & \cdots & \hat{i}_{1N_{RX}}(k) \\ \vdots & \ddots & \vdots \\ \hat{i}_{i1}(k) & \cdots & \hat{i}_{iN_{RX}}(k) \\ \vdots & \ddots & \vdots \\ \hat{i}_{IN_{STS}1}(k) & \cdots & \hat{i}_{IN_{STS}N_{RX}}(k) \end{bmatrix} \quad (2.7)$$

$$\left| \hat{h}_{i,j}^k \right|$$

N_{RX}^1 N_{TX}^1

where $\hat{h}_{i,j}^k$ can be calculated by the Maximum Likelihood (ML) estimation algorithm

[³⁶]. Define $\hat{h}_{i,n}^k$ to be the HE-LET symbol received by the i -th antenna of the receiver up to the n th HE-LET symbol, for a single airtime flow

(e.g., Single Input Single Output (SISO) or Single Input Multiple Output (SIMO) systems) channel estimation can be performed in the following manner:

$$\hat{h}_{i,n}^k = \frac{\hat{h}_{i,n}^{LTF}(k)}{H_{ELTF}(k)} \quad (2.8)$$

And for a system with two spatial streams, i.e., $N_{STS}=2$ (e.g., a 2×2 MIMO system) there are

$$\hat{h}_{i1}(k) = \frac{h_{L1,i}(k) \otimes h_{L2,i}(k)}{2 \otimes HELTF} \quad (2.9)$$

$$\hat{h}_{i2}(k) = \frac{h_{L1,i}(k) + h_{L2,i}(k)}{2 \otimes HELTF} \quad (2.10)$$

This is due to the fact that the data subcarrier part of the HE-LTF needs to be multiplied in both the spatial and temporal domains of definition with an orthogonal matrix P_{HELTf} , which is applied to the mapping of 1-4 streams, each row representing a null-time stream.

$$P_{HELTf} = \begin{bmatrix} 1 & -1 & 11 \\ 1 & 1 & -11 \\ \hline 1 & 1 & 1 \\ 1 & 1 & 11 \end{bmatrix} \quad (2.11)$$

For the FG subcarriers, the mapping relationship is different, the FG information on each stream is the same, and they are not orthogonal to each other, so the channel estimation cannot be performed by the above method. For the guided-frequency subcarrier, only one HE-LTF is needed, and multiple copies are sent for compatibility with other data subcarriers. This processing can increase the robustness of the guided-frequency subcarrier, and at the receiver, the multiple carriers can be averaged to eliminate some of the noise effects, which makes the frequency bias estimation using the guided-frequency more reliable. In addition, the continuity of the frequency domain can be exploited by using the interpolation method to^[37] The channel response at the pilot subcarrier is estimated. Two data subcarriers are taken from the left and right sides of the pilot subcarrier for calculation, and a three-time interpolation estimation method is described as follows:

For the guided frequency subcarrier k_p , the channel response is estimated as follows:

$$\hat{h}_{ij}(k_p) = \frac{1}{a} a_0 + \frac{1}{a} a_1 + \frac{1}{a} a_2 + a_3 \quad (2.12)$$

where a_0, a_1, a_2, a_3 are defined as
ows

23 0

$$a_0 = \hat{h}_{ij}^{(k+2)} \otimes \hat{h}_{ij}^{(k+1)} \otimes \hat{h}_{ij}^{(k-1)} + \hat{h}_{ij}^{(k-2)} \quad (2.13)$$

$$a_1 = \hat{h}_{ij}^{(k-2)} \otimes \hat{h}_{ij}^{(k-1)} \otimes a_0 \quad (2.14)$$

$$a_2 = \hat{h}_{ij}^{(k+1)} \otimes \hat{h}_{ij}^{(k-2)} \quad (2.15)$$

$$a_3 = \hat{h}_{ij}^{(k-1)} \quad (2.16)$$

In summary, the estimated channel matrix is $\hat{H}(k)$ with internal noise $N(k)$, and the relation is as in equation (2.17).

$$\hat{H}(k) = H(k) + N(k) \quad (2.17)$$

After obtaining the above CSI, the receiver can equalise the data portion, usually by linear equalisation.

The computational complexity is low and easy to implement in hardware. The commonly used MIMO linear equalisation methods are Zero Forcing (ZF) equalisation and Minimum Mean Square Error (MMSE) equalisation. In order to simplify the analysis process, the following analysis omits the subcarrier subscripts.

(1) ZF Equaliser

In ZF equalisation, the received signal is assumed to be $y = Hx + n$, and the estimated channel matrix $H^{\hat{}}$ is directly pseudo

The inverse operation^[38] **The matrix G**, which is obtained by multiplying the received signal y , is then directly multiplied with the received signal y to recover the original data. (2.18)

$$G = H^{\hat{}} \dagger = (H^{\hat{}} * H^{\hat{}})^{-1} H^{\hat{}} *$$

where the * operation is the Hermitian transpose and † is the pseudo-inverse operation. The equalised received signal z has the following expression.

$$z = Gy = x + Gn \quad (2.19)$$

It can be seen that ZF equalisation eliminates ICI and is an ideal equalisation method when there is no channel noise. However, when noise is present, ZF equalisation amplifies the noise and the performance degrades when the signal-to-noise ratio is low.

(2) MMSE Equaliser

In practice, channel equalisation is usually performed using the MMSE method, where the objective of the MMSE equaliser is to minimise the MSE, i.e. to solve for the

$$\min_{\|} E \| x - Gy \| \quad (2.20)$$

The final result is obtained as

$$G = (H^* \otimes N_0 I) H^{-1*} \quad (2.21)$$

where N_0 is the estimated received signal noise. It can be seen that the MMSE equaliser takes into account the effect of signal noise.

When performing equalisation, the amplification of noise is smaller than that of ZF and the performance is better, but the computation amount is larger than that of ZF equaliser. When the noise is 0, the MMSE equaliser degrades to the ZF equaliser.

After the receiver obtains the channel matrix by estimation, it feeds the CSI to the transmitter, which can adjust the transmission strategy based on this information, such as the selection of the modulation order and the operation of beamforming using the estimated channel matrix.

2.2.2 beamforming

In the 802.11 protocol family, beamforming technology was first introduced in 802.11n, and its application scenario is that an access point (AP) with multiple antennas transmits signals to wireless terminals (station (STA)) with a small number of antennas (usually only 1-2). In order to make full use of the multiple antenna resources of APs, MU-MIMO is introduced in 802.11ac, which can simultaneously transmit signals to multiple antennas.

The efficiency of wireless transmission is improved by sending different signals from different STAs. 802.11ax further increases the number of multiple users to cope with the increasing number of wireless terminals. In MU-MIMO, beamforming is used to enable different sets of antennas to be pointed at different user terminals, so that the terminals receive only their own signals and are not interfered by other signals.

According to the different ways of acquiring CSI at the transmitter, beamforming can be divided into two categories: Explicit beamforming and Implicit beamforming.

(1) Explicit beamforming

Display beamforming is a way for the receiver to obtain CSI through channel estimation and then send it back to the transmitter. First the AP sends a probe frame to the STA to obtain the channel information, and then the STA estimates the channel information and sends it back to the AP. in 802.11ax, the AP first sends a Null Data Packet (NDP) which is a type of wireless data frame that does not contain a data portion, i.e., it only contains a leading portion, and can measure the passing wireless channel to obtain the channel information. The channel information is obtained. Then the channel matrix information is fed back to the transmitter through data compression to calculate the beamforming coefficient matrix, the specific flow is shown in Fig. 8.

The receiver performs channel estimation through the HE-LTF sequence in the NDP preamble to obtain the channel matrix \mathbf{H} , which is then subjected to Singular Value Decomposition (SVD):

$$\mathbf{H} = \mathbf{U}\Sigma\mathbf{V}^* \quad (2.22)$$

Where \mathbf{U} and \mathbf{V} are the You matrices, Σ is the diagonal array, and its elements are called singular values, which are arranged in descending order of non-negative magnitude. The advantage of using the SVD decomposition is that a linear receiver can achieve maximum likelihood performance, thus simplifying the design and increasing the computational efficiency of the device. 802.11ax devices compress the \mathbf{V} matrix obtained from the feedback when implementing beamforming: \mathbf{V} is decomposed into the angle-dependent

parameters ϕ and ψ by rotating the Givens matrix, and then inverted into the V matrix by rotating the Givens matrix.

The quantised values fed to these angles can be used to achieve different data volumes and computational complexity by choosing the number of bits of quantisation^[39]. The signal received at the receiver can be represented as follows:

$$\mathbf{y} = \mathbf{h}\mathbf{v}\mathbf{x} + \mathbf{n} = \mathbf{u}\Sigma\mathbf{x} + \mathbf{n} \quad (2.23)$$

where \mathbf{X} is the transmitted signal and \mathbf{N} is the noise at the receiving end. The receiver processes the received signal to estimate the channel matrix as $\mathbf{H}' = \mathbf{U}\Sigma$, which can be obtained:

$$\begin{aligned} \mathbf{X} &= \mathbf{H}'^{-1} \otimes = (\mathbf{U}\Sigma)^{-1} \mathbf{Y} \\ &= (\mathbf{U}\Sigma)^{-1} (\mathbf{U}\Sigma\mathbf{V}^*) \mathbf{V}\mathbf{X} + (\mathbf{U}\Sigma)^{-1} \otimes = \mathbf{X} + \mathbf{N}' \end{aligned} \quad (2.24)$$

Due to the nature of the You matrix, the power of the equivalent noise \mathbf{N}' is constant and the above communication system is equivalent to several parallel Additive White Gaussian Noise (AWGN) channels.

In summary, SVD-based beamforming not only decouples the transmit signal at the receiver end, but also does not amplify the noise without error transmission.

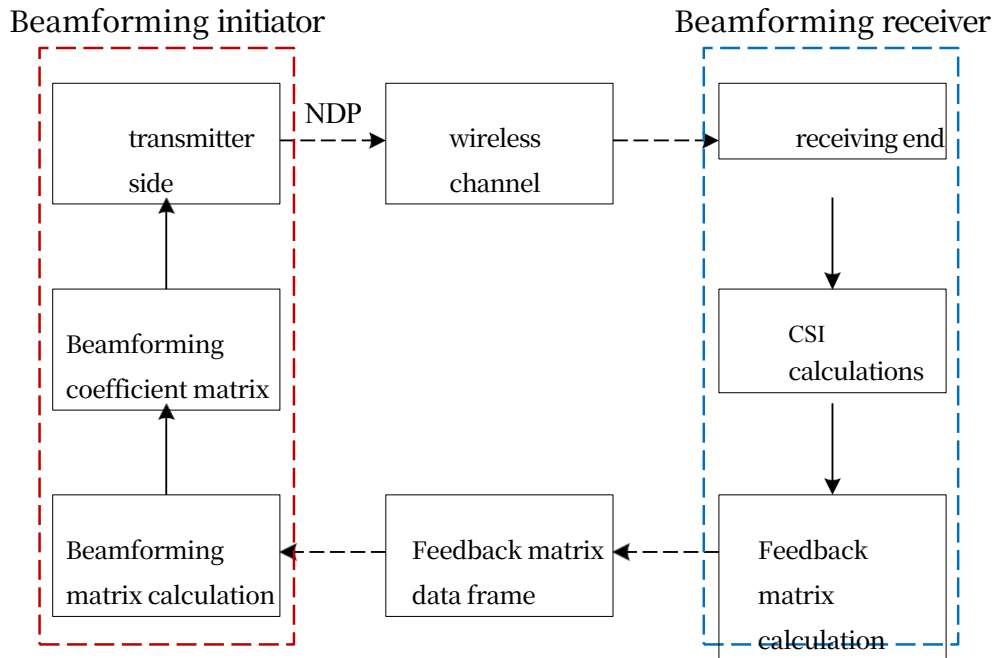


Fig. 8 Beamforming flow

(2) implicit beamformin g

Implicit beamforming is premised on the assumption that Time Division Duplexing (TDD) systems are reciprocal, i.e., the CSIs of the uplink and downlink channels on the same frequency band are the same. Based on the above assumption, the STA directly applies the CSI obtained in the uplink receive direction to the downlink direction. Due to the complexity of the implementation of implicit beamforming, protocols from 802.11ac onwards specify that beamforming is only performed using the display method.

Unlike analogue beamforming techniques, which operate directly on the phase at the RF antenna end, all of the above beamforming techniques fall into the category of digital precoding, which is the result of direct mathematical processing of the transmitted signal. In addition, hybrid precoding techniques can be used to enhance the performance of the communication system.

2.2.3 Transmit Rate Adaptive

Rate adaptive technology is a technology in the communication system, the transmitter according to the detection of the real-time state of the channel, change the modulation of the transmitted signal, and then change the transmission rate to improve the throughput performance of the system. The core of the rate adaptation algorithm is to obtain the current channel state information in real time and adjust the transmission rate. Throughput is one of the standards to measure the performance of the communication system, throughput is not only related to the choice of modulation method, but also the BER of the received signal. When a higher transmission rate is selected, the BER of the communication system will also be increased. The purpose of the adaptive rate algorithm is to find a balance between the transmission rate and the BER performance to meet the effectiveness and reliability requirements of the communication system, which is in line with the needs of WAIC.

The 802.11ax standard provides 12 different rate MCSs at the physical layer, but does not specify a rate selection strategy. The common adaptive rate algorithms^[40] are classified into the following four main categories:

(1) The most typical algorithm to determine whether to adjust the MCS is based on the number of consecutive successes or failures of transmitted data frames, such as the Automatic RateFallback (ARF) algorithm.^[41] The most typical algorithm is the Automatic RateFallback (ARF) algorithm. When the receiver does not receive two consecutive Acknowledge (ACK) frames, the MCS is lowered by one notch and a timer is started to send data again; when 10 consecutive frames are received correctly or the timer reaches a predetermined time, the MCS is raised. The disadvantage of this method is that it is difficult to adapt to the rapid changes in the channel. The AARF algorithm^[42] The AARF algorithm enhances the adaptability to rapid channel changes by using an exponential threshold.

(2) Data metrics such as BER, SNR, etc. obtained using physical layer measurements or estimations. The channel information obtained from data frame measurements is fed back to the transmitter for MCS adjustment. The disadvantage is that the physical layer metrics may not have a strong correlation with the throughput, and the performance is poor in specific implementations.

(3) The quality of the current channel is estimated by sending probe frames with different MCSs at regular intervals. In this way, the transmission capability of different MCSs in the current channel can be well estimated. However, when too many probe frames are sent, it may lead to misjudgment and affect the system performance. A typical algorithm is SampleRate^[43] SampleRate.

(4) The MCS is adjusted by calculating the statistics of the received signals over a period of time. A typical algorithm is RRRA.^[44] This algorithm counts the frame loss rate and other information during a window of time and compares it with the corresponding threshold value to adjust the MCS. This method avoids false judgement caused by dropped frames, and when the window is set appropriately, it can respond to rapid changes in the channel.

The above rate control algorithms can also be categorised according to transmitter-based and receiver-based, e.g., (1)(2) and (3) belong to transmitter-based rate control algorithms, which do not require modification of the physical data frame format, and are widely used in practical communication devices. While (4) belongs to the rate control algorithm based on the receiver side, by performing data statistics at the receiver and then feeding back to the transmitter side, the advantage is that it can react to the rapid change of the channel in time, the disadvantage is that it needs to modify the management frame format to transmit the information, and the compatibility is poor.

2.3 IEEE 802.11 Applicability in WAIC Technology Simulation

2.3.1 Simulation analysis of beamforming technology

The experiment is simulated based on the 802.11ax single-user point-to-point communication scenario, and the experimental flow is shown in Fig. 9. The avionics cabin model used in the experiment is the passenger cabin, and the channel fading obeys the Rice distribution, which will be further modelled and simulated in Chapter III.

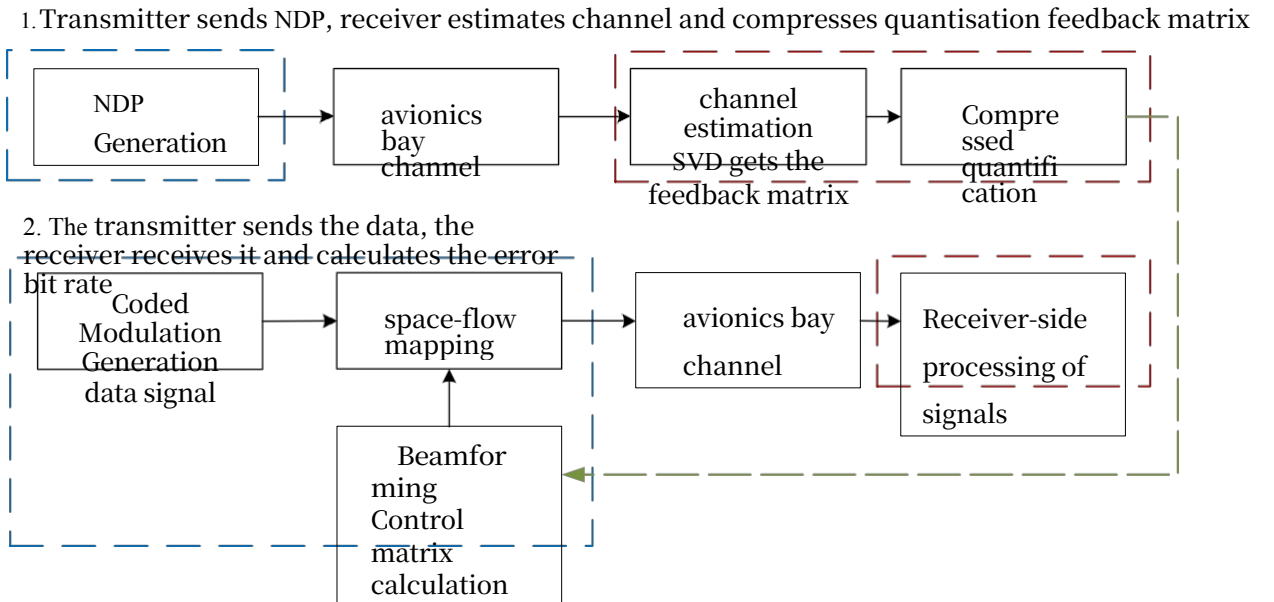


Fig. 9 Flow of detecting at the transmitter and beamforming at the receiver

In this experiment, the number of antennas at the transmitting end is set to be 4, the number of antennas at the receiving end is set to be 2, the number of airtime streams is set to be 2, the communication bandwidth is 20MHz, and the length of transmitting data is set to be 1000 Bytes, and a total of 1000 packets are transmitting. Simulation MCS3 (modulation 16QAM, code rate 1/2) and MCS5 (modulation 64QAM, code rate 2/3) two different signals with three different bit counts of compressed beamforming are used to calculate the Packet Error Rate (PER) at the receiving end with the following settings:

- (1) No compressed quantisation is performed and the complete V matrix is fed back;
- (2) Set the number of bits in ϕ to 4 and the number of bits in ψ to 2;
- (3) Set the number of bits in ϕ to 6 and the number of bits in ψ to 4.

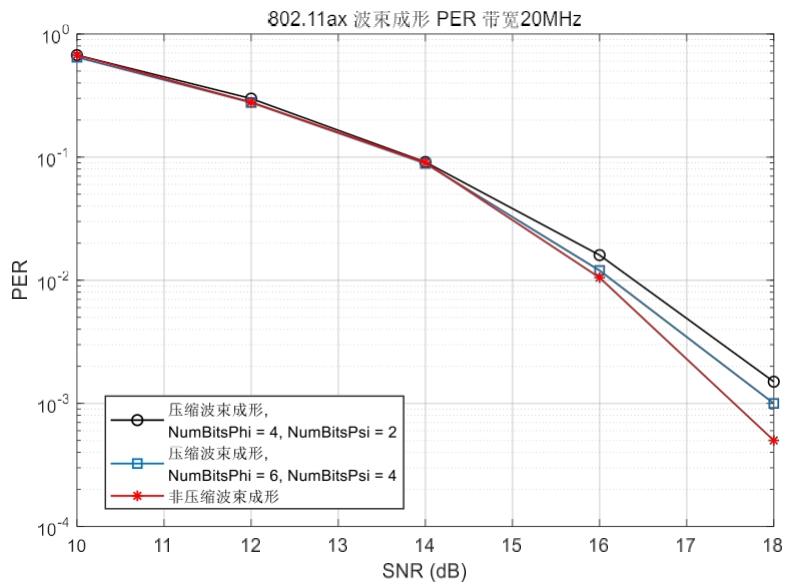


Fig. 10 Comparison of the performance of MCS3 quantised beamforming PER with different bits.

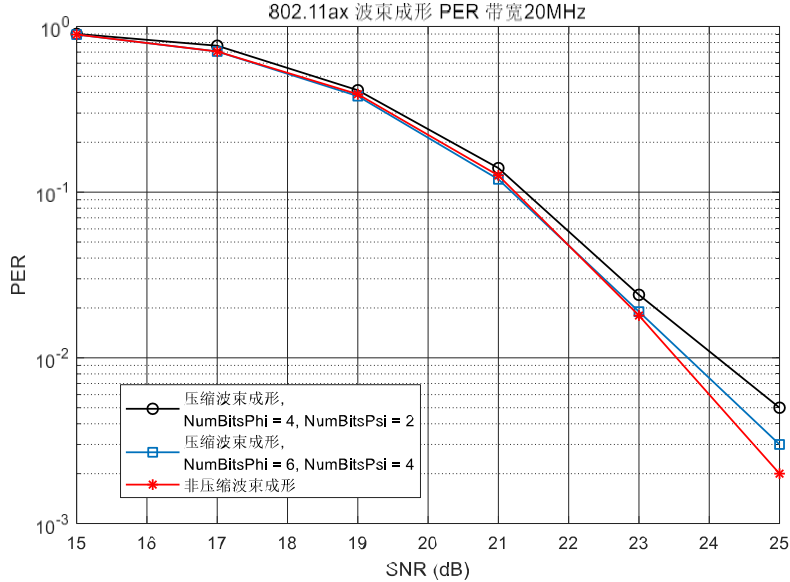


Fig. 11 Comparison of the performance of MCS5 quantised beamforming PER with different bits.

Fig. 10 shows the simulation results of MCS3 and Fig. 11 shows the simulation results of MCS5. It can be seen that the variation curves of PER curves quantised with different number of bits are the same, but the slopes of the PER curves are different in the high SNR domain. This is due to the fact that the unquantised control matrix has a higher gain, the larger the number of quantised bits is, the more channel information is saved, the larger the gain can be obtained by the transmitter, and the larger the absolute value of the slope of the PER curve is in the high SNR domain, but at this time, the amount of data that needs to be sent to the transmitter will also become larger, which affects the delay characteristics of the system, and a compromise needs to be made between the number of quantised bits and the throughput performance of the actual hardware equipment. In the actual hardware equipment, it is necessary to make a compromise between the number of quantisation bits and the throughput performance.

2.3.2 Simulation Analysis of Rate Adaptive Techniques

In order to simplify the implementation process, this experiment considers the implementation of the rate adaptive algorithm by measuring the physical layer metrics. Let the BER requirement of WAIC be 10^{-6} , and measure the SNR value required to reach this BER when different MCSs are set, and take it as the threshold value of MCS switching for the rate

adaptive algorithm. Fig. 12 shows the BER and PER curves obtained by simulating MCS 0-5, and the relationship between BER and PER can be observed by taking the average value of multiple simulations, when BER drops to 10^{-6} , PER also drops to 10^{-2} , and the SNR value at this time is taken as the threshold value for rate switching, as shown in Table 4.

Table 4 Signal-to-noise ratio with PER reduced to 10^{-2}

Modulation (bit rate)	Eb_N0
BPSK (1/2)	3
QPSK (1/2)	10
QPSK (3/4)	14
16QAM (1/2)	18
16QAM (3/4)	24
64QAM (2/3)	29

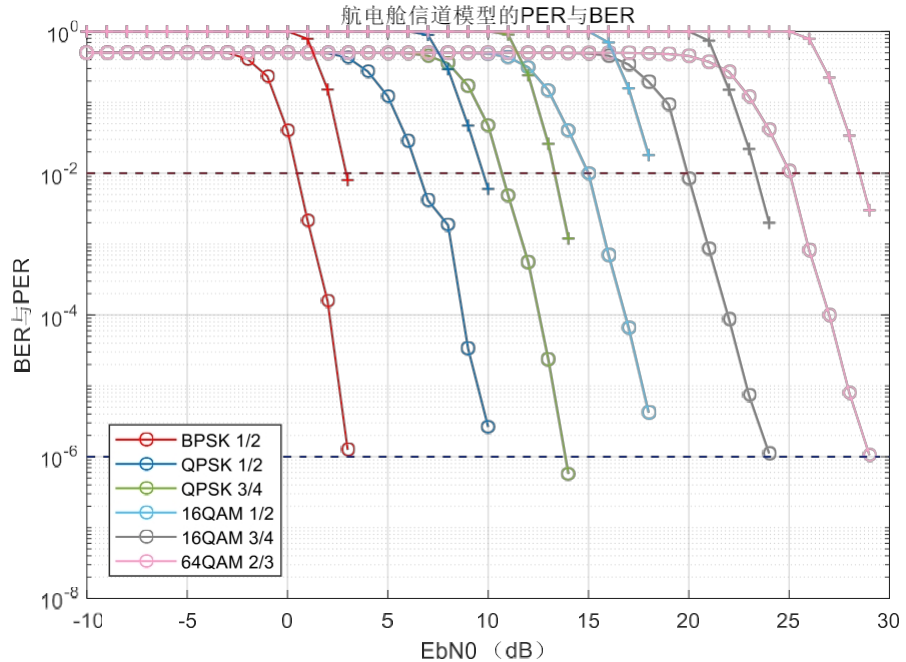


Fig. 12 BER and PER with different MCS settings

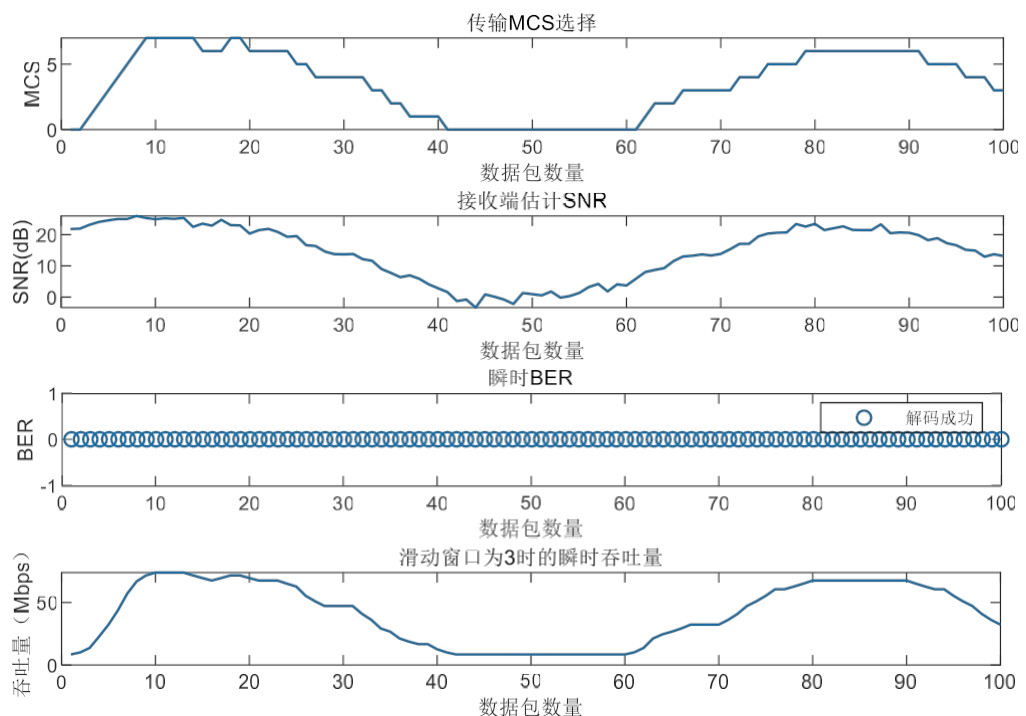


Fig. 13 Simulation results of adaptive rate algorithm

Conversion from E_b / N_0 to SNR:

$$SNR (\text{dB}) = E_b / N_0 (\text{dB}) + 10 \log_{10} \frac{(M^{N_{\text{used}}})}{N_{\text{fft}}} \quad (2.25)$$

where M is the constellation map N_{used} is the number of subcarriers
order of the selected MCS. carrying data 234, N_{ft}

The number of FFT points required for OFDM modulation is 256. a set of SNR switching thresholds is calculated as $\{5, 8, 11, 14, 18, 21, 24, 26\}$. In the actual simulation system, in order to switch the MCS more smoothly, two more thresholds are also set

(The MCS is increased when the measured SNR is greater than threshold+rcaAttack and decreased when the measured SNR is less than threshold-rcaRelease. The simulation is set in a scenario where the SNR transform is continuously varied by a cosine function. The simulation is set in a scenario where the SNR variation is controlled by a cosine function that varies continuously, and the average value of SNR is

15dB with a variance of 14dB. In the simulation environment where both the transmitter and receiver antennas are single antennas, set rcaAttack=0 and rcaRelease=1, the simulation results are shown in Fig. 13, which shows that the designed system can track the continuous changes of the current channel well. In the face of different communication environments, the two parameters of racAttack and racRelease can be reasonably adjusted to adapt.

2.4 Summary of the chapter

This chapter firstly analyses the principle of the applicable technologies of IEEE 802.11 WLAN in WAIC, and then explains the principle of the transmitter CSI acquisition technology and the rate adaptive algorithm which are required in WAIC. Then it explains the principles of transmitter CSI acquisition, beamforming and rate adaptive algorithms, which can be used as the performance guarantee mechanism of WAIC. CSI acquisition can track the channel status in real time, which provides the basis for the subsequent beamforming and rate adaptive algorithms. The beamforming technique focuses the signal and provides gain to the receiver to enhance the system performance and communication quality. The rate adaptive algorithm can adjust the modulation and coding scheme of the transmitter according to the

CSI information in real time to match the channel state, so as to ensure that the system has better communication performance. Finally, the beamforming and rate adaptation algorithms are simulated and analysed in the practical application scenario of avionics cabin. The simulation results show that the beamforming technique can provide a certain gain for the signal at the receiving end, and the proposed adaptive rate control algorithm can track the real-time state of the channel and make timely adjustments to the MCS at the transmitting end in the scenarios where the signal-to-noise ratio of the channel changes rapidly, which enhances the communication performance of the system, and thus achieves the purpose of guaranteeing the performance of the WAIC.

Chapter III Study of the Effective Capacity of Avionics Wireless Communications

The WAIC high-rate communication scenario of interest to this topic is the in-flight communication in the avionics cabin. Due to the lack of the conditions for the actual measurement and research in the avionics cabin, and the fact that the current WAIC communication actual measurement and research is based on the passenger cabin or the external communication scenario, this topic will use the simulation method to carry out the modeling research on the wireless channel in the equipment cabin. In addition, focusing on the QoS performance of transmit data in the physical layer buffer queue, the delay of equipment signal transmission is analysed by studying the effective bandwidth and effective capacity model of the transmitter buffer queue, and simulating and analysing the upper bound of queuing delay of the transmitter buffer queue.

3.1 Avionics wireless channel modelling

The random characteristics of the wireless channel will affect the throughput of the communication system as well as the QoS performance and other indicators, and the study of the statistical characteristics of the wireless channel fading is an indispensable step in analysing the performance of the communication system. The commonly used methods for analysing channel fading characteristics include measurement and simulation. Measurement analysis is performed by transmitting the set signals in real communication scenarios and analysing them at different locations of the receivers, and the results obtained can be used as empirical data to guide the signal processing in similar scenarios afterwards. Simulation analysis is a method to simulate the physical processes such as reflection, refraction or diffraction experienced by the signal through computer modelling of physical models and statistical information at the receiver when the conditions for real analysis are not available.

Regarding the WAIC channel, the existing studies are based on the cabin model for actual measurement or simulation analysis. Literature [45] simulated the signal propagation characteristics of the cabin model of A340 aircraft at 2GHz using ray tracing algorithm based on geometrical optics theory. Literature^[46-48] The ray-tracing algorithm is used to simulate and evaluate the cabin channel model based on Ultra Wide Band (UWB) communication technology, measure the delay power spectrum of the multipath channel, and calculate the root-mean-square delay expansion, which is in line with the characteristics of multi-cluster multipath. Literature [49] measured the signal propagation characteristics in the ISM bands (2.4GHz and 5.8GHz) inside the cabin channel in a line of sight (LOS) scenario and fitted the channel fading distribution as a Rice distribution. Literature [50] added a passenger movement scenario in the cabin to analyse the time-varying channel characteristics in the cabin, and the faster the speed of the passengers, the shorter the channel coherence time.

Based on the above analysis, the goal of this project is to model the avionics equipment bay, in which there is no large amount of object movement, which is a quasi-static channel. Due to the difficulty of measuring the internal environment of the equipment bay, this paper adopts the ray tracing algorithm to model and simulate the avionics equipment bay channel for analysis.

3.1.1 Ray tracing algorithms

Ray tracing algorithms are a technique often used in communication scenarios to predict the propagation paths of wireless signals, and can discern all possible paths that a signal may take in a multipath channel. Based on the theory of radio wave propagation, the transmission time, amplitude attenuation, and phase variation of the signal on each path can be calculated, and combined with the carrier frequency and bandwidth, the

The final result of the synthesis is obtained at the receiving point.

Ray tracing algorithms are usually classified into Shooting and Bouncing Rays Method (SBR) and Image Method. In SBR, the positions of the transmitter point T_x and receiver point R_x are specified, and rays are emitted uniformly from the transmitter point to the surrounding area. Fig. 14 shows a schematic diagram of SBR ray emission and reception. A receiving sphere of fixed radius is specified at the receiving point, and the rays emitted from T_x are judged to pass through the inner part of the receiving sphere of R_x after different reflections at each point.

is successfully received. The radius of the receiving sphere is proportional to the length of the rays and the average degree between the rays, and when the degree between the rays is reduced in order to increase the number of rays, the radius of the receiving sphere will also become smaller. Physical phenomena such as refraction, diffraction and scattering can also be considered in the SBR algorithm, but due to the complexity of the computation, only refraction is considered in the simulation without affecting the accuracy of the final results.

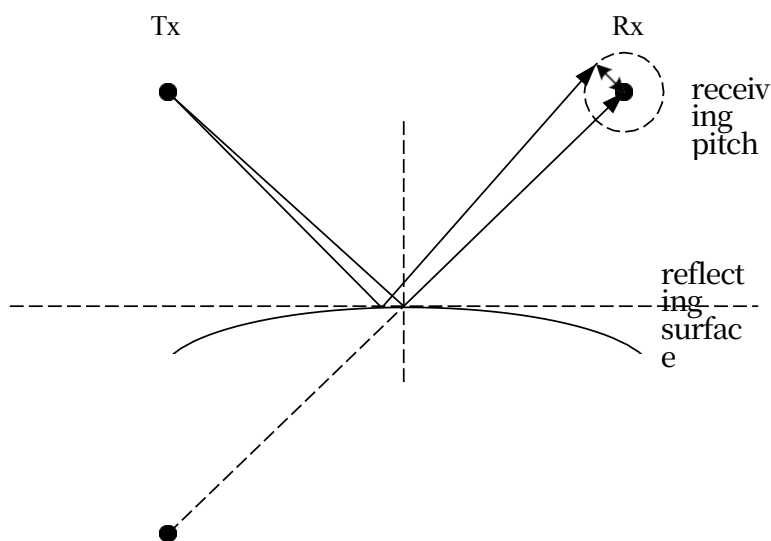


Figure 14 SBR Receiving Schematic

The mirror method mirrors the emitting node based on the reflection surface, determines whether the mirror point and the receiving point can be connected by a straight line, and if they can be determined to be

reasonable paths, obtains the final path by repeating the above steps, and calculates parameters such as the distances between the emitting mirror point and the receiving point. The computational complexity of the SBR is linearly related to the number of reflecting points, whereas the computational complexity of the mirror method is exponentially related to the number of reflections. In addition, the mirror method cannot calculate the information such as the time series of the received ray and the reflection angle. Taken together, the SBR algorithm is adopted in this project for modelling the channel of avionics cabin.

The avionics bay consists of a large number of metal devices and composite materials, which is a closed communication environment, similar to an indoor communication scenario, and can be described by a typical multipath channel model. After ray tracing to get the electric field strengths of the signals of different paths at the receiving end, the field strength of the final signal is then obtained by vector summation operation. Assuming that the transmitted signal is

$$x(t) = \operatorname{Re}\{s(t)e^{j2\pi f_C t}\}$$

where $s(t)$ is the baseband signal corresponding to $x(t)$, f_C is the carrier frequency, and $\operatorname{Re}\{\cdot\}$ is the real part taking operation. Neglecting the noise, the received signal $y(t)$ is the sum of all ray-traced resolvable multipath signal components, as follows

$$y(t) = \operatorname{Re} \left\{ \sum_{i=0}^N \beta_i(t) s(t - \tau_i(t)) e^{-j2\pi f(t - \tau_i(t))} \right\} \quad (3.2)$$

where N is the number of distinguishable multipaths, $i = 0$ is the shortest path, which corresponds to a direct signal when a direct ray path exists. The length of each ray path is $d_i(t)$ and its corresponding delay is $\tau_i(t) = d_i(t) / c$, c is the transmission rate of the radio wave, i.e., the optical velocity. $\beta_i(t)$ is denoted as the large-scale decay factor, such that $\phi_i(t) = 2\pi f C \tau_i(t)$, which simplifies the signal expression as

$$y(t) = \beta \operatorname{Re} \left\{ \sum_{i=0}^N \beta_i(t) e^{-j\phi_i(t)} s(t - \tau_i(t)) \right\} e^{-j2\pi f t} \quad (3.3)$$

Amon
g
them.

$$r(t) = \sum_{i=0}^N \beta_i(t) e^{-j\phi_i(t)} s(t - \tau_i(t)) \quad (3.4)$$

is the baseband signal corresponding to the received signal. $\beta_i(t)$ depends on the path loss and shadow fading, $\phi_i(t)$ depends on the delay, which

The two stochastic processes can usually be assumed to be independent of each other. From the above analysis, the equivalent impulse response of the baseband signal can be obtained as

$$h(t, \tau) = \sum_{i=0}^N \beta_i(t) \delta(t - \tau_i(t)) = \sum_{i=0}^N \alpha_i(t) \delta(t - \tau_i(t)) \quad (3.5)$$

Usually $\alpha_i(t) = \beta_i(t) e^{-j\phi_i(t)}$ is taken as the channel fading coefficient of the

baseband signal. By obtaining the information about the delay and fading of the multipath channel in the results obtained from ray tracing, the channel response amplitude at the receiver can be calculated for subsequent analysis of the fading distribution.

3.1.2 Simulation and analysis of wireless channels in avionics cabin

Due to the complexity of the aircraft structure, the internal communication environment is different from the common scenarios, and the channel characteristics need to be analysed based on specific simulation or real measurement data. Since it is not possible to conduct real measurements in the actual scenario of avionics cabin, this topic adopts the simulation method to analyse the channel characteristics, which is based on the cabin data modelled on SolidWorks. Firstly, the cabin model of Boeing 737-200 is modelled with reference to the data in [51], and the multipath channel simulation is carried out by the SBR algorithm. The transmitter is located at the top of the cabin with a height of 2m, and the receiver is located at the armrest of the seat with a height of 0.6m, and the receiver is located at the armrest of the seat with a height of 0.6m.

The horizontal distance between the two is 1 m. The relative dielectric constant of the bulkhead material is 14, the conductivity is 1×10^{-5} S/m, and the propagation speed of the wireless signal is set to be the speed of light, and the simulation results are shown in Fig. 15.

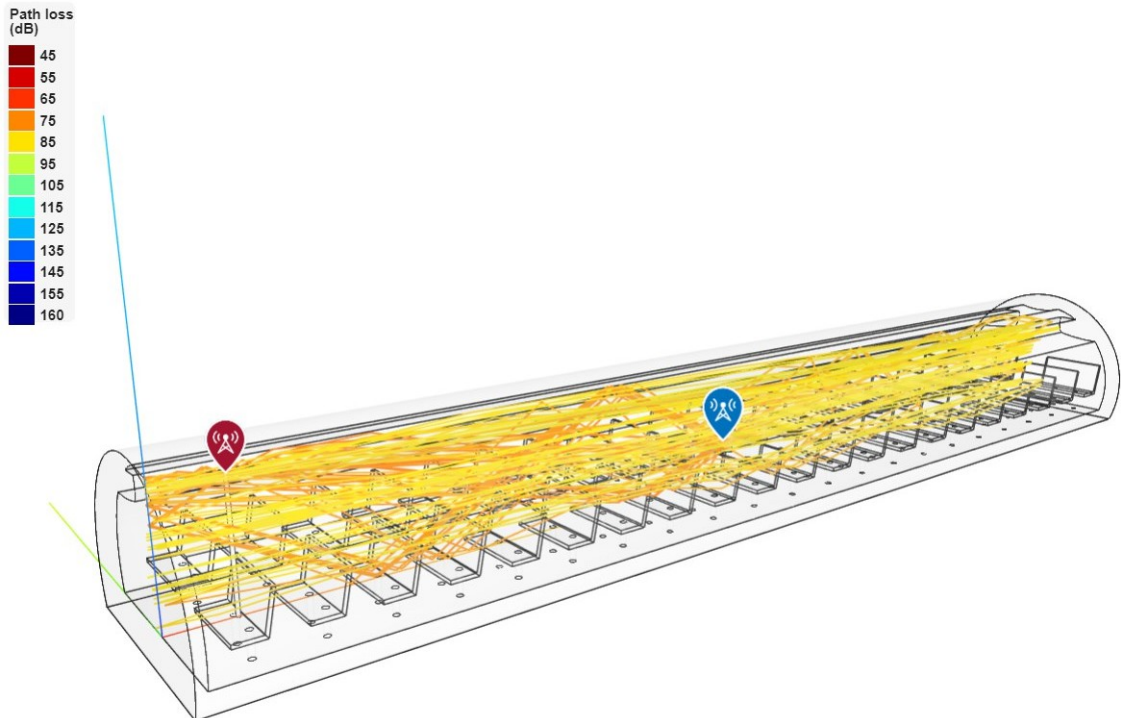


Figure 15 Boeing 737-200 cabin channel simulation

According to the results obtained from SBR, the Delay Power Profile (PDP) of the channel can be drawn from each ray path parameter, and then the Root Mean Square (RMS) delay expansion of the multipath channel can be obtained from the PDP calculation as follows:

$$\tau_{rms} = \sqrt{\frac{1}{P_T} \sum_i^L P_i \tau_i^2 - \bar{\tau}^2} \quad (3.6)$$

$$\bar{\tau} = \sqrt{\frac{1}{P_T} \sum_i^L P_i \tau_i} \quad (3.7)$$

where L is the number of multipaths obtained from the SBR simulation, i.e., the number of rays, P_T and P_i are the total power and the number of rays in the i -th direction, respectively.

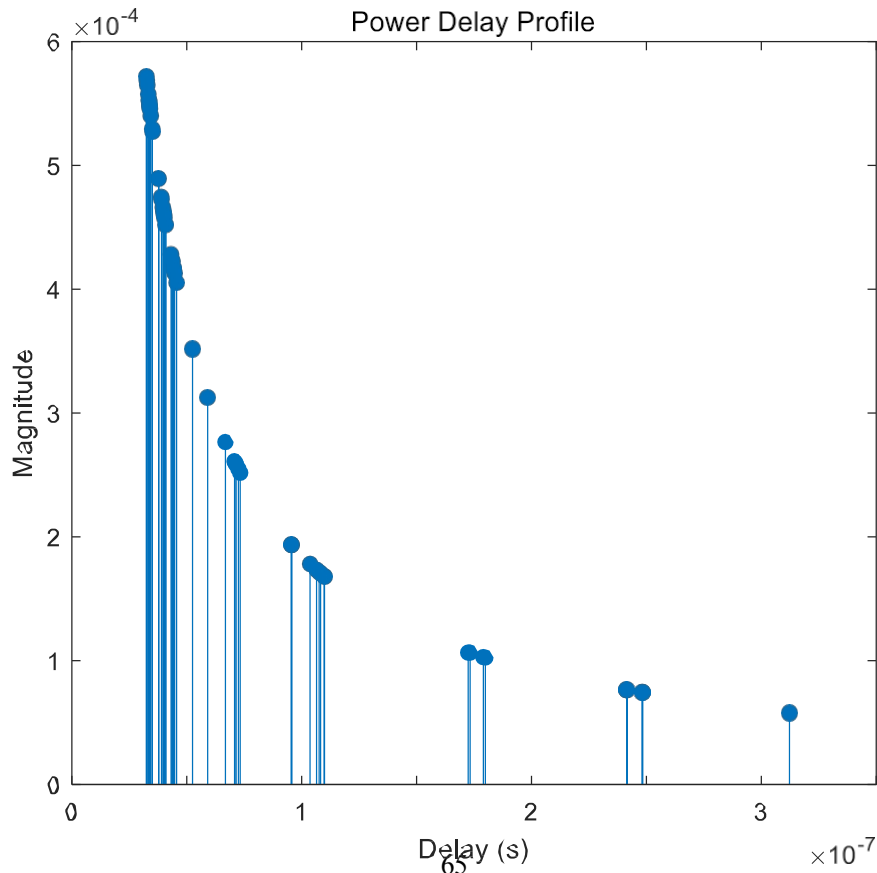
power of a path, and τ is the average delay extension. Based on these parameters it is possible to characterise the correlation properties of multipath channels, as defined by the coherence bandwidth: there exists a frequency interval in which the complex frequency transfer function of the channel is strongly correlated, characterised by the correlation coefficient. The coherence bandwidth BC_{50} with a correlation coefficient of 50%, as defined in the literature [34], is calculated as:

$$BC_{50} = \frac{1}{5\tau_{rms}} \quad (3.8)$$

And the coherence bandwidth BC_{90} with a correlation coefficient of 90% is calculated as:

$$BC_{90} = \frac{1}{50\tau_{rms}} \quad (3.9)$$

Figure 16 shows the PDP obtained from a cabin channel simulation, from which it can be seen that the multipath channel has more obvious multi-cluster multipath characteristics, that is, there are several different signal clusters in the multipath channel, the signal delay difference within each cluster is very small and has similar frequency, phase and delay, but the time difference between these clusters is very large, and the envelope of the different clusters is in line with exponential fading characteristics, and the amplitude of the channel response inside the clusters is also in line with the exponential fading characteristics. Within these clusters, the amplitude of the channel response similarly conforms to the exponential fading characteristics.



0.5 1.5 2.5 3.5

Figure 16 Boeing 737-200 cabin channel PDPs

The RMS delay extension of each cabin channel simulation is calculated, and the average value of 500 simulations is counted, as shown in Fig. 17. Comparing with the simulation results in the literature [48], the average RMS delay extension obtained in this experiment is about 14ns, which is close to the measured results, and this confirms the validity and feasibility of the SBR method adopted in this project, and it can be used in the subsequent experimental simulation.

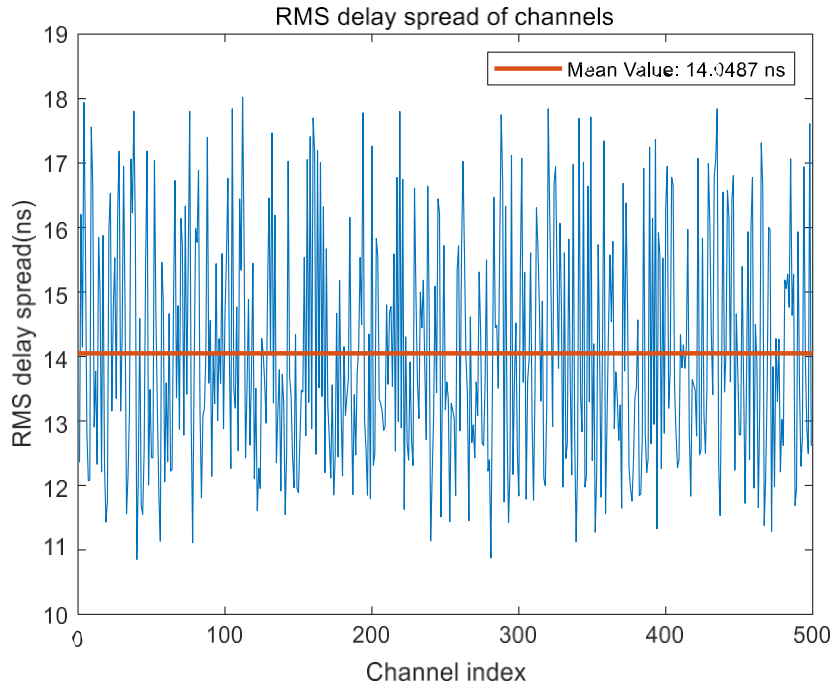


Fig. 17 RMS delay extensions calculated from 500 cabin simulations

3.1.3 Simulation and analysis of wireless channel in avionics bay

The A777-200 avionics bay was modelled using SolidWorks software, as shown in Figure 18, and the tolerance was set to 5.90 mm when exporting the STL model, in which the dimensions of the communication equipment on the avionics racks refer to the standards set by the Allied Standard Avionics Architecture Council (ASAAC).^[52] The dimensions of the communication equipment on the equipment rack are defined by the Allied Standard Avionics Architecture Council (ASAAC), which are 20 mm in width (can be increased to 30 mm or 40 mm if required) 160 mm in height, and 233.45 mm in length. The avionics equipment on the equipment rack generally consists of Line Replaceable Units (LRUs) and modules (Line Replaceable Modules (LRMs)). The ASAAC standard is not designed for LRMs or LRUs, but is applicable to a wide range of systems and equipment on the aircraft, and is mostly compatible with civil aviation equipment.^[53] The ASAAC standard is not designed for LRMs or LRUs.

Table 5 Avionics modelling dimensional information

typology	Length/mm	Width/mm	Height/mm
1	324	40	200
2	324	100	200

3	324	200	200
4	324	300	200
5	324	450	200

In order to simplify the modelling process, this topic uses different types of avionics equipment containing five sizes placed in the equipment

The channel modelling is carried out on the racks, and the data are shown in Table 5. Two different types of equipment racks are used, the height of the racks is set to 250 mm, and the width of the racks is set to 3000 mm. The equipment rack 1 is 6-tier, and the equipment rack 2 is 3-tier, and the two racks are placed opposite to each other with reference to the internal structure of the actual avionics equipment bay in Fig. 19. Since it is difficult to measure the actual parameters, in order to get more reliable simulation data, the simulation is carried out in three scenarios with different spacing between equipment, which are 60, 75 and 90 cm respectively.

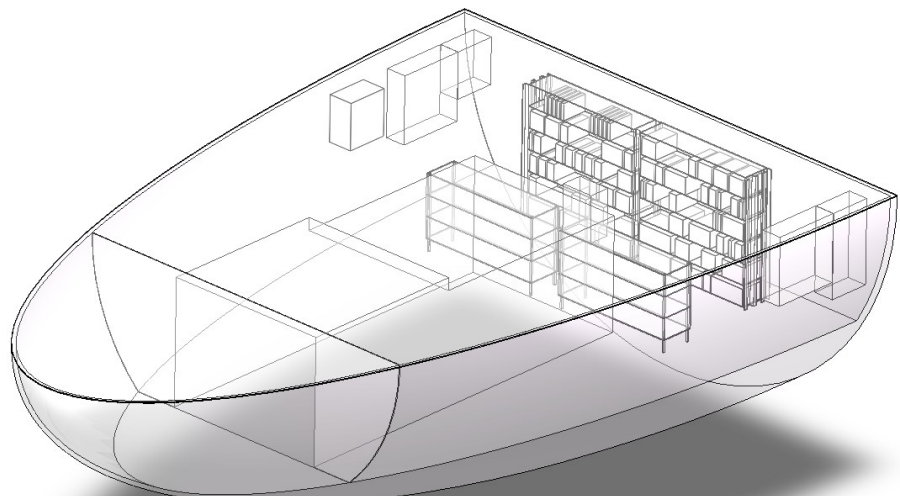


Figure 18 Avionics module model



(a) Placement of avionics equipment on equipment rack 1

(b) Relative placement of equipment racks

Figure 19 View of A777-200 avionics bay

Set the relative positions of the transmitter and receiver to be on the

diagonal of the two equipment racks, as shown in Fig. 20, when the direct signal will pass through the farthest distance of the inter-device communication. The transmit signal bandwidth is set to be 20 MHz, which is the basic signal bandwidth specified by the 802.11 protocol, and the centre frequency is 4.3 GHz, corresponding to the signal wavelength $\lambda = 69.77$ mm. The SBR method is a deterministic channel modelling method, and randomly generated variables need to be introduced to study the random characteristics of the avionics cabin channel. In this experiment, the fixed transmitter position is unchanged, and the receiver position is set to be the fixed sphere centre, with a uniform radius of $\lambda/2$ on the sphere.

The sampled points were statistically simulated through 5000 simulations and are shown in Table 6.

Table 6 Equipment bay ray tracing statistics

Equipment rack distance/cm	RMS delay extension/ns	Coherent Bandwidth	
		BC ₅₀ /MHz	BC ₉₀ /MHz
60	7.03	28.42	2.84
75	8.32	24.03	2.40
90	7.34	27.22	2.72

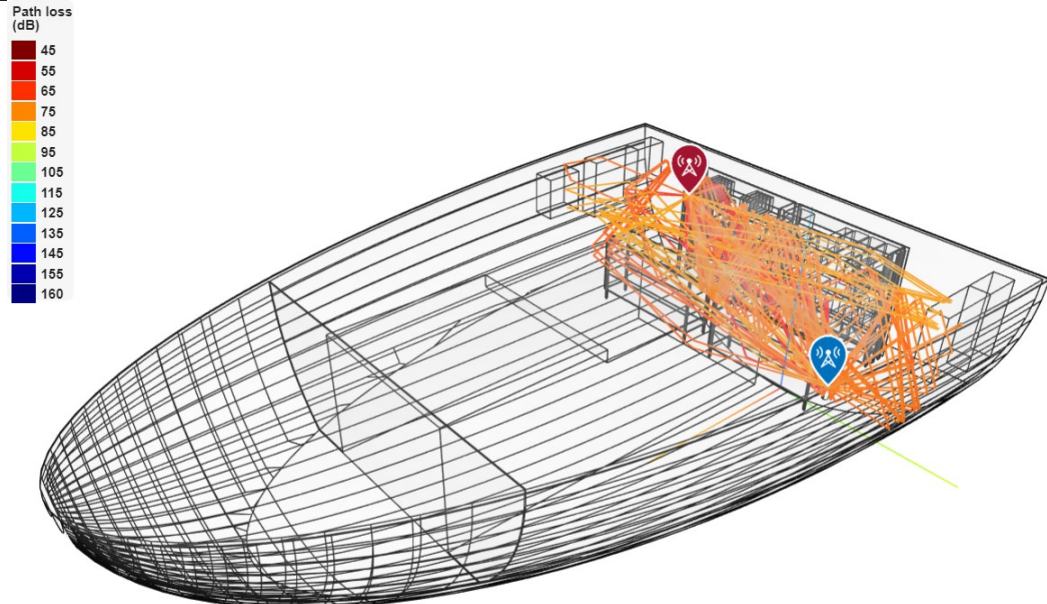


Fig. 20 Ray tracing simulation results of avionics equipment compartment

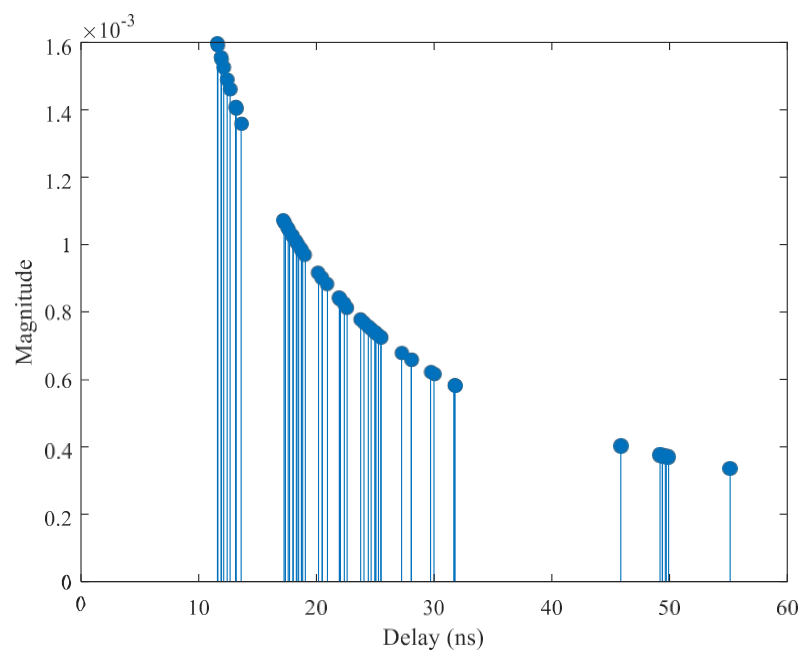


Figure 21 PDP of the equipment bay channel obtained in one simulation.

Taking the PDP of a simulation as shown in Fig. 21, it can be seen that the equipment bay channel obtained from the simulation has the characteristics of multi-cluster multipath, which is consistent with the characteristics of multipath channel. From the results in Table 6, it can be seen that the avionics equipment bay channel is a quasi-stationary channel (flat fading channel) with weak frequency selectivity in the definition of coherence bandwidth BC_{50} and in the basic communication bandwidth of 20MHz. In the coherent bandwidth BC_{90} , it is a frequency-selective channel, and the signal needs to be

Row equalisation. In the subsequent capacity analysis, it is necessary to distinguish between the different effects caused by flat fading and frequency-selective fading, while the different performance of the channel is also related to the size of the bandwidth and the division of the channel.

3.2 Upper bound analysis of queuing delay based on effective capacity

The effective capacity in wireless communication and the effective bandwidth in wired communication are dyadic concepts, and this model considers the QoS constraint problem of queuing delay in buffer queue. Based on the effective capacity model, the upper bound of queuing delay in the buffer queue at the transmitter can be calculated and analysed, and by controlling the rate of arriving traffic, the queuing delay can be controlled within the desired range, thus satisfying the QoS requirements in WAIC and evaluating the effectiveness and reliability of the communication system.

3.2.1 Theoretical Models of Effective Capacity and Effective Bandwidth

Wireless communication environments are diverse, with different channel characteristics in different communication environments. Signal propagation is affected by physical phenomena such as reflection, refraction or diffraction as well as moving objects, and the channel response has certain random characteristics. The theoretical upper bound of the maximum rate that can be supported by the transmitter is determined by the Shannon capacity, but the Shannon capacity is an idealised model

assuming error-free transmission under AWGN channel conditions, and does not take into account the BER and queuing delay and other QoS metrics.

The effective capacity model is a model that can be used for performance analysis of wireless communication networks, which is based on the Stochastic Network Calculus (SNC) theory, and can describe the impact of uncertainty and randomness of wireless fading channels on the performance of communication systems. In the network algorithm theory, the performance of communication system is usually measured by delay, packet loss rate and bit error rate. The effective capacity model adopts the methods and tools of SNC to model the uncertainty and randomness of the wireless channel as a stochastic process, and uses its properties to calculate the effective capacity of the channel, which is a measure of the maximum transmission rate that can be supported by the wireless channel under the guarantee of a certain BER and delay requirements.

In communication networks, traffic with random characteristics cannot be provided with deterministic QoS guarantees and needs to be analysed using statistical methods. The Large Deviation Principle (LDP) is a mathematical method for exponentially asymptotic estimation of the probability of rare events, and the effective bandwidth and effective capacity models derived on this basis are often used to analyse the performance of communication networks with random characteristics.

As shown in Fig. 22 is a model of a transmitter with an infinite length buffer queue in a wireless communication system, where the data source

The launch rate, i.e., the buffer queue arrival rate at the transmitter, is μ , the number of data bits in the buffer queue at moment t is $Q(t)$, and the instantaneous transmission rate of the wireless fading channel is $r(t)$. To simplify the analysis process, the following assumptions are made:

- (1) discretised model, the arrival rate and the number of bits transmitted by the channel in time slot n are $A[n]$ and $S[n]$, respectively;
- (2) The channel is set up as a packet fading channel model, i.e., the impact response characteristics of the channel remain constant over a packet time slot^[19], and the length of a data frame sent is equal to the length of a packet T_f ;
- (3) In time slot n , the arrival rate is $R[n] = \frac{A[n]}{T_f}$ and the service rate is $C[n] = \frac{S[n]}{T_f}$, and they are in no

independent and identically distributed (i.i.d.) in the same time slot.

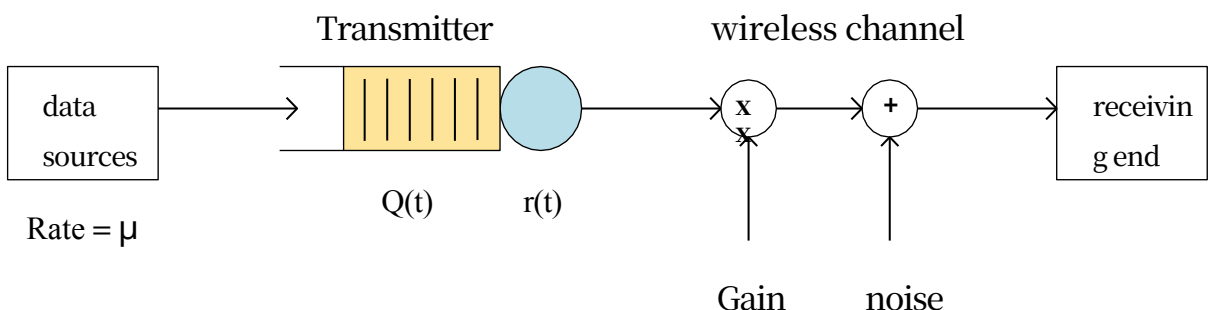


Figure 22 Launch-side buffer queue queuing model

In summary, the arrival bits $A[1], A[2], \dots$ are the values of the random variable A in different time slots, and the service bits $S[1], S[2], \dots$ are the values of the random variable S in different time slots. According to the effective capacity theory and using the Gartner-Ellis theory, the moments of arrival bits A and service bits S as random variables are defined as follows:

$$\Lambda_A(\theta) = \log \frac{\mathbb{E}[\exp(\theta A)]}{\mathbb{E}}$$

$$(-\theta) = \log(\mathbb{E}[\exp(-\theta S)]) \quad (3.10)$$

where the parameter θ is the delay exponent and $\mathbb{E}[\cdot]$ is the expectation operator. The effective bandwidth of the arriving traffic is defined as follows:

$$\alpha^{(b)}(\theta) = \frac{\Lambda_A(\theta)}{\tau_f \theta} \quad (3.12)$$

As a pairwise concept, the effective bandwidth of the service rate is defined as follows:

$$\alpha^{(c)}(\theta) = \frac{\Lambda_S(-\theta)}{\tau_f \theta} \quad (3.13)$$

Suppose that $\Lambda_A(\theta)$ and $\Lambda_S(-\theta)$ are finite-valued and derivable for all θ . If there exists a unique $\theta^* > 0$ Full

Adequ

ate:

$$\alpha^{(b)}(\theta^*) = \alpha^{(c)}(\theta^*) \quad (3.14)$$

failing

$$\lim_{x \rightarrow \infty} \frac{\log(\Pr(Q(\infty) > x))}{x} = -\theta^* \quad (3.15)$$

agree

ment

where $\Pr(\cdot)$ is the event probability and x is the boundary of the number of bits in the buffer queue. When the value of θ^* is large, it means that the probability of buffer non-empty fades very fast, and the QoS constraints are more stringent in this case. In wireless communication systems, the service data bits S can be determined by the capacity of the fading channel. In summary, the effective capacity model can be derived from Shannon's capacity, and the equilibrium problem between QoS and throughput needs to be considered in the process of system design to solve the QoS performance when the

The throughput maximisation problem.

An approximate formula for the buffer bit backlog can be obtained from equation (3.15):

$$\Pr(Q(\infty) > x) \approx e^{-\theta^* x} \quad (3.16)$$

For smaller values of x , there exists a more accurate

approximation of the equation^[11]:

(3.17)

$$\Pr(Q(\infty) > x) \approx \Pr(Q(t) > 0) e^{-\theta^* x}$$

where $\Pr(Q(t) > 0)$ is the buffer non-empty probability. Based on the assumptions it can be deduced that within the time slot n , sending a

Approximate formula for the delay

violation probability of a data frame: $) \approx \Pr(Q[n] > 0) e^{-\theta^* \mu D}$ (3.18)

$$\Pr(D[n] > D_{\max})$$

where D_{\max} is the specified maximum delay and the buffer non-empty

probability can be approximated as^[16] :

$$\Pr(Q[n] > 0) \approx \frac{\mathbb{E}[R[n]]}{\mathbb{E}[C[n]]} \quad (3.19)$$

In fact, the approximation obtained by the calculation of equation (3.18) is the upper bound of the buffer delay violation probability. Based on LDP, usually for very small probability events exceeding the delay threshold, the smaller the value of the delay violation probability, the more accurate the results obtained.

The expected value of the probability of delay violation is generally set in experiments to be taken below 10^{-3} ^[54]. In the experiments, the expected value of delay violation probability is generally set to be below 10^{-3} . In real wireless communication scenarios, the QoS performance of the system can be further improved by using measures such as error correction codes.

3.2.2 Effective capacity analysis of frequency selective channels

The premise assumption of the above effective capacity modelling formula is that the wireless channel is flat fading over the entire communication band, whereas with a large communication bandwidth, it is difficult to maintain a flat fading over the entire band, and it is necessary to analyse the frequency-selective channel and derive the corresponding formulae for the frequency-selective channel.

The conceptual pairing of a constant service rate transmit queue with the presence of N i.i.d. sources with the transmit queue of a constant arrival rate frequency selective channel with N i.i.d. sub-channels is performed^[55]. Let $Q^N(\infty)$ be the length of the queue that is in the smooth state when there are N smooth i.i.d. superimposed sources with a service rate of $N \times r$, where r is a fixed constant. Define $A^N(t)$

is the total amount of aggregated arrival traffic in the $[0, t)$ time period, assuming that the length of the buffer queue is infinite, when the total data source

As the number tends to infinity, define the logarithmic momenta function as follows:

$$A_t(u) = \lim_{N \rightarrow \infty} \frac{1}{Nt} \log \left(\mathbb{E} \left[\exp \left(u(A^N(t) \otimes Nrt) \right) \right] \right) \quad (3.20)$$

The above equation holds for all $u > 0, t > 0$. Based on the concept of effective bandwidth, by introducing the prefactor $\beta^{(s)(r)}$ 获得更

The exact approximate formula

for the probability of delay violation is as follows: $\Pr\{D^N(\infty) \geq D_{\max}\} \approx \beta^{(s)(r)} e^{-\eta^{(s)(r)} N \theta_B(N, r)}$ (3.21)

$$\Pr\{D^N(\infty) \geq D_{\max}\}$$

where $D^N(\infty)$ is the delay in the \max state and D is the set maximum delay threshold. The product $\beta^{(s)(r)e^{-\eta^{(s)(r)} N}}$ is the probability of the buffer being non-empty, $\theta_B(N, r) = \theta_B(N, r)Nr$ is a function of N and r , and $\theta_B(N, r)$ is the inverse function of the effective bandwidth. $\eta^{(s)(r)}$ 定义如下：

$$\eta^{(s)(r)} = \lim_{t \rightarrow \infty} \frac{1}{t} \log \left(\mathbb{E} \left[\exp \left(u(A^N(t) \otimes Nrt) \right) \right] \right) \quad (3.22)$$

Bringing

equation (3.20)

into the equation

yields

$$\eta^{(s)(r)} = \lim_{t \rightarrow \infty} \frac{1}{t} \log \left(\mathbb{E} \left[\exp \left(u(A^N(t) \otimes Nrt) \right) \right] \right) \quad (3.23)$$

$$(3.23) \quad \mathbb{E} \left[\exp(\theta_B) \right]$$

Based on the conceptual dyad, the effective capacity under the frequency selective channel model with N i.i.d. sub-channels can be derived.

The arrival traffic rate is set to a constant μ and is served by a frequency-selective channel with $1/N$ fragments, referred to later as the

$1/N$ channels. Introducing the prefactor $\beta^{(c)(\mu)}$, the delay violation probability is approximated as follows:

$$Pr \{ D(\infty) \geq D_{\max} \} \approx \beta^{(c)}(\mu)^{e^{-\eta^{(c)}(\mu) N e^{-\theta_v(\mu) D_{\max}}}} \quad (3.24)$$

where $D(\infty)$ is the delay in the smooth state, μ is the rate of arriving traffic, $\theta_N(\mu) = \mu N \alpha^{-1}(\mu)$, and $\alpha^{-1}(\cdot)$ is the inverse function of the effective capacity of the individual sub-channels. $\eta^{(c)(\mu)}$ is likewise obtained according to the pairwise relation:

$$\eta^{(c)}(\mu) = \frac{1}{N} \mathbb{E} \left[\exp \left(-\alpha^{-1}(\mu)(\mu - r(T)) \right) \right] \quad (3.25)$$

where $r_N(t)$ is the number of bits served by the $1/N$ channel in $[0, t)$ time and T_f is the length of the data frame. The approximate formula for the non-null probability can be obtained from Eq. (17) and Eq. (15) in literature [53]:

$$\gamma_N(\mu) \approx \beta^{(c)}(\mu)^{e^{-\eta^{(c)}(\mu)N}} = \gamma_1(\mu)e^{(I-N)\eta^{(c)}(\mu)} \quad (3.26)$$

where $\gamma_N(\mu)$ and $\gamma_1(\mu)$ denote the buffer non-empty probability for $1/N$ channel service and single sub-channel service, respectively, and the upper The computational procedure of the above equation is equivalent to the computation of the probability of delay violation at service time for all frequency selective channels containing N i.i.d. sub-channels. It is obtained from the concave function property of negative exponential function and Jensen's inequality:

$$\mathbb{E} \left[\exp \left(N \alpha^{-1} \left(\frac{T \otimes r(T)_f}{\mu} \right) \right) \right] \leq \exp \left(N \alpha^{-1}(\mu) \left(\mu T \otimes \mathbb{E} \left[\frac{r(T)}{\mu} \right] \right) \right) \quad (3.27)$$

The right-hand side can be used as an approximate upper bound for the expectation calculation. Substituting Eqs. (3.25), (3.26) & (3.27) into (3.24) yields the following formula for delay violation probability calculation:

$$\Pr_{\max} \left\{ D(\infty) \geq D \right\} \approx \left(\frac{\mu}{\mu T} \exp \left(N \alpha^{-1}(\mu) \otimes \mathbb{E}_f \left[\frac{r(T)}{\mu} \right] \right) \right)^{\frac{N \tau^2}{D}} \Pr_{\max} \left\{ N \alpha^{-1}(\mu) \right\} \quad (3.28)$$

3.2.3 Effective bandwidth analysis of arrival traffic with exponentially distributed data frame lengths

One of the assumptions of the above effective capacity model is that the arrival traffic maintains a constant rate, while in the actual communication network, the arrival traffic usually has certain random characteristics, in order to analyse the performance of the communication network more realistically, it is assumed that the number of data bits A arriving at the traffic within the time τ_f of transmitting a data frame obeys the parameter λ exponential distribution, and its probability density function is

The Probability Density Function (PDF) is the

number of

$$f_A(a) = \begin{cases} \frac{1}{\lambda} \exp(-\frac{1}{\lambda} a) & (a \geq 0), \\ 0 & (a < 0). \end{cases} \quad (3.29)$$

The average arrival rate $\mu = \lambda / T_f$. Calculated from the definition of effective capacity in 3.2.1, the effective bandwidth of the exponential arrival process

For:

$$\begin{aligned}
 a^{(b)}(\theta) &= \frac{\log E[\exp(\theta A)]}{T_f \theta} \\
 &= \frac{1}{T_f \theta} \log \int_0^\infty \exp(\theta a) f_A(a) da \\
 &= \frac{1}{T_f \theta} \log \frac{1}{1 - \lambda \theta}
 \end{aligned} \tag{3.30}$$

In order for the above formula to exist, the range of values of θ should be $(0, 1/\lambda)$, and from the derivation, it can be seen that the specificity of the exponential distribution reduces the computational complexity, and the use of the computation of the effective bandwidth instead of the complex integral operation of the effective capacity can further simplify the analysis process. Let the number of buffer bits in different time slots be a sampling of the random variable Q . From the literature [56], Chen

The statement can be obtained that the buffer non-empty probability can be approximated by the following equation:

$$\Pr(Q > 0) \approx 1 - \lambda\theta^* = 1 - \lambda_{Tf}\theta^*$$

And for the delay violation probability there is

$$\begin{aligned} \Pr\{D(\infty) \geq D_{\max}\} &\approx \Pr(Q > 0) \exp(-\theta^* \alpha^{(b)}(\theta^*) D_{\max}) \\ &= (1 - \lambda\theta^*)^{\frac{D_{\max}}{\eta} + 1} \end{aligned} \quad (3.32)$$

In summary, for the exponential arrival process as well as the buffer queue delay analysis in the case of wireless fading channel service, the parameter θ^* can be computed by Eq. (3.14) and then Eq. (3.32) can be used for the approximation of the delay violation probability.

3.3 Simulation analysis of transmitter-side buffer queue queuing

In the analysis of queuing delay of WAIC transmitter-side buffer, it is firstly necessary to fit the distribution of fading channel according to multipath channel simulation, derive the expression of effective capacity through the probability density formula of the distribution, and obtain the exponential fading factor θ , and further compute the probability of delay violation by solving the nonlinear equations of the effective bandwidth and effective capacity equation. By comparing the queuing simulation with the theoretical calculation, it is proved that the effective capacity model has certain usability.

3.3.1 Channel distribution fitting analysis

According to the ray tracing algorithm, the amplitude, phase, and delay information of each signal path in the multipath channel can be calculated, and the modelling of the time-invariant channel model can be carried out by assuming that there is no influence of the time factor in this communication model due to the small influence of the moving objects in the avionics equipment cabin. Setting the centre frequency of the transmitted signal as 4.3 GHz, the delay on the i th path as τ_i , and the

channel gain as a_i , the total channel complex gain is:

$$h(f) = \sum_i^{L_a} \exp(\otimes j2\pi f_{ti}) \quad (3.33)$$

Calculate the amplitude of the channel response, $h(f)$, by taking the data | obtained from 5000 simulations when the equipment racks are 75cm apart in 3.1.3.

Perform distribution fitting. Four distributional assumptions were set: the Rayleigh, Weber, Nakagami-m, and Rice distributions. The fit of these four distributions was evaluated by means of the K-S test with the following assumptions:

- (1) Null hypothesis (H_0) the data conforms to a set particular distribution;
- (2) Alternative hypothesis (H_1) the data do not conform to a set particular distribution.

Setting the significance level α to 1% and calculating the p-values for the four distribution settings, the results are shown in Table 7, which can be

It can be seen that only the Rice distribution passes the hypothesis test, and the channel fading distribution is best fitted to the Rice distribution. The Cumulative distribution function (CDF) of the four distributions is shown in Fig. 23, which shows that the Rice distribution is the closest to the channel data distribution.

Table 7 K-S test results for channel distribution with $\alpha = 1\%$.

Setting distribution	p-value
Rayleigh distribution (math.)	1.5602×10^{-32}
Weber distribution	1.5507×10^{-8}
Nakagami-m Distribution	0.0013
Rice distribution	0.0283

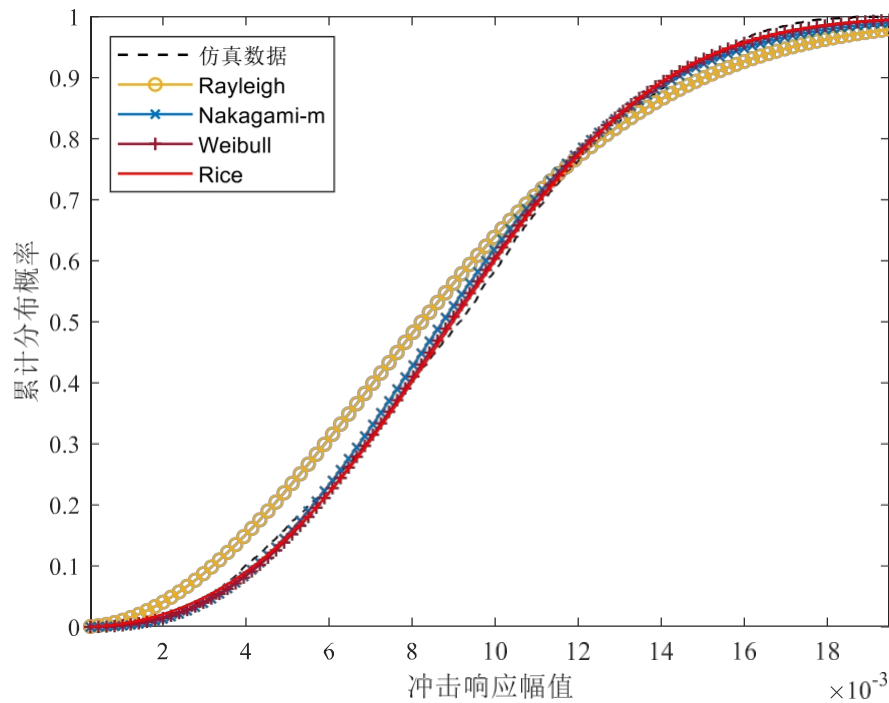


Fig. 23 Fitting results of channel distribution of avionics equipment bay

Based on the assumption that the avionics equipment bay channel obeys the Rice distribution, the derivation of an analytical expression for the effective capacity can be carried out. The PDF for the channel gain $x = h(f)^2$ obeying the Rice distribution is

$$p(x) = \frac{(1+K)e^{-K}}{\Phi} \exp\left(-\frac{(1+K)x}{\Omega}\right) I_0\left(\frac{2\sqrt{K(1+K)x}}{\Omega}\right) \quad (3.34)$$

where K is a shape parameter defined as the ratio of the power of the direct path to the remaining multipath, Ω is a scale parameter defined as the total power of all paths, and $I_0(\cdot)$ is the first type of zero-order corrected Bessel function, which can be computed as a channel parameter by using moment estimation or log-likelihood estimation methods^[57]. The channel parameters can be calculated using moment estimation or log-likelihood estimation. The channel data obtained from 5000 simulations using equipment racks separated by 75 cm are used to calculate the channel parameters by using the

Maximum likelihood 1.72 , $\Omega = 9.80 \times 10^{-5}$.

estimation^[58] to obtain the channel parameters, $K =$

Bringing the PDF of the Rice distribution into the effective capacity calculation formula, the following analytical expression for the normalised effective bandwidth can be derived:

$$\begin{aligned} a^{(c)}(\rho, \theta) &= \frac{\alpha_{AS}(-\theta)}{B} = \frac{1}{B} \log \left(\frac{1}{2} \Gamma \left[(1 + \rho x)^{-\beta} \right] \right) \\ &= \frac{K T_f B}{\beta \ln 2} + \left(\frac{\beta}{\Omega \rho} \right) \sum_{n=0}^{\infty} \frac{U \left(\beta ; \beta \otimes n ; \frac{1+K}{\Omega \rho} \right)}{\Gamma(n+1)} \end{aligned} \quad (3.35)$$

where $\rho = \frac{E_S}{N_0}$ is the ratio of the transmitted signal E_S to the noise N_0 at the receiver, and B is the transmitted signal bandwidth.

$\beta = 1/\theta_T B$ is the QoS factor. $\int_0^\infty t^{x-1} e^{-t} dt$ is the gamma function and $U(\cdot)$ is the Tricomi hypergeometric function^[59]. $U(\cdot)$ is the Tricomi hypergeometric function.

The complex transcendental function integrals included in the calculation can be replaced by a unified closed formula using Meijer's G-function for multiple fading channels^[60], and the derivation of the above effective capacity formula is shown in Appendix A.

$$U \left(\beta ; \beta \otimes n ; \frac{1+K}{\Omega \rho} \right) = \frac{1}{\Gamma(n+1)\Gamma(\beta)} {}_{G_{2,1}} \left(\frac{1+K}{\Omega \rho} \middle| \begin{matrix} 1 \otimes \beta \\ 0, n+1 \otimes \beta \end{matrix} \right) \quad (3.36)$$

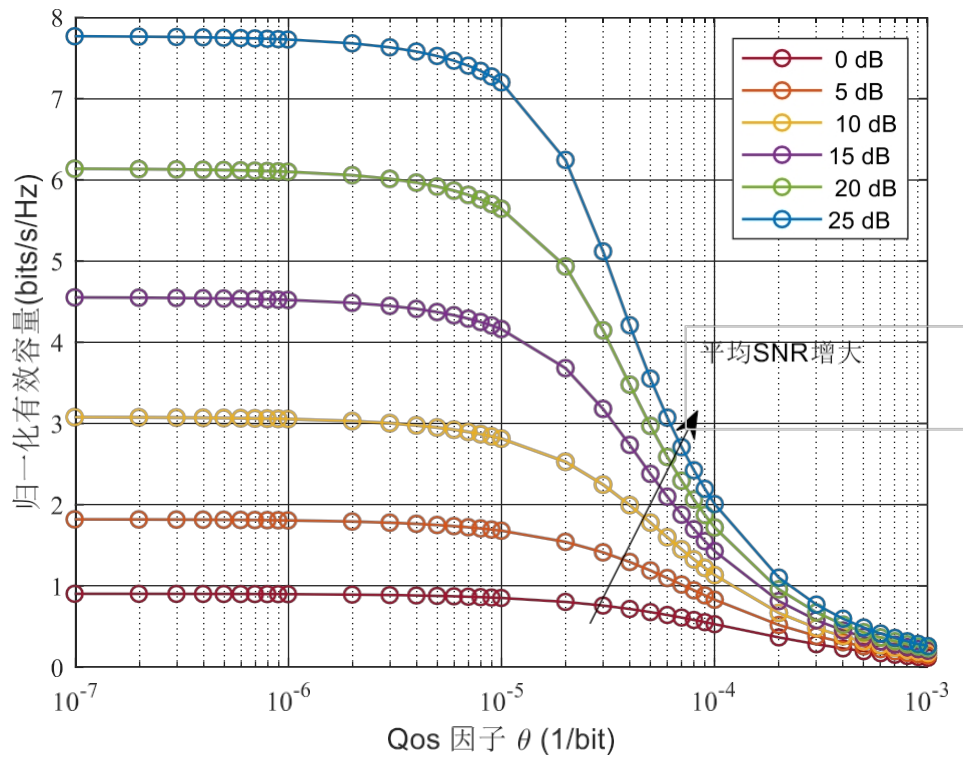


Fig. 24 Normalised effective capacity at different average SNRs

Set the data frame duration $\tau_f=2\text{ms}$ and the channel bandwidth to the base bandwidth of 802.11 protocol 20MHz based on the

For the above analysis, the channel is considered to be flat fading for a coherent bandwidth of $BC_{50} > 20$ MHz, and the normalised effective bandwidth is calculated for different values of θ . The results are shown in Fig. 24. As the average SNR, i.e., ρ , increases, the effective capacity also increases; as the QoS factor θ increases, the effective capacity decreases. As $\theta \rightarrow 0$, the QoS for the channel

The constraint becomes smaller, meaning that the transmitter can tolerate a delay of any size, at which point the value of the effective capacity tends to be Shannon

capacity; while when $\theta \rightarrow \infty$, the QoS requirement of the channel becomes higher, and the corresponding effective capacity value becomes smaller.

3.3.2 Queuing Simulation Parameter Settings

In the communication environment of avionics equipment cabin under 802.11ax communication protocol, the base bandwidth of the transmit signal is set to 20MHz, the transmit power is set to 15dBm, and the noise power at the receiving end is set to -65dBm. In the simulation, the parameters of the Rice distribution fitted in 3.3.1 are used to generate the random numbers obeying the Rice distribution as the channel gain coefficients.

Based on the correlation bandwidth analysed in 3.1.3, the signal is flat fading over the entire channel when using the BC_{50} definition, and when using the BC_{90} definition, for the convenience of the analysis, we take $BC_{50} = 2.5$ MHz, in which case the 20 MHz bandwidth can be regarded as a frequency-selective channel consisting of eight uncorrelated sub-channels, each of which is a frequency-selective channel.

all obey the Rice distribution. Consider a time-sensitive network that can be combined with wireless communication, where upper layer wired data frames are most

The maximum length is 1522 bytes, and the duration of the wireless data frame can be up to 1.2ms when the lowest modulation strategy is used. 802.11

protocol frame aggregation feature, i.e., aggregating 2-8 data frames to be sent at the same time, the simulation parameters are set as follows: transmit The packet length of the delivered data frame is $T_f=2\text{ms}$ and the simulation duration is 2000s. In the literature of effective capacity studies^[11], the usual The delay violation probability is set to 10^{-3} , considering the requirement of avionics communication for delay guarantee, the desired delay violation probability is set to a more stringent requirement of 10^{-4} in this experiment. In order to analyse the influence of arrival traffic distribution and service channel distribution on the queuing delay of the buffer queue at the transmitter side, the following four types of communication scenarios are designed:

- (1) The arrival traffic is constant rate μ and the service channel is a flat fading channel;
- (2) The arrival traffic data frame lengths obey an exponential distribution with parameter λ . The service channel is a flat fading channel;
- (3) The arrival traffic is constant rate μ and the service channel is a frequency selective fading channel;
- (4) The length of the arrival traffic data frame obeys an exponential distribution with parameter λ . The service channel is a frequency selective fading channel.

The simulation procedure calculates the number of remaining unserved bits in the buffer queue every 2ms, divides it by the expected value of Shannon's capacity as the delay within the current time slot, then counts the number of time slots exceeding the set threshold delay and divides it by the total number of simulation time slots to estimate the size of the delay violation probability, and compares it with that obtained by the theoretical formula.

3.3.3 Queuing Simulation and Theoretical Analysis

The following four scenarios of queuing simulation are performed by the above simulation scheme to compare with the theoretical calculations.

(1) Constant Rate Arrival Traffic with Flat Fading Service Channel

Setting the arrival traffic rate at the transmitter to 50, 55 and 60 Mbit/s for simulation, the results are shown in Fig. 25.

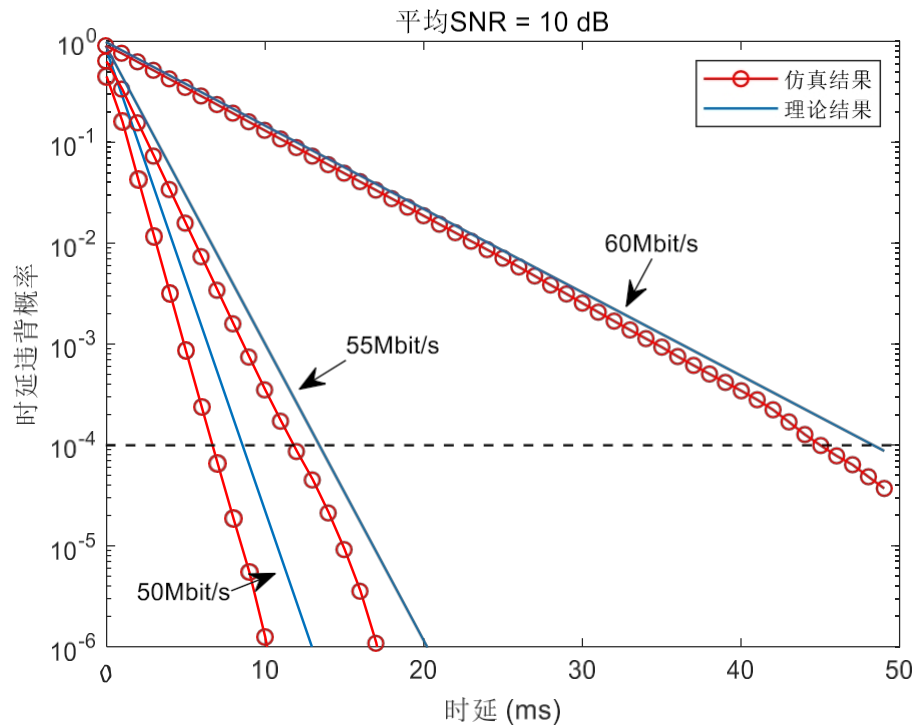


Fig. 25 Scene 1 Queuing Simulation and Theoretical Calculation Results

From the figure, it can be seen that as the rate of arrival traffic decreases, the delay of data arriving at the buffer queue also decreases. The theoretically calculated delay violation probability curve is the upper bound of the delay violation probability obtained from the actual simulation statistics, when the arrival traffic rate is closer to the theoretical Shannon limit, the more likely that the transmitted data will pile up in the buffer queue and a delay violation event will occur. If the arrival traffic rate of the control transmitter is below 55Mbit/s, the queuing delay of the buffer queue can be controlled below 20ms.

(2) Constant Rate Arrival Traffic and Frequency Selective Fading Service Channels

The number of uncorrelated sub-channels N of the frequency-selective

channel is set to 4 and 8 (corresponding to the channel state of the avionics equipment bay) and the arrival traffic constant rate is 60Mbit/s, and the results are shown in Fig. 26.

From the figure, it can be seen that as the number of subchannels of the frequency selective channel increases, the probability of a delay violation event for data in the buffer queue decreases for the same arrival rate at the transmitter. This suggests that frequency selective channels can introduce frequency diversity to the communication system, which in turn improves the delay performance of the wireless channel. When the coherent bandwidth of the channel is reduced, it means that the wireless channel contains more multipath channels with large differences in delay, and the receiver can obtain more copies of signals transmitted through different paths, which improves the system performance through the diversity gain. At this point, 60 Mbit/s reaches

The rate-induced delay can be controlled to less than 20ms.

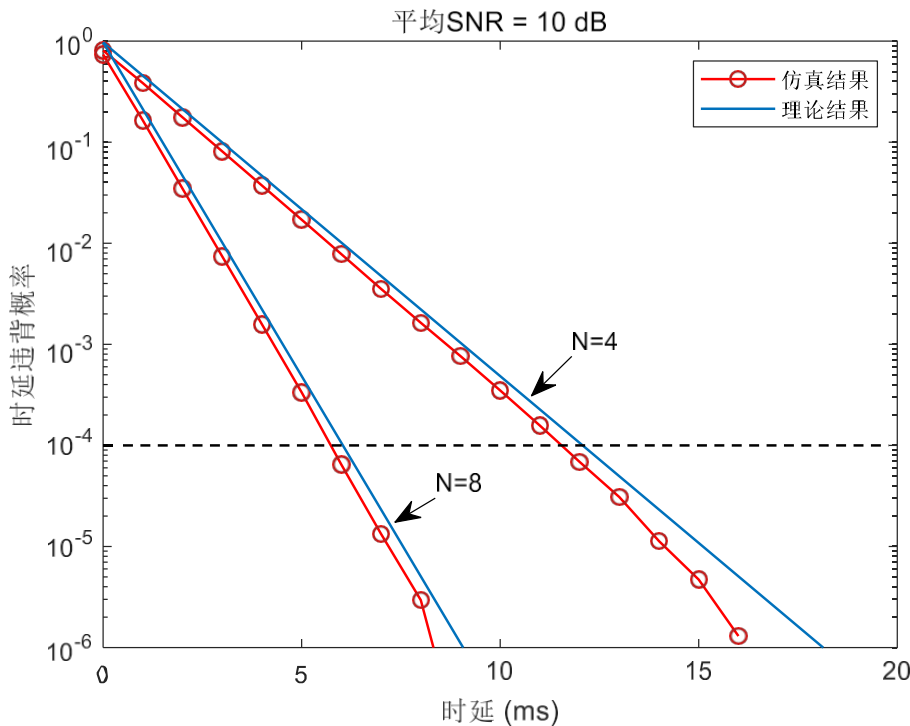


Fig. 26 Scene 2 queuing simulation and theoretical calculation results

(3) Exponential arrival traffic with flat fading service channel

Setting the length of the arrival traffic obeys the exponential distribution with parameters $\lambda = 90, 100$ and 110Kbit , the average arrival traffic rates are $45, 50$ and 55Mbit/s , respectively, and the queuing simulation results at this time are shown in Fig. 27.

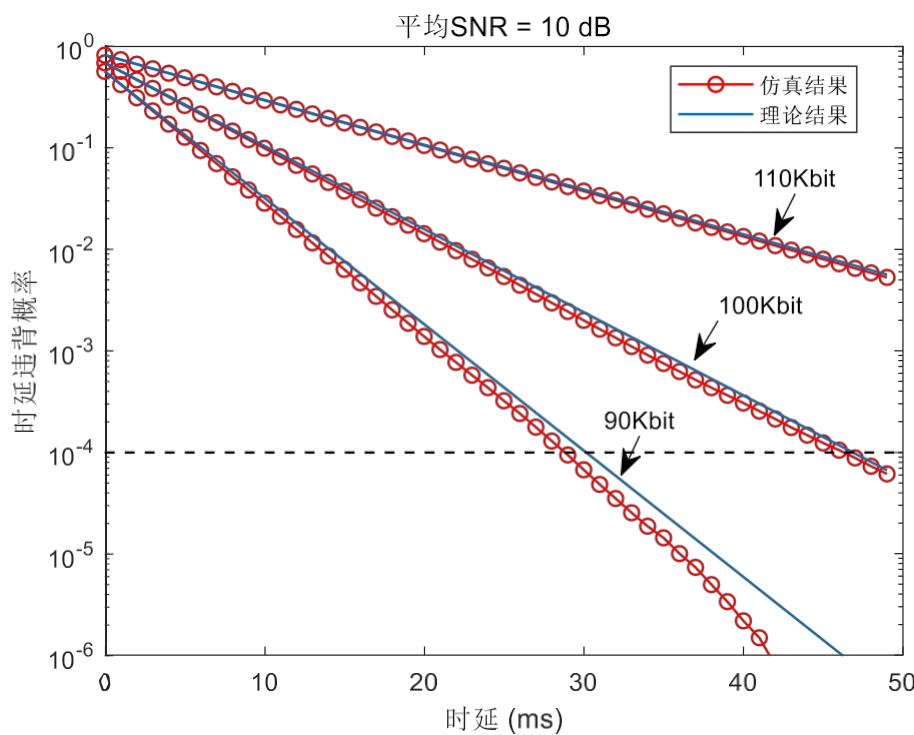


Fig. 27 Scene 3 queuing simulation and theoretical calculation results

From the figure, it can be seen that as the average data length of the exponential arrival traffic increases, the probability of the buffer queue experiencing a delay violation event also increases. Unlike the constant rate arrival traffic, the data length of the arrival traffic that obeys a certain random distribution introduces a certain degree of burstiness to the communication system, which may result in a situation where the instantaneous data flow is too large to be processed.

The simulation of Scenario 3 is closer to the real situation when the avionics system sends signals, and it can be seen from the figure that when the average data length of the arrival traffic is 90Kbit, the delay in the buffer queue can be controlled below 40ms.

Fig. 28 shows the images of effective capacity and effective bandwidth at different values of θ ($0 < \theta < 10^{-5}$), at this time $\lambda = 100\text{Kbit}$, it can be seen that as the value of θ grows, i.e., with the increase of QoS constraints, the value of effective capacity gradually decreases while the value of effective bandwidth continues to grow, and the two are intersected¹⁰at a point, when the state of buffer queue is kept stable.

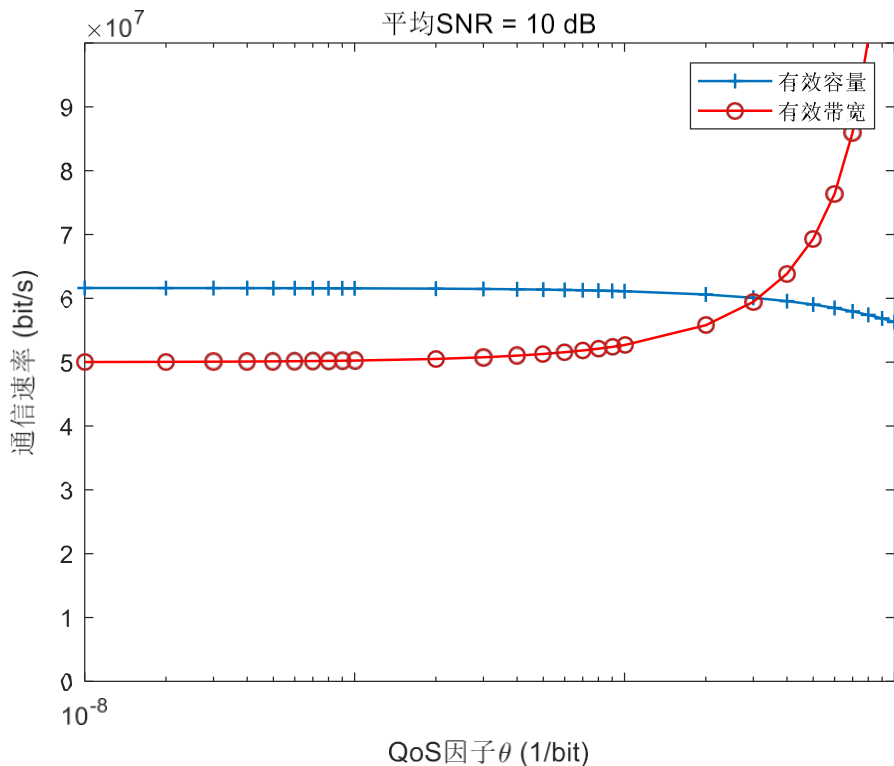


Figure 28 Effective Capacity vs. Effective Bandwidth Curve

(4) Exponential Arrival Traffic and Frequency Selective Fading Service Channels

The length of the arrival traffic is set to obey an exponential distribution with parameter $\lambda = 90\text{bit}$, and the number of uncorrelated subchannels N of the frequency-selective channel is set to be 4 and 8, respectively, and the results are shown in Fig. 29.

From the figure, it can be seen that when the length of arrival data obeys an exponential distribution, the buffer non-empty probability decreases, but the frequency-selective service channel does not play a certain role in improving the delay violation probability under the two sub-channel numbers is theoretically bounded to be the same, and there is no significant difference in the simulation results. The analysis concludes that for the large random variation characteristics to

arriving traffic and the frequency selectivity of the channel does not provide a good performance improvement, the rate of arriving traffic should be controlled in such scenarios so as to reduce the queuing delay of data sending.

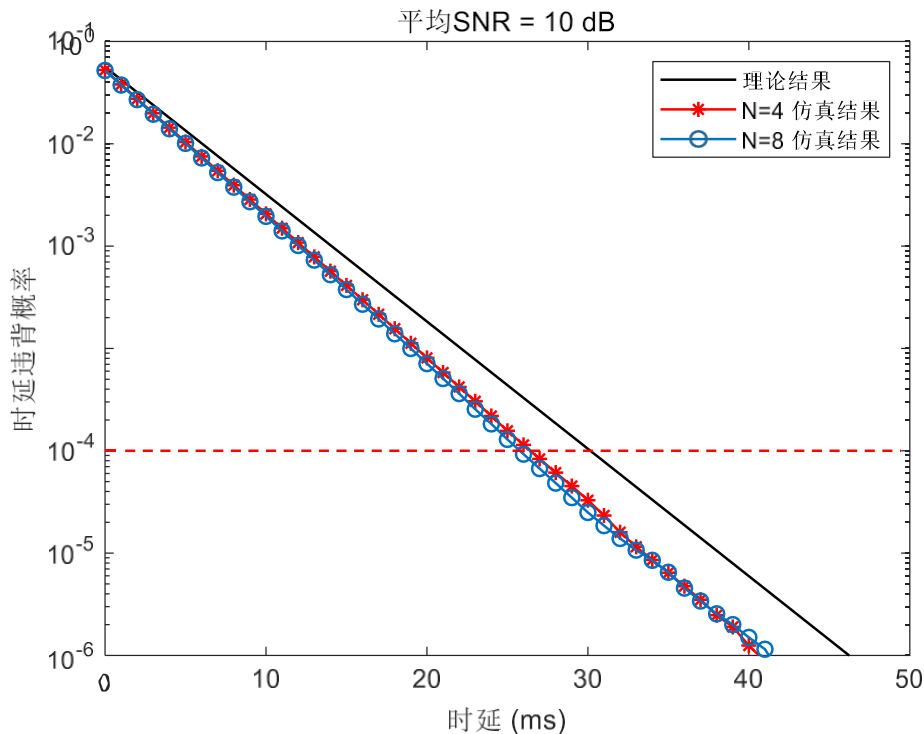


Fig. 29 Scene 4 Queuing Simulation and Theoretical Calculation Results

3.4 Summary of the chapter

This chapter investigates the channel modelling of avionics intra-flight communication scenarios based on ray tracing algorithms and the analysis of the queuing phenomenon of transmitter signals in buffer queues. The mathematical tools of effective capacity and effective bandwidth are used to derive a closed formula for the effective capacity of the buffer queue, which is solved as a nonlinear equation equal to the effective bandwidth. The delay violation probability of buffer queue data queuing is analysed for four types of scenarios with different stochastic characteristics of the arrival traffic and the service channel, which are compared with the simulation statistics. The simulation and analysis results show that the frequency selective channel has a certain improvement on the queuing delay of constant rate arrival traffic, while

the improvement on the exponential arrival process is not significant; therefore, in order to control the magnitude of the data sending delay in the buffer queue, it is more effective to use the method of controlling the rate of arrival traffic.

Chapter 4: Avionics Wireless LAN Code Forwarding Relay Technology Research

The complex avionics communication network has a wide variety of communication devices, which can use relay nodes for collaborative communication to improve the capacity of the multi-user system, and in the scenario of wireless LAN communication there can be many relay nodes for forwarding messages. Considering the requirements of avionics system for effectiveness and reliability, the use of relay nodes for encoding and forwarding of information, and the provision of a copy of the sent message at the destination node can effectively enhance the ability of the system to deal with signal transmission errors. At the same time, for the delay requirements in the information transmission process, QoS analysis is also required in the relay collaborative communication process. The main research content of this chapter is to study the equilibrium and optimisation of QoS and throughput of the relay cooperative communication system under the coded forwarding mechanism in the context of the effective capacity model, and to reasonably design the power allocation strategy of the transmitter and forwarder nodes.

4.1 Selection of transmission modes for relay collaborative communications

Wireless communication is difficult to achieve open system interconnection like wired communication due to its special air-port communication characteristics.

(The link layer control of relay communication is closely related to the channel state of the physical layer, which is independently optimised in different layers of the Open System Interconnect (OSI) model. Based on the rich multi-device communication environment in WAIC, we consider adopting relay cooperative communication, which introduces relay nodes, adopts appropriate signal forwarding strategy, sends signal copies to the receiver at

the appropriate time, and introduces diversity gain to enhance the stability of the system. Meanwhile, in order to evaluate the QoS performance of the communication system, the QoS analysis of the delay of the buffer queue at the transmitter end of the physical layer can be performed based on the effective capacity model that takes into account the QoS constraints. In a simple point-to-point communication scenario, the effective capacity model is affected by a variety of factors such as channel distribution, QoS factors, bandwidth, and data frame length. Under high QoS requirements, the capacity of the communication system may tend to zero, and outages may occur, affecting the effectiveness and reliability of the system.^[22] In this case, a relay node is introduced to carry out the message. The introduction of relay nodes for message forwarding can improve the degradation of channel throughput and reduce the probability of interruptions due to high QoS requirements.

Traditional collaborative communication consists of two basic types of relay node operations: amplify and forward (AF) and code and forward (DF).^[61] Traditional collaborative communication consists of two basic types of relay node operation: amplify-and-forward (AF) and code-and-forward (DF) AF is simple and computationally small, only need to multiply the received signal by the corresponding transmit power, the disadvantage is that the amplification of the original signal also amplifies the noise; while the DF mode decodes and checks the signal at the relay node, so that the wrong transmission of the signal can be detected in time to make the appropriate decisions, but there are problems such as computational complexity. However, there are problems such as large amount of computation and complicated operation. Considering the communication scenario with direct path, in order to simplify the analysis process, the source node (Source, S) is assumed,

The relay node (Relay, R) and the destination node (Destination, D) are on the same straight line, normalise the distance i.e. set the distance between S and R to d, and the distance between R and D to 1-d, as shown in Fig. 30. γ_1 , γ_2 and γ_3 are respectively

The channel gains on the S-D, S-R and R-D paths, the transmit power of transmitter S and relay node R are p_s and

P_r

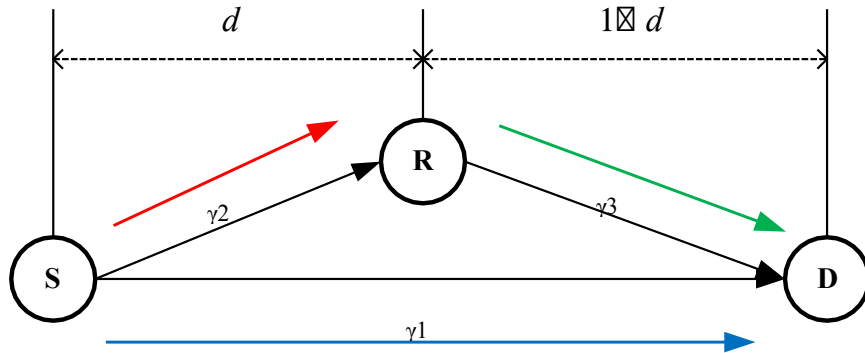


Figure 30 Schematic diagram of the trunking collaborative communications system

For further simplified analysis, the following explanation is given for the above communication system:

- (1) It is assumed that the channel is flat fading on all three paths of the signal transmission and the channel gain remains constant during the signal transmission, i.e., the channel is a packet fading channel with channel bandwidth B and packet duration T_f ;
- (2) The three channels are independent of each other and the channel amplitudes $h_{i,j}, i \in \{s,r\}, j \in \{r,d\}$ and $i \neq j$ obey a Rayleigh distribution.

Then the channel gain $\gamma_{s,d} = h_{s,d}^2$, $\gamma_{s,r} = h_{s,r}^2$ and $\gamma_{r,d} = h_{r,d}^2$ obey the exponential distribution with parameters $\lambda_1 = 1$, $\lambda_2 = d^\alpha$ and $\lambda_3 = (1 \otimes d)^\alpha$.

Let the random variable Γ obey an exponential distribution with parameter λ . The PDF is:

$$\pi_\Gamma(x) = \lambda \exp(-\lambda x) \quad (4.1)$$

- (3) The noise at the receiver side is zero-mean additive Gaussian white noise with unit variance, i.e., $\sigma_i^2 = 1, i \in \{r,d\}$;
- (4) Assuming that the CSI can be estimated at the receiver side and fed back to the transmitter side, the delay caused by the transmitter feedback

information is negligible, and the transmitter side adjusts the transmit rate based on the CSI obtained from the feedback by using an adaptive rate control algorithm.

Consider the implementation of half-duplex relay forwarding protocol with less complexity, unlike full-duplex, at this time the coded forwarding node R and the source node S can not send messages simultaneously in the same frequency band and the communication efficiency of the system is reduced, but the orthogonal sending protocol eliminates the problem of signal interference that exists between S and R. In the above relay collaborative communication system, the signal

The sending process is divided into two phases, both with a duration of $T_f/2$: In the first stage, the source node S sends a message to the relay node R with

The destination node D sends the signal; in the second stage, the relay node processes the received signal accordingly and then forwards it to the destination node D. Finally, multiple copies of the signal are merged at the destination node D to obtain the final signal. In the second stage, the relay node processes the received signals in the appropriate way and then forwards them to the destination node D. Finally, multiple copies of signals are merged at the destination node D to obtain the final signal.

4.1.1 Amplify-and-forward relay communication protocol

In the AF transmission mode, the first stage of the system sending signal, the relay node R receives the data from the source node S without any demodulation or decoding operation, but only performs a simple amplification and forwarding operation, which is known as the non-regenerative relay or analogue relay scheme. Suppose the source node sends a signal as $x_s = [x_s[0], \dots, x_s[M-1]]$, the first stage R and D of the

The received

signal is given by

$$y_r[m] = h_{s,r} \sqrt{P_s} x_s[m] + n_r[m] \quad (4.2)$$

$$y_d^{(1)}[m] = h_{s,d} \sqrt{P_s} x_s[m] + n_d^{(1)}[m] \quad (4.3)$$

where $m = 0, \dots, M-1$, $n_r[m]$ and $n_d[m]$ are Gaussian white noise at the receiver.

In the second stage, the relay node R first scales the signals received by

(4.2), and for all m, there are

$\mathbb{E} \left[\frac{x_r[m]^2}{r} \right] = 1$. If the instantaneous gain at the relay node $h_{s,r}$

$$G_r = \frac{1}{\sqrt{P_s |h_{s,r}|^2 + \sigma_r^2}} \quad (4.4)$$

Multiplying the received signal

gives the transmitted signal $y_d^{(1)}[m] = \frac{P_s}{\sqrt{P_s |h_{s,r}|^2 + \sigma_r^2}} + n_d^{(1)}[m]$ as

$$x_r[m] = G_r y_d^{(1)}[m] = \frac{P_s}{\sqrt{P_s |h_{s,r}|^2 + \sigma_r^2}} + \frac{n_d^{(1)}[m]}{\sqrt{P_s |h_{s,r}|^2 + \sigma_r^2}} \quad (4.5)$$

where the channel gain is constantly changing during transmission and hence is also known as variable gain AF. After that, R multiplies the signal by the power P_r and forwards it to the destination node D. The received signal can be expressed as

$$\begin{aligned} y_d^{(2)}[m] &= h_{r,d} \sqrt{P_r} x_r[m] + n_d^{(2)}[m] \\ &= \sqrt{\frac{P_s P_r}{P_s |h_{s,r}|^2 + \sigma_r^2} + \sigma_r^2} h_{s,r} x_s[m] + \sqrt{\frac{P_r}{P_s |h_{s,r}|^2 + \sigma_r^2} + \sigma_r^2} h_{s,r} n_d^{(1)}[m] + n_d^{(2)}[m] \end{aligned} \quad (4.6)$$

Considering the communication scenario with the presence of a direct path, the reception scheme with divided set merging at the destination node D is used with a Maximal Ratio Combining (MRC) receiver, and the signal processing at the receiving end is as follows:

$$\tilde{y}_d = \frac{\sqrt{P_s h_{s,r}^*} y_d^{(1)}}{\sigma_d^2} + \frac{\sqrt{\frac{P_s P_r}{P_r} \left| h_{s,r}^* \right|^2 + \sigma_r^2}}{\frac{\left| h_{r,d} \right|^2}{\left| h_{s,r}^* \right|^2 + \sigma_r^2} + \sigma_d^2} y_d^{(2)} \quad (4.7)$$

At this point the equivalent signal-to-noise ratio at the receiving end is

$$\begin{aligned}
 \gamma_{AF} &= \frac{\frac{P_s |h_{s,d}|^2}{\sigma_r^2}}{\frac{P_s |h_{s,r}|^2}{\sigma_r^2} + \frac{P_r |h_{r,d}|^2}{\sigma_d^2}} \\
 &= \gamma_1 P + \frac{\gamma_2 P \gamma_3 P_r}{1 + \gamma_2 P_s + \gamma_3 P_r}
 \end{aligned} \tag{4.8}$$

Consider the nodes S and R only at T_f . The signal is sent during the time period of $T_f/2$, in order to ensure that the total number of signals sent during the entire data sending time

Power limitation, the transmission power is replaced by two times the original power, which defines the rate R_{AF} that the system can support at this time as

$$\begin{aligned}
 R_{AF} &= \left(\frac{T_f B}{2} \right) \log_2 \left(1 + \gamma_{AF} \right) \\
 &= \left(\frac{T_f B}{2 + \log_2} \right) \left| 1 + \frac{4 \gamma_2 P \gamma_3 P_r}{1 + 2 \gamma_1 P_s + \frac{P + 2 \gamma_3 P_r}{2 \gamma_2 P_s}} \right|
 \end{aligned} \tag{4.9}$$

The total power constraints of the communication system are

where P is the average transmit power of the system.

4.1.2 Coded Forwarding Relay Communications Protocol

In DF transmission mode, in the first phase of the system sending signals, the relay node R receives the data from the source node S, displays and decodes the message, and then forwards a newly generated signal to the destination node, which is known as the regenerative relay scheme. The signalling process in the first phase is the same as AF. In the second phase, it is assumed that the relay node R can correctly decode the received message, and then re-encode the signal into a new codeword x_r by the same codebook, when the

$x_r = x_s$, the destination node D receives the signal as

$$y_d^{(2)} = h_{r,d} \sqrt{P_{rxs}} [m] + n_d^{(2)} [m] \quad (4.11)$$

Continue to combine the received signals (4.3) and (4.11) using the MRC receiver as follows:

$$\tilde{y}_d[m] = \left(P \left| h_{s,d} \right|^2 + P \left| h_{r,d} \right|^2 \right) x_s[m] + \sqrt{P_s} h_{s,d}^* n^{(1)}[m] + \sqrt{P_r} h_{r,d}^* n^{(2)}[m] \quad (4.12)$$

At this point the equivalent signal-to-noise ratio at the receiving end is

$$\frac{\left| h_{s,d} \right|^2}{\sigma_d^2} + \frac{\left| h_{r,d} \right|^2}{\sigma_d^2} = P \gamma + \sigma_d^2 \quad (4.13)$$

Same as the AF mode, the transmit power is replaced by 2 times. Considering that the relay node R can successfully send the information in the second stage on the premise that R successfully decodes the signal in the first stage, and the transmission rate of the source node S must not exceed the capacity of the S-R link, in summary, we can get that the system can support the rate of R_{DF} as follows

$$\frac{R}{\log_{DF}} = \left(\frac{T_f B}{2} \right) \min \left(\log_2 \left(1 + 2\gamma P \right), \left(\log_2 \left(1 + 2\gamma P + 2\gamma P \right) \right) \right) \quad (4.14)$$

4.2 Study of node power allocation problem based on effective capacity model

From the above analysis, the relay cooperative communication system with direct path can obtain multiple copies of signals at the receiving end, and adopt suitable merging method to obtain diversity gain to improve the communication performance of the system. For the QoS communication performance guarantee, which is a concern in WAIC, relay cooperative communication technology can be adopted to analyse the node power allocation problem based on the effective capacity model, and optimise the performance of the communication system under the conditions of total power limitation and QoS factor constraints. Considering the effective capacity model as the upper bound of the maximum communication rate that can be achieved by the communication system under the specified QoS factor θ constraints, the node power allocation problem under the two forwarding modes of AF and DF is modelled with this capacity maximization as the optimization objective, and the optimal power allocation strategy is solved.

4.2.1 AF node power allocation method study

Consider the three-node relay collaborative communication system in Fig. 30 in the presence of a direct path, where the node power allocation strategy is a function of the instantaneous transmission SNR vectors $\gamma = (\gamma_1, \gamma_2, \gamma_3)$ of the three signal transmission paths S-D, S-R, and R-D, and the

introduction of an effective

After the capacity model, the node power allocation is also related to the QoS factor, defining the network state information vector \mathbf{v}

SNR and QoS factors, when the corresponding node power allocation policy is $\mathbf{P}(\mathbf{v})$

Using the AF strategy, the instantaneous communication rate of the system is similarly modelled as a function of \mathbf{v} :

$$R_{AF}(\mathbf{v}) = \frac{T_B}{2} \log \left(1 + \frac{4\gamma P_{2s}(\mathbf{v}) \gamma P_{3r}(\mathbf{v})}{1 + 2\gamma P_{2s}(\mathbf{v}) + 2\gamma P_{3r}(\mathbf{v})} \right) \quad (4.15)$$

Given the QoS factor θ , the effective capacity maximisation problem under the total power constraint is formulated according to the definition of effective capacity under flat fading channels and modelled as follows:

$$(P1) \quad \arg \max_{\mathbf{P}(\mathbf{v})} \left[\log \left(\frac{1}{\theta} \sum_{s=1}^S \exp(-\theta R_{AF}(\mathbf{v})) \right) \right] \quad (4.16)$$

The restrictions are as follows:

$$\begin{aligned} & \left\lfloor \frac{\gamma P_s(v) + P_r(v)}{\gamma P_s(v) + P_r(v)} \right\rfloor^{\beta} \\ & \quad \left\{ \begin{array}{l} P_s(v) \geq 0 \text{ and } P_r(v) \\ \geq 0 \end{array} \right. \end{aligned} \quad (4.17)$$

Due to the monotonically increasing property of the logarithmic function $\log(\cdot)$, the above optimisation problem can be equivalently transformed, while observing that $R_{AF}(v)$, as a function of the power allocation policy $P(v)$, is not a convex function. In order to construct a convex function to further solve the optimisation problem, the following approximation is made under high SNR conditions:

$$1 + 2\gamma P_{2s}(v) + 2\gamma P_{3r}(v) \approx 2\gamma P_{2s}(v) + 2\gamma P_{3r}(v) \quad (4.18)$$

$$\begin{aligned} R_{AF}(v) &= \log_{\theta T_f B} \left(\frac{1 + 2\gamma P(v)}{P_{2s}(v) + P_{3r}(v)} \right) \\ &= \log_{\theta T_f B} \left(\frac{1 + 2\gamma P(v)}{P_{2s}(v) + P_{3r}(v)} \right) \quad (4.19) \end{aligned}$$

The substitution yields $R_{AF}(v)$ as an upper bound for $R_{AF}(v)$ under high SNR conditions in the power allocation strategy $P(v)$ open

which are strictly convex functions in the linear space, the solution process is simple. At low to medium SNR, the above approximation is still accurate enough to be used for approximating^[22].

The problem P1 is then equivalently transformed into the minimisation problem P1'.

$$(P1') \quad \arg \min_{P(v)} \left\{ \left(\frac{2\gamma P(v) \gamma P(v)^{-\frac{\beta}{2}}}{\gamma P_{2s}(v) + \gamma P_{3r}(v)} \right)^2 \right\} \quad (4.20)$$

where $\beta = \theta T_f B / \ln(2)$, is the normalised QoS factor.

In order to solve the above optimisation

problem, the Lagrange function is created as follows: $\mathbb{E}_\gamma \left[\left(\frac{1 + 2\gamma P(v)}{\gamma P_{2s}(v) + \gamma P_{3r}(v)} \right)^2 + \lambda \mathbb{E}_\gamma [P_{2s}(v) + P_{3r}(v)] \right]^{1/\beta}$ (4.21)

$$\mathcal{L}(P(v), \lambda) =$$

The above equation omits the condition $P_i(\mathbf{v}) \geq 0, i \in \{s, \square\}$. Since the constraints of the optimisation problem P1' are inequalities according to

The Karush-Kuhn-Tucker (KKT) condition for solving the minimum value has

$$\frac{\partial \mathcal{L}(\mathbf{P}(\mathbf{v}), \lambda)}{\partial p_i(\mathbf{v})} = 0, i \in \{s, \square\} \quad (4.22)$$

The system

of equations

is calculated

$$\begin{aligned} & \left\| \gamma + \frac{\gamma^2 \gamma_{3r}^2(\mathbf{v})}{\|\gamma P_{2s}(\mathbf{v}) + \gamma P_{3r}(\mathbf{v})\|_2^2} \right\|_1 = \gamma_0 \\ & \left\| \frac{\gamma^2 \gamma_{23s}^2(\mathbf{v})}{\|\gamma P_{2s}(\mathbf{v}) + \gamma P_{3r}(\mathbf{v})\|_2^2} \right\|_1 = \gamma_0 \end{aligned} \quad (4.23)$$

Where $\gamma_0 = \lambda / \beta$ is the SNR threshold calculated from the average power constraints, which can be obtained by solving the power constraints in equation (4.17). Solving the above system of equations yields the following node power allocation strategy:

$$\begin{cases} P_s(v) = uP_r(v) \\ P_r(v) = \frac{1}{\left(\frac{\gamma_0}{\gamma_1 + c} \right)^{\frac{2}{\beta+2}}} \\ \gamma_0 = \frac{\gamma_3(\gamma_1 + c)}{(2c\gamma(\gamma + c)^2)^{\frac{3}{\beta+2}}} \end{cases} \quad (4.24)$$

When $P_s(v) > 0$ and $P_r(v) > 0$, the parameters in Eq. are calculated as follows:

$$\begin{cases} u = \frac{\gamma_3(\gamma_1 + c)}{(\gamma_3 - \gamma_1)\gamma_2^2} \\ v = \frac{2c\gamma(\gamma + c)^2}{(\gamma_3 - \gamma_1)\gamma_2(\gamma_3 + c)} \end{cases} \quad (4.25)$$

where $\sqrt{\gamma_1\gamma_3 + 2\gamma_3\gamma_2}$.

$$c = \gamma_1\gamma_2$$

Note that Eq. (4.25) is a feasible solution when $u > 0, P_r(v) > 0$. When the above condition is not satisfied, i.e., $\gamma_1 > \gamma_3$, the AF protocol degenerates to direct link communication, where only the direct signal is transmitted and no integration of the signals is performed at the receiving end. Bringing $P_r(v) = 0$ into problem P1', the degraded optimisation problem P1'' is obtained as follows:

$$(P1'') \quad \arg \min_{\substack{\gamma \\ \mathbb{E}_{P(v)}}} \left\| \left(1 + 2\gamma P_s(v) \right)^{\frac{-\beta}{2}} \right\|_F^2 \quad (4.26)$$

The

restriction

$$s \text{ are } \mathbb{E}_{\gamma} \left\| P_s(v) \right\|_F^2 \leq P \quad (4.27)$$

Similarly construct the Lagrange

$$\begin{aligned} & \text{function as follows: } \mathbb{E}_{\gamma} \left[\left(1 + 2\gamma P_s(v) \right)^{\frac{-\beta}{2}} \right] + \bar{\lambda} \mathbb{E}_{\gamma} \left\| P_s(v) \right\|_F^2 \\ & \quad = \infty \end{aligned}$$

$$2\gamma P(v)^{\otimes_2}$$

$$(4.28) \quad \frac{d}{d\gamma}(\gamma) + \lambda \left(\int_0^{\infty} 2P_s(v) f_{\Gamma}(\gamma) d\gamma - 1 \right)$$

Solving the partial differential equation yields the following node power allocation strategy:

$$(4.29) \quad \begin{cases} P_s(v) = \frac{1}{2} \left[\frac{1}{1 + 2\gamma} \right]^{1/2} \\ P_r(v) = 0 \end{cases}$$

where $[x]^+ = \max \{x, 0\}$. Notice that for consistency in the derivation of the formulae, the work in the constraints part of Eq. (4.28)

The rate constraint is set to 1, which should be multiplied by the factor P again in the actual simulation. The above formula degenerates to the power allocation strategy of the water injection method for direct link transmission as $\theta \rightarrow 0$. The impact of the QoS constraint on the power allocation strategy and the universality of the analysis based on the effective capacity model can be seen.

In summary, under the QoS and total power constraints, the AF node power allocation method is as follows:

- (1) When $\gamma_1 \geq \gamma_3$, regardless of the QoS constraint factor θ , the direct transmission link channel state is better than the relay channel state at this time, and the signalling strategy is degraded to the direct link transmission, and the node power allocation is performed through equation (4.29);
- (2) When $\gamma_1 < \gamma_3$, the optimal power allocation policy between the source and relay nodes is equation (4.24).

4.2.2 Research on DF node power allocation method

In the same way as the AF node power allocation methodology study above, the following modelling of the optimisation problem in DF mode is carried out. The instantaneous communication rate of the system is a function of \mathbf{v} :

$$R_{DF}(\mathbf{v}) = \left(\frac{\gamma_1}{2} + \frac{P(\mathbf{v})}{2} \right) \min \left(\frac{\gamma_1 + P(\mathbf{v})}{2}, \frac{\gamma_1 + 2\gamma P(\mathbf{v}) + P(\mathbf{v})}{2} \right) \quad (4.30)$$

The maximisation problem of the effective capacity model in the DF mode is modelled as:

$$(P2) \quad \arg \max_{\mathbf{P}(\mathbf{v})} \left\{ \frac{1}{\theta} \log \mathbb{E}_{\gamma} \left[\exp \left(-\theta R_{DF}(\mathbf{v}) \right) \right] \right\} \quad (4.31)$$

The restrictions are the same as in equation (4.17). The monotonicity properties

$$\mathbb{E}_{\gamma} \left[\left. \mathbb{E}_{\gamma} \left[\mathcal{F}_1(\mathbf{v}), \mathcal{F}_2(\mathbf{v}) \right] \right| \mathbf{v} \right]$$

of the logarithmic function and the negative exponential function are converted equivalently for problem P2:

$$(P2') \quad \arg \min_{\mathbf{P}(\mathbf{v})} \left\{ \begin{array}{l} \mathcal{R}(\mathbf{v}) = (1 + 2\gamma P_{2s}(\mathbf{v}))^{\frac{\beta}{2}} \\ \mathcal{F}_1(\mathbf{v}) = (1 + 2\gamma_{1s} P_1(\mathbf{v}) + 2\gamma_{3r} P_3(\mathbf{v}))^{\frac{\beta}{2}} \end{array} \right. \quad (4.32)$$

among
others

$$\begin{cases} \mathcal{R}(\mathbf{v}) = (1 + 2\gamma P_{2s}(\mathbf{v}))^{\frac{\beta}{2}} \\ \mathcal{F}_2(\mathbf{v}) = (1 + 2\gamma_{1s} P_1(\mathbf{v}) + 2\gamma_{3r} P_3(\mathbf{v}))^{\frac{\beta}{2}} \end{cases} \quad (4.33)$$

It can be seen that the optimisation problem P2' is a strictly convex function for which there exists a unique solution. The following discussion of the above optimisation problem considers two different types of scenarios under different conditions:

- (1) $\gamma_1 > \gamma_2$: for $P_r(\mathbf{v}) > 0$, there is $\gamma_1 > \gamma_2$ holds, and the above when optimisation problem

Degraded to $\mathbb{E}_{\gamma} [\mathcal{R}(\mathbf{v})] \}$
problem P2": $\arg \min_{\mathbf{P}(\mathbf{v})} \left\{ \begin{array}{l} \mathbb{E}_{\gamma} [\mathcal{R}(\mathbf{v})] \\ \mathcal{F}_1(\mathbf{v}) \end{array} \right. \quad (4.34)$

(P2")

At this point, in order to save the transmit power of the system, the transmit power of the relay node should be $P_r(v) = 0$. The constraints of P2 "

Also $\mathbb{E}_{\gamma} / \mathbb{P}_s(v) \leq P$, at which point the optimisation problem is equivalent to a direct transmission from source node S to relay node R

d to

Link problem. Same as the solution process in AF, the node power allocation strategy in this case is as follows:

$$\begin{cases} \mathbb{P}(v) = \frac{1}{2} \left[\left(\frac{\gamma_1^2 + 2\gamma_2}{2} \right)^{-1} \right] & \gamma_2 \leq \gamma_1 \\ \mathbb{P}_r(v) = 0 & \text{otherwise} \end{cases} \quad (4.35)$$

(2) $\gamma_1 \leq \gamma_2$: In order to solve the optimisation problem

P2', solve the following equation relation: $\mathcal{F}_1(v) = \mathcal{F}_2(v)$

(4.36)

The relationship

between the node $P_r(v) = \tilde{u}P_s(v)$

powers is obtained as

where $u = (\gamma_2 - \gamma_1) / \gamma_3$. At this point the optimisation problem degenerates into problem P2 " with the constraints defined by equation (4.37) with total power

$\mathbb{E}_{\gamma} / \mathbb{P}_s(v) \leq P$ consists of. Construct the Lagrange function as limit follows:

$$\begin{aligned} \mathcal{L}_3(P_s(v), \lambda) &= \mathbb{E}_{\gamma} [\mathcal{F}(v)] + \lambda \mathbb{E}_{\gamma} / \mathbb{P}_s(v) + P_r(v) \\ &= \mathbb{E}_{\gamma} \left[\left(1 + 2\gamma_2 P_s(v) \right)^{-1} \right] + \mathbb{E}_{\gamma} \left[(1 + \tilde{u}) P_s(v) \right] \end{aligned} \quad (4.38)$$

From the KKT condition, solve strategy is derived as follows:

the partial differential equation:

$$\underline{\frac{\partial \mathcal{L}}{\partial v}}$$

The node power allocation

$$\partial P_S(\mathbf{v})$$

$$_3(P_s(\mathbf{v}), \lambda) = 0$$

$$P_s(\mathbf{v}) = \frac{1}{\Gamma((1+u)\gamma_0)^{\frac{2}{\beta+2}} \gamma_2^{\beta+2}} \quad (4.39)$$

$$P_r(\mathbf{v}) = \tilde{u} P_s(\mathbf{v})$$

In summary, under the QoS and total power constraints, the DF node power allocation method \mathcal{S}_1 is as follows:

- (1) When $\gamma_1 > \gamma_2$, the node power allocation is performed by Eq. (4.35), at this time, the relay node does not transmit signals, and the transmit power of the source node is determined by the SNR of the S-R link γ_2 ;

(2) When $\gamma_1 \leq \gamma_2$, the node power allocation is performed by Eq. (4.39), and the power of the source node and the relay node are linearly related.

Notice that as $\theta \rightarrow 0$, the effective capacity obtained using the above power allocation strategy is given by the following equation:

$$C_1 = \left(\frac{T_f B}{\log_2 \left(1 + \frac{P_s}{2\gamma_1} \right)} \right) \max_{\gamma} \min_{P} \left\{ \frac{\log_2 \left(1 + \frac{P_s}{2\gamma_1} \right)}{\gamma_1}, \frac{\log_2 \left(1 + 2\gamma_1 P + \frac{P_r}{2\gamma_1} \right)}{\gamma_1} \right\} \quad (4.40)$$

And the traversal capacity (the capacity of each state) of the actual DF communication system is formulated as follows^[62] ::

$$C_2 = \left(\frac{T_f B}{\log_2 \left(1 + 2\gamma_1 P_{1s} \right)} \right) \max_{\gamma} \min_{P} \left\{ \log_2 \left(1 + 2\gamma_1 P_{2s} \right), \log_2 \left(1 + 2\gamma_1 P_{3r} \right) \right\} \quad (4.41)$$

By the nature of the concave function of \min_{P} C_2 constant holds. This shows (·) and Jensen's inequality, we have $C_1 < C_2$ that the above DF node work

The rate allocation algorithm degrades without QoS constraints to obtain the system capacity does not reach the theoretical upper bound, which is due to the fact that the two formulas adopt different transmission strategies. In the formula₁, the relay node R receives the signal sent by the source node S and sends it out to the destination node D immediately after the decoding and re-encoding process without considering the current state information of the sending channel; while in the formula₂, the relay node R does not send out the signal immediately after processing it, but

It is retained in the buffer, and then forwarding operation is carried out when the status of the sending channel is monitored to turn good, thus obtaining a higher communication capacity. However, the stay of signal in the buffer will increase the delay of signal transmission. In WAIC scenarios where the actual QoS delay requirement is higher, the immediate forwarding strategy will be more in line with the system communication requirements.

4.2.3 Analysis of improvement strategies for DF node power allocation methods

In order to meet the requirement of avionics for reliability, more

attention is paid to the performance of the communication policy when the QoS constraint is high in the WAIC system. When the QoS factor $\theta \rightarrow \infty$, the effective capacity is degraded to zero interruption capacity^[22]. Considering the original DF node power allocation policy \mathcal{S}_1 derived in the previous subsection, it is integrated into a unified expression as follows:

$$\begin{cases} P(v) = \frac{\sigma}{2\gamma_2} \\ P_r(v) = uP_s(v) \mathbb{I}(\gamma_1 \leq \gamma_2) \end{cases} \quad (4.42)$$

where $\sigma = \lim_{\theta \rightarrow \infty} \gamma_0^{-2/\beta+2} - 1$, with $\mathbb{I}(\cdot)$ is the indicator function. Since γ_0 is still a function of the normalised QoS factor β , it is necessary to

It is difficult to derive analytical expressions to solve the integral equation containing the transcendental function obtained from the total power constraint of the system. It has been shown in the literature [22] that $\otimes \theta \rightarrow \infty, \sigma = 0$, the zero-interruption capacity of the system is 0 and cannot support higher

QoS requirements. The analysis of the system outage probability under the S_1 policy in reference [63], although using a fractional set of merged reception scheme, but the diversity order of the system is still 1. This is due to the fact that in this strategy, the relay nodes need to successfully decode the received signals before collaborative communication can be realised, and the reachable rate of the system is affected by the channel capacity of the S-R link. In order to reduce the limitation of the link capacity of the relay node, the destination node can be allowed to $\gamma_1 > \gamma_2$.

The signals sent from the source node are processed directly without considering the link channel state of the relay node. Based on the above analysis, the improved power allocation method for DF nodes₂ is as follows:

- (1) When $\gamma_1 > \gamma_2$, the node power allocation is performed by Eq. (4.29), at which time the relay node does not send signals, and the communication link degenerates into a straight shot link of S-D;
- (2) When $\gamma_1 \leq \gamma_2$, the node power allocation is performed by equation (4.39).

Similarly, as $\theta \rightarrow \infty$, the derivation yields the unified expression as follows:

$$\begin{aligned} P(v) &= \frac{\sigma}{2\gamma_2} I(\gamma_1 \leq \gamma_2) + \frac{\sigma}{2\gamma_1} I(\gamma_1 > \gamma_2) \\ P_r(v) &= uP_s(v) \chi(\gamma_1 \leq \gamma_2) \end{aligned} \quad (4.43)$$

It has been shown in the appendix of the literature [22] that at this point $\sigma = 0$, the zero-interrupt capacity of the system is still 0. In order to further improve the above phenomenon, it is necessary to relax the communication conditions for the use of direct injection links, and in more scenarios to directly process the signals received by the S-D link. In order to maintain the two-phase transmission strategy, i.e., only the source node S sends signals outward in the first phase, and only the relay node R sends signals outward in the second phase, the opportunistic collaboration strategy analysed in the literature [64] is considered, and the diversity order of the opportunistic collaboration mechanism is larger compared to the original DF

communication. The improved DF node power allocation method₃ is as follows:

(1) When $\gamma_1 > \gamma_2$ or $\gamma_1 > \gamma_3$, i.e., $\gamma_1 > \min\{\gamma_2, \gamma_3\}$, the node power allocation is performed by Equation (4.29);

(2) When $\gamma_1 \leq \min\{\gamma_2, \gamma_3\}$, the node power allocation is performed by equation (4.39). When $\theta \rightarrow \infty$, the unified expression for the₃ allocation strategy is as follows:

$$\begin{aligned} P(v) &= \frac{\sigma}{2\gamma_1} \mathbb{I}_{\gamma_1 > \min\{\gamma_2, \gamma_3\}} + \frac{\sigma}{2\gamma_2} \mathbb{I}_{\gamma_2 < \min\{\gamma_1, \gamma_3\}} \\ p_r(v) &= \tilde{u}_{Ps}(v) \mathbb{I}_{\gamma_1 \leq \min\{\gamma_2, \gamma_3\}} \end{aligned} \quad (4.44)$$

A lower bound for σ has been derived in the literature [22]:

$$\sigma > 2P/\lambda - \left(\frac{1}{\lambda_2} \log \left| 1 - \frac{1}{\lambda_2} \right| + \frac{1}{\lambda_3} \log \left| 1 - \frac{1}{\lambda_3} \right| + \frac{1}{\lambda_1} \log \left| \frac{1}{\lambda_1} \left(1 + \frac{1}{\lambda_1} \right) \right| \right) \quad (4.45)$$

It can be seen that under the policy₃, the zero interrupt capacity of the system does not decay to 0 when the QoS constraint is high.

4.3 Simulation validation of code-forwarding technique based on effective capacity model

In order to analyse the performance of relay collaborative communication in terms of effectiveness and reliability in WAIC, the effective capacity model with QoS constraints is used for theoretical analysis and simulation verification. Since the calculation of the theoretical value of the effective capacity of relay collaborative communication contains a complex integration operation process, this study adopts the Monte Carlo method to simulate the relaying process and calculate the statistical data for analysis and verification.

4.3.1 Relay communication simulation parameter setting

In a WAIC network based on 802.11ax protocol, as shown in Fig. 31 the AP is set as the relay node R, the source node S and the destination node D are set as the STA, at this time R has the ability to decode and forward the received signals, and the simulation and analysis of relay collaborative communication in this scenario is considered.

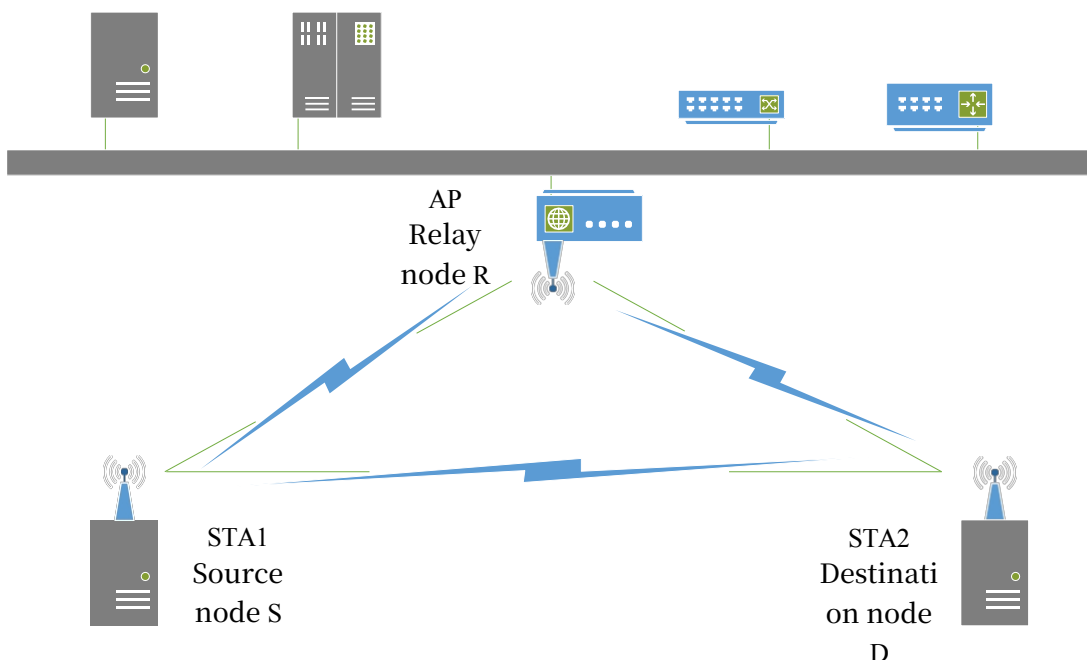


Figure 31 Schematic diagram of trunk collaboration in a WAIC network

The communication bandwidth of the system is set to be the base bandwidth of 20MHz, and the data frame transmission time is 2ms. in order to simplify the analysis process, the relative position relationship of the relay node R is considered to have an impact on the communication capacity of the system, and the distance between S-D is normalised, and the fading channel between the nodes is set to obey an independent Rayleigh distribution. Since the communication capacity is affected by the channel bandwidth and the signal-to-noise ratio at the receiving end, the total transmit power is set to be limited to 10 dB, and the noise power at the receiving end to be 0 dB. The expected value of the channel gain in the direct link is 1, and the expected value of the signal-to-noise ratio at the receiving end is kept at 10 dB. the distance d between S and R is at

The QoS factor θ takes values uniformly in the range $[0.01, 0.99]$ and the QoS factor θ takes values in the range $[10^{-7}, 10^{-3}]$.

Referring to the empirical parameter of path loss in different communication scenarios of aircraft measured by ITU-R, it is 2 in the cabin interior and 3.46 in the scenarios where the cabin interval contains facilities such as partitions and seats.^[6] Considering that the interior of avionics cabin is a closed communication scenario with metal devices, the path loss parameter will increase because metal walls, obstacles and metal frames will hinder the signal propagation and reduce the signal strength continuously. In addition, the centre frequency of WAIC carrier is 4.3GHz, the penetration ability of high-frequency signal is weakened, and the loss will increase when propagating between complex obstacles. Generally, in indoor or shaded outdoor environments, a path loss parameter greater than 4 can be observed.^[65] In summary.

Set the path loss parameter $\alpha = 4$ in the simulation and perform 100000 simulations in each scenario to calculate the average value.

4.3.2 Analysis of simulation results of relay communication

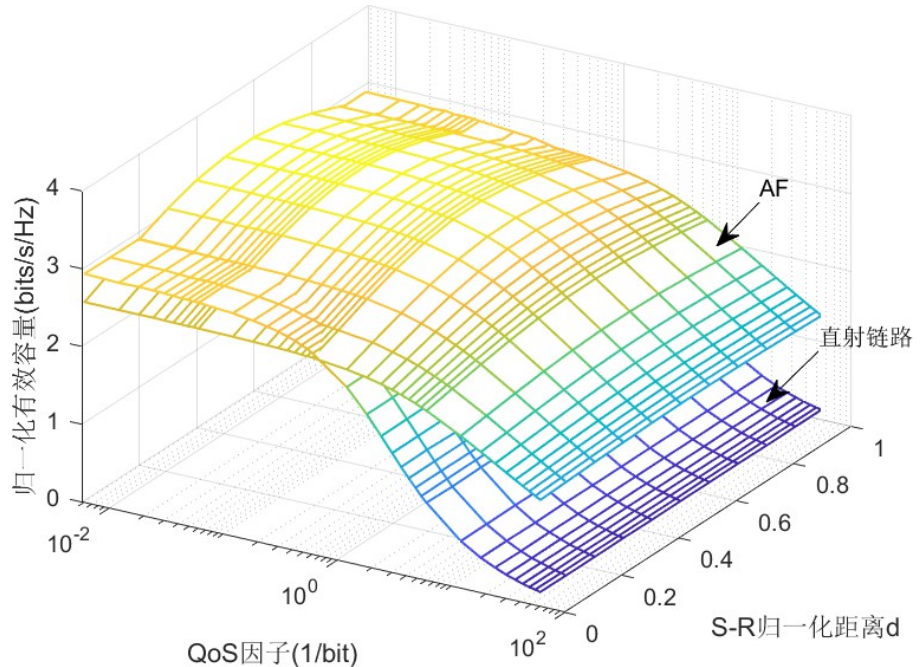


Fig. 32 Normalised effective capacity of AF node power allocation method with direct communication link

Based on the above parameter settings, the simulation of the optimal node power allocation method is carried out in AF and DF modes, respectively, and

the effective capacity statistics are calculated and compared with the direct communication link.

As shown in Fig. 32 are the results of normalised effective capacity calculations for the optimal node power allocation method in AF mode with direct shot links at different S-R distances. From the figure, it can be seen that when the QoS factor is small, the effective capacity values of relayed collaborative communication and direct link are very close to each other. When the QoS factor increases, i.e., when the QoS constraints are enhanced, the effective capacity of the direct link will decay rapidly until 0. At this time, the zero-interruption capacity of the system is 0, which cannot satisfy the reliability requirements of WAIC. The relay collaborative communication link with AF mode, on the other hand, when the QoS value increases, the effective capacity decreases but does not decay to 0, and it can support communication scenarios with higher QoS requirements, which is due to the fact that the receiving end diversity the received signal copies.

The merger acquires some diversity gain.

Since there is no relay node in the direct shot communication link, the value of its effective capacity is not affected by the normalised distance d . From the figure, it can be seen that the value of the effective capacity reaches its maximum when the relay node is at an equal distance relative to the source node and the destination node in the relay collaborative communication scenario.

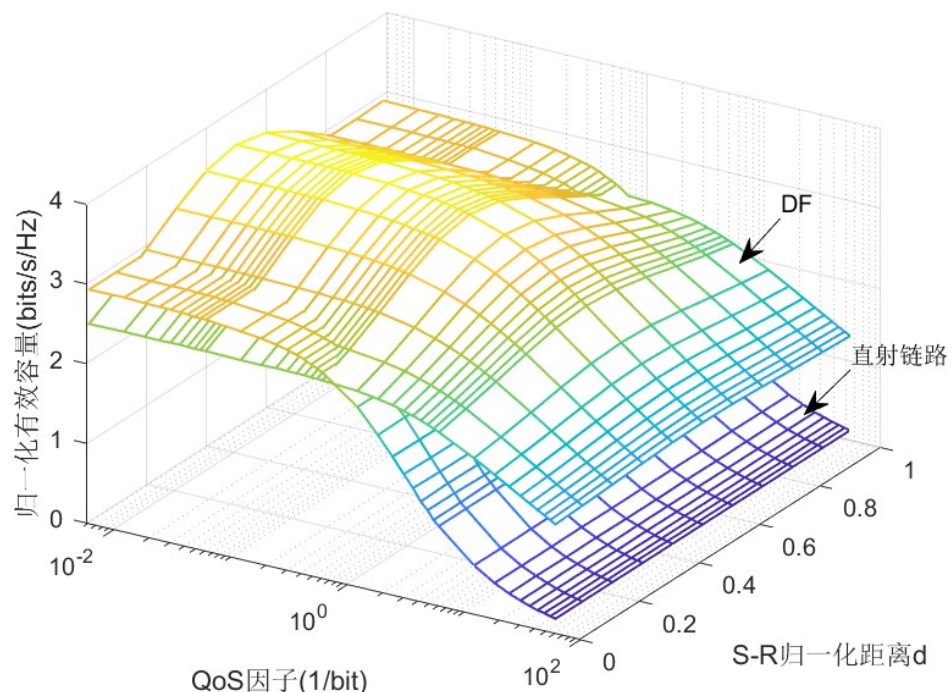


Figure 33 DF node power allocation method₃, Normalised effective capacity with direct communication links

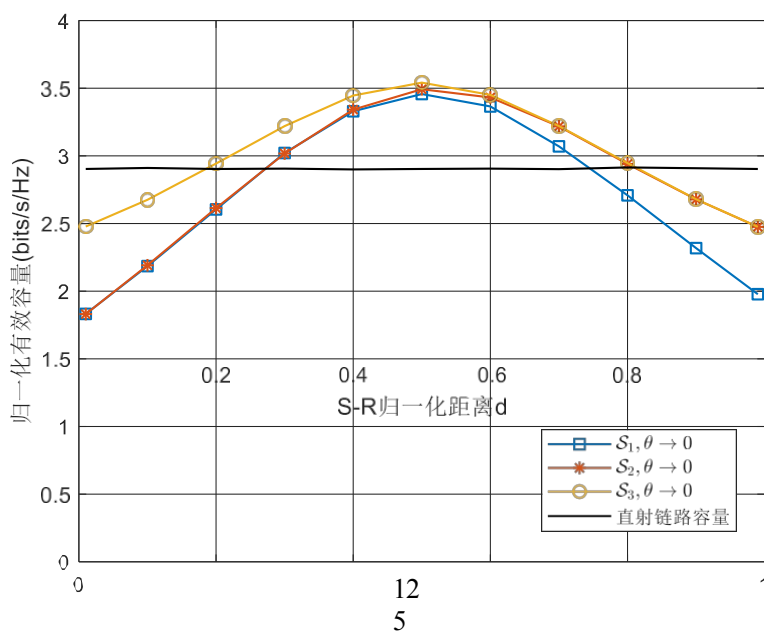


Fig. 34 Effective capacity of three different DF node power allocation methods with direct-fire links as $\theta \rightarrow 0$

Fig. 33 shows the normalisation of the optimal node power allocation method₃ in DF mode with the direct link at different S-R distances.

The effective capacity is calculated. Similar to the AF mode, the relay cooperative communication system in the DF mode has better performance in higher QoS demand, can support a certain rate of communication, and meets the WAIC reliability requirements.

Fig. 34 shows the performance of three different optimal node power allocation methods ₁, ₂, and ₃ in the DF mode with the direct shot link when the QoS factor $\theta \rightarrow 0$, i.e., when there is no QoS requirement. From the figure, it can be seen that all the three methods reach the maximum value when the S-R distance $d = 0.5$. Method ₃ can achieve the largest capacity value, followed by Method ₂, and Method ₁ the most.

Smaller. In addition, Methods ₁ and ₂, the relative position of the relay nodes also leads to a small difference in the trend of the effective capacity values, as can be seen in the figure, when the relay node is closer to the destination node, the capacity degradation is smaller.

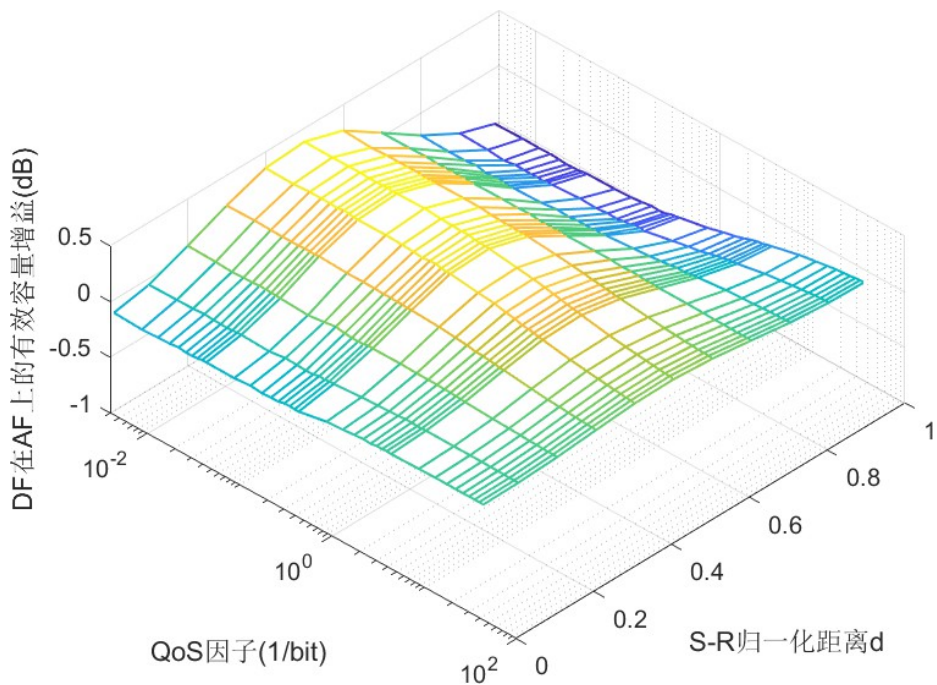


Fig. 35 Comparison of effective capacity values for DF and AF

Figure 35 shows the effective capacity of the node allocation method, in DF mode on the optimal node allocation method in AF mode

Gain: When the QoS factor is small and the relay node is in the middle position, i.e., $d=0.5$, the effective capacity value of DF collaboration improves significantly over AF collaboration up to a maximum of about 0.4 dB. When the QoS factor is increased and the position of the relay node is close to the two ends, the performance of DF collaboration improves over AF collaboration.

From the above results, it can also be observed that there is an inferior performance in terms of effective capacity performance compared to the direct shot link when relayed collaborative communication is used, due to the limitation of the half-duplex communication mechanism, which can only be applied to half of the communication system since the

by degree. The performance of relay collaborative communication may be improved even more if some more advanced relaying techniques are used, such as full-duplex communication or bi-directional communication.

4.4 Summary of the chapter

This chapter investigates the performance simulation analysis of relay collaborative communication scenarios based on the effective capacity model in WAIC scenarios. In order to satisfy the effectiveness and reliability requirements in WAIC, a reasonable node power allocation strategy needs to be adopted under higher QoS constraints. The simulation results show that under different relay node positions and QoS constraints, the zero-interruption capacity of the system does not decay to 0 with the improved DF node power allocation method, which can better support the communication scenarios with QoS requirements in WAIC. In the process of QoS factor increase, the overall performance of DF collaboration is better compared with AF collaboration.

Chapter 5 Avionics Wireless LAN Simulation Evaluation Study

This chapter describes the simulation of an avionics communication system based on the IEEE 802.11ax protocol and the physical testing based on software radios for performance evaluation of an avionics wireless local area network (WLAN). Software modelling and simulation analysis of the parameters of several components of the WAIC-applicable WLAN, including channel model, modulation and demodulation, coding and decoding, etc., were performed. Semi-physical testing of communications using the software radio platform was conducted to further validate the credibility and accuracy of the software simulation results.

5.1 MATLAB-based Avionics Wireless LAN Communication Simulation

Avionics WLAN with flexible deployment and mature COTS technology is suitable for WAIC solution. Based on the MATLAB software toolbox of IEEE 802.11ax protocol, the avionics WLAN is simulated and modelled, and the software simulation performance is analysed and evaluated.

5.1.1 Parameter settings for wireless LAN simulation

Considering a simple point-to-point SISO communication scenario, the rate adaptive technique proposed in Section 2.2.3 and modelled in Section 3.1.3 are used to obtain the avionics bay wireless channel, and the WAIC is simulated and analysed with the parameter settings shown in Table 8.

Table 8 WAIC WLAN Simulation Parameters

Physical meaning of parameters	parameterisation
Transmit signal bandwidth	20MHz
Centre frequency of transmitted signals	4.3GHz
Upper layer packet length	1000 Byte
Protection interval length	0.8us
FEC Code Type	BCC

firing power	15dBm
receiver thermal noise	-90.9dBm

Using the above parameter settings, the transmitter sends 100 packets and the receiver demodulates to restore the original signal for BER, PER and throughput and other indicators of the statistical calculation, the signal processing flow is shown in Figure 36.

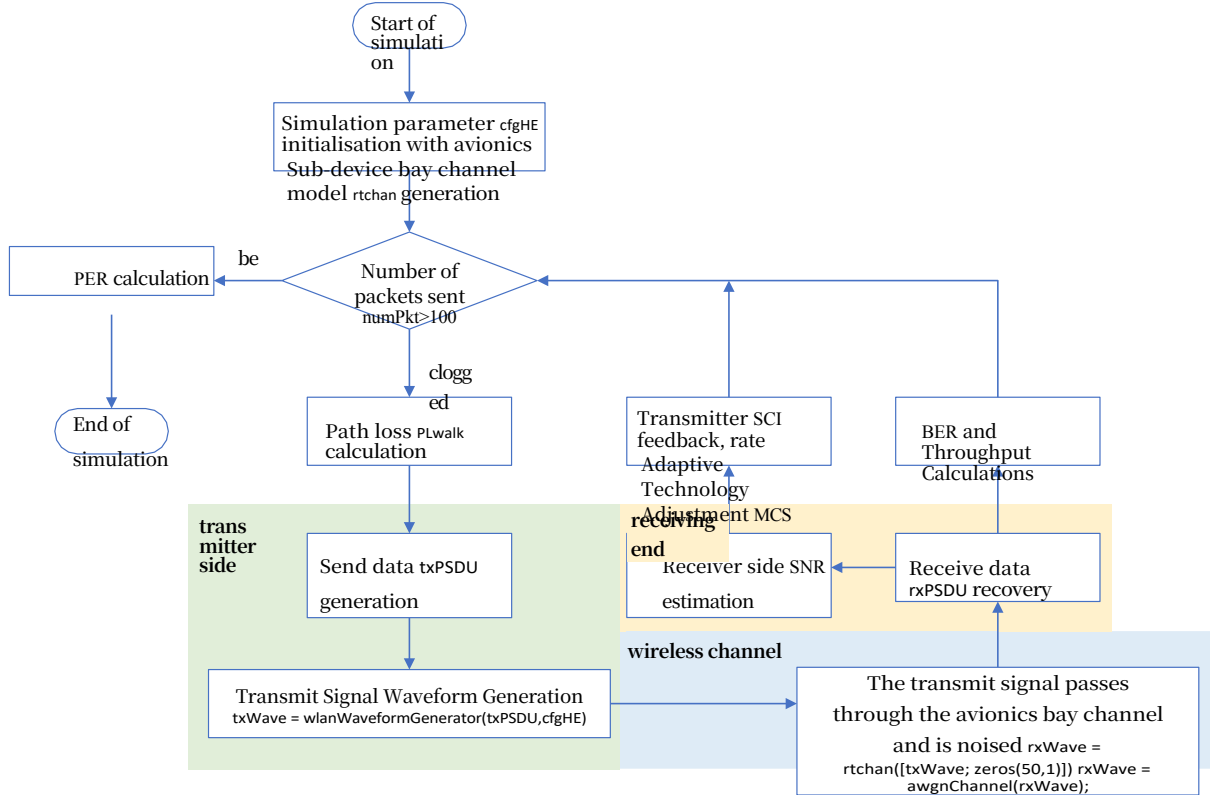


Fig. 36 MATLAB simulation flowchart

Since the avionics bay channel is a deterministic channel model, when the transmitter and receiver positions are determined, the path loss is also unique. In order to analyse the WLAN communication performance under different SNRs, the channel gain is normalised and the path loss is set to vary with time, i.e., the path loss experienced by different transmitter packets is continuously varied under the control of the cosine function, and the transmitter signal passes through the channel model that removes the influence of the path loss, and then multiplied by the path loss obtained from the above calculation. Set the average value of the path loss to 80dB, and the amplitude of the cosine function to 20, i.e., the path loss is in the [60dB,100dB] norm.

The signal is demodulated at the receiving end to recover the original signal and compare it with the transmitted signal. The receiver demodulates the original signal and compares it with the transmitted signal to get the statistical information such as BER, PER and throughput. At the same time, the receiver also needs to estimate the SNR of the received signal, which is fed

back to the transmitter to adjust the MCS setting for the next packet.

5.1.2 Analysis of wireless LAN simulation results

Figure 37 shows the deterministic multipath channel model obtained by the ray tracing algorithm, where the blue nodes are the transmitters and the red nodes are the receivers. By selecting one of the rays, the simulation data can be viewed, including the number of reflections, the path loss, the phase change, the transmission distance, the departure and arrival angles, etc. Figure 38 shows the delay power spectrum as well as the departure and arrival angles of the channel model. Fig. 38 shows the delay power spectrum of the channel model and the three-dimensional diagrams of the departure and arrival angles.

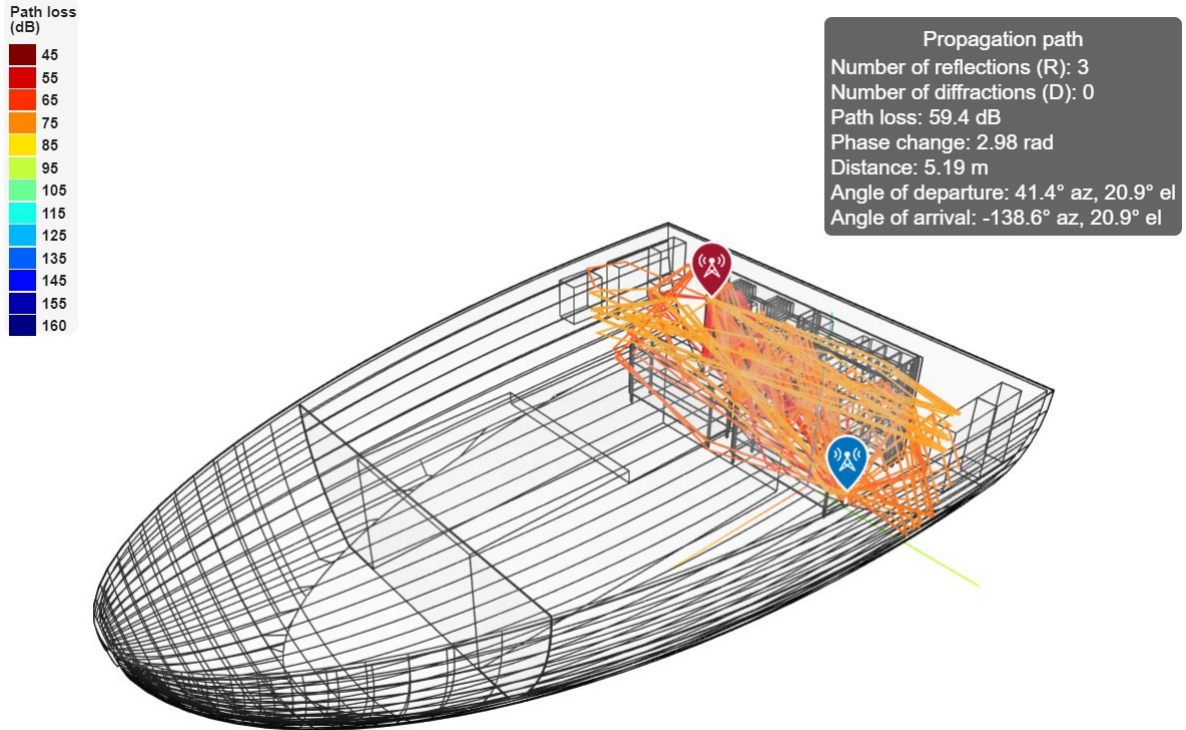


Figure 37 Avionics bay ray tracing algorithm results

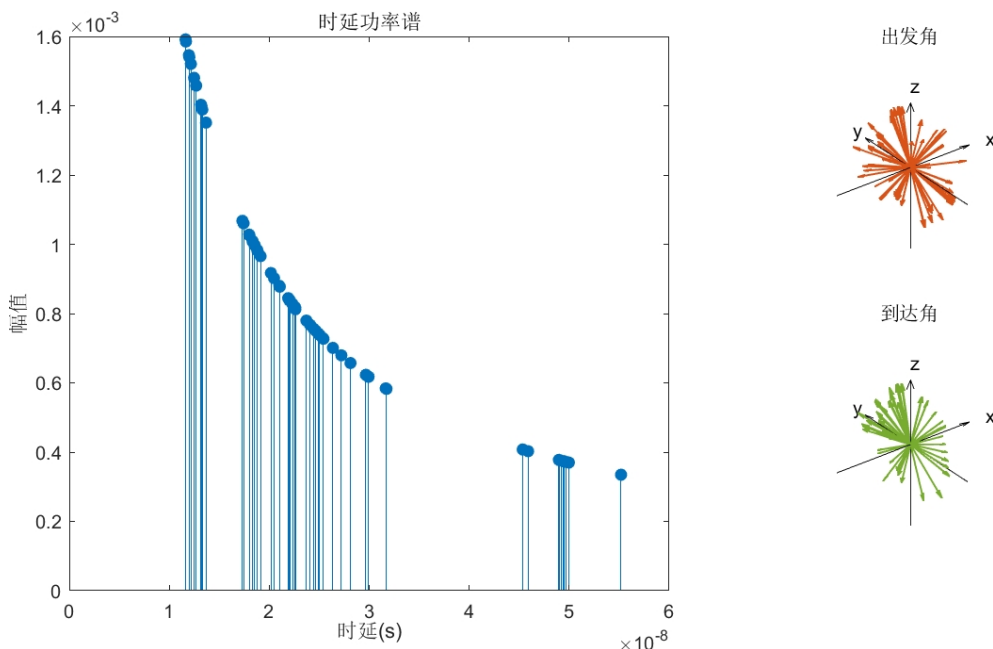


Fig. 38 3D plot of delay power spectrum with departure and arrival angles

The initial MCS of the transmitter is set to 4, i.e., the modulation mode is 16QAM and the code rate is 3/4. Fig. 39 shows the information of the received signal of packet 1 in the simulation, and the SNR is estimated to be 32.7192 dB, and Fig. 40 shows the constellation diagram of the received signal of packet 1, and it can be seen that, after the synchronization of the

receiving end, the estimation of the frequency deviation, and the equalization of the channel, the constellation diagram of the received signal can be well matched with the reference constellation point, which is the same as that of the received signal. It can be seen that after synchronisation, frequency offset estimation and channel equalisation at the receiving end, the received signal constellation and the reference constellation point can match well.

字段	值
RxPSDU	<i>8056x1 int8</i>
EqDataSym	<i>234x12 complex double</i>
RxWaveformLength	4306
NoiseVar	1.1918e-12
EstimatedSNR	32.7192
rxWave	<i>4306x1 complex double</i>

Fig. 39 Received signal information when simulating the transmission of packet 1

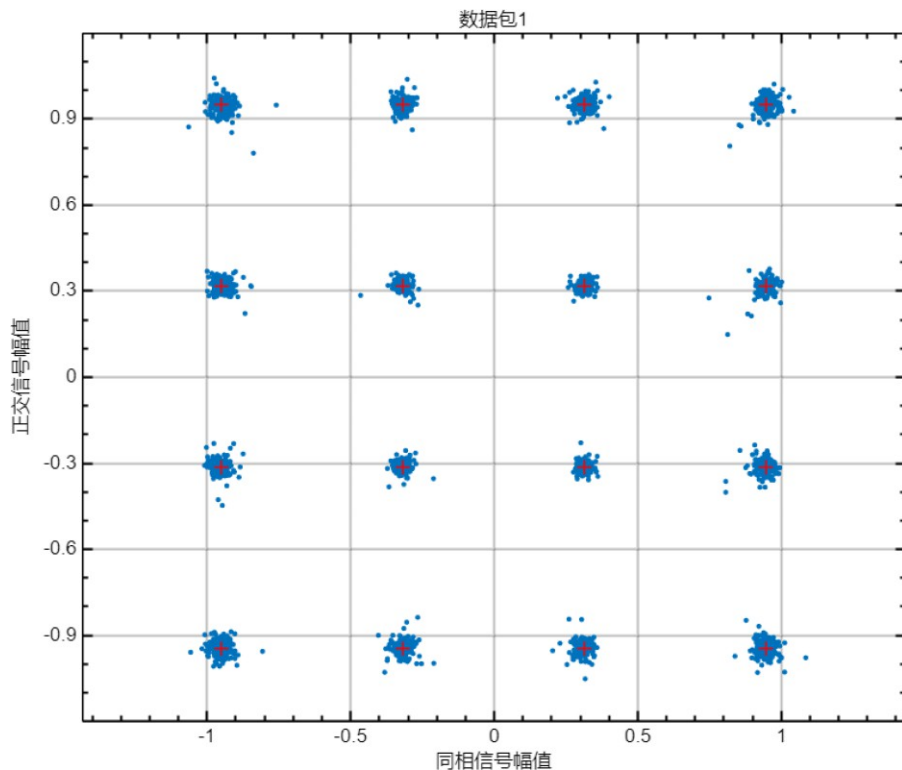


Fig. 40 Constellation diagram of packet 1 with MCS 4

Fig. 41 shows the power of the transmitted and received signals measured by the spectrum analyser, from which it can be seen that the power of the transmitted signals is 15 dBm on the frequency axis, while the received signals have different degrees of attenuation on the frequency axis, which is due to the effect of multipath channels, resulting in frequency-selective channels so that the signal gain is different at different frequency points, which can be estimated through the channel state information of the pilot sequence. Channel equalisation is performed to counteract some of the effects of the multipath channel. At the same time, it can be seen that the frequency selectivity of the multipath channel is weak, and the variation is not large, which is due to

the fact that the channel environment in the avionics bay is a quasi-stationary communication environment, and there is no Doppler effect from the moving objects. According to the simulation results in subsection 3.1.3, it can also be seen that the coherent bandwidth of the channel is large, and it can be approximated as a flat fading channel. Fig. 42 shows the statistics obtained by sending 100 packets, from which it can be seen that the SNR value is still at the same level as that in When the communication system modulation is within the tolerance range, the transmitter can track the channel state changes well, while when the SNR value is close to or even less than 0dB, the received signal will fail to be decoded, and then the BER requirement of WAIC will not be supported.

At this point, the statistically obtained PER is 0.12 and the average throughput of the system is 19.9012 Mbps.

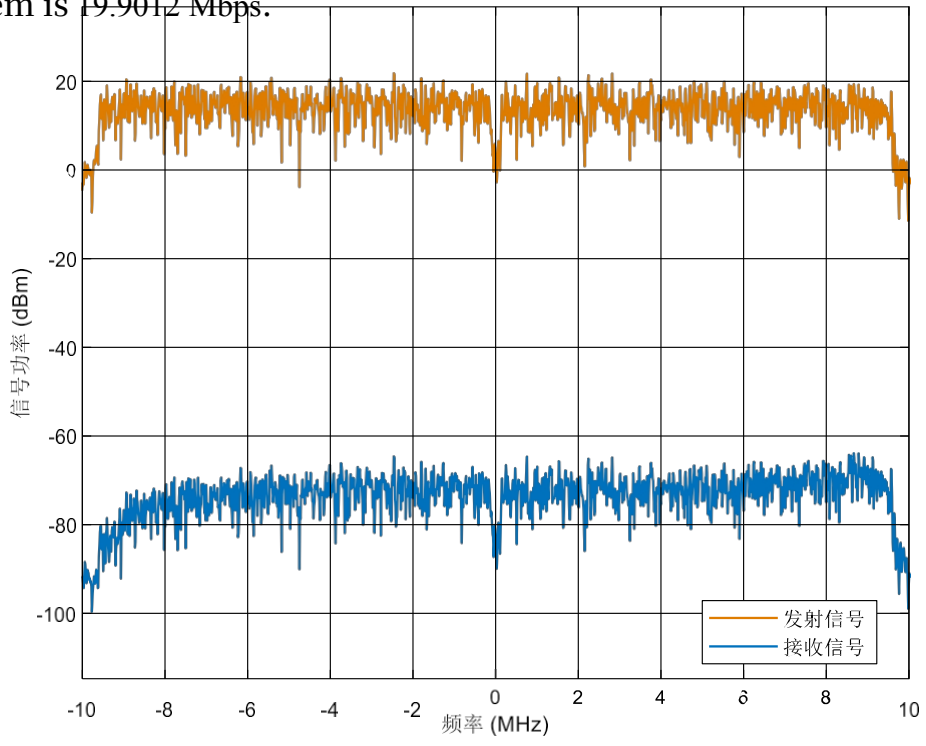


Fig. 41 Power spectra of transmitted and received signals

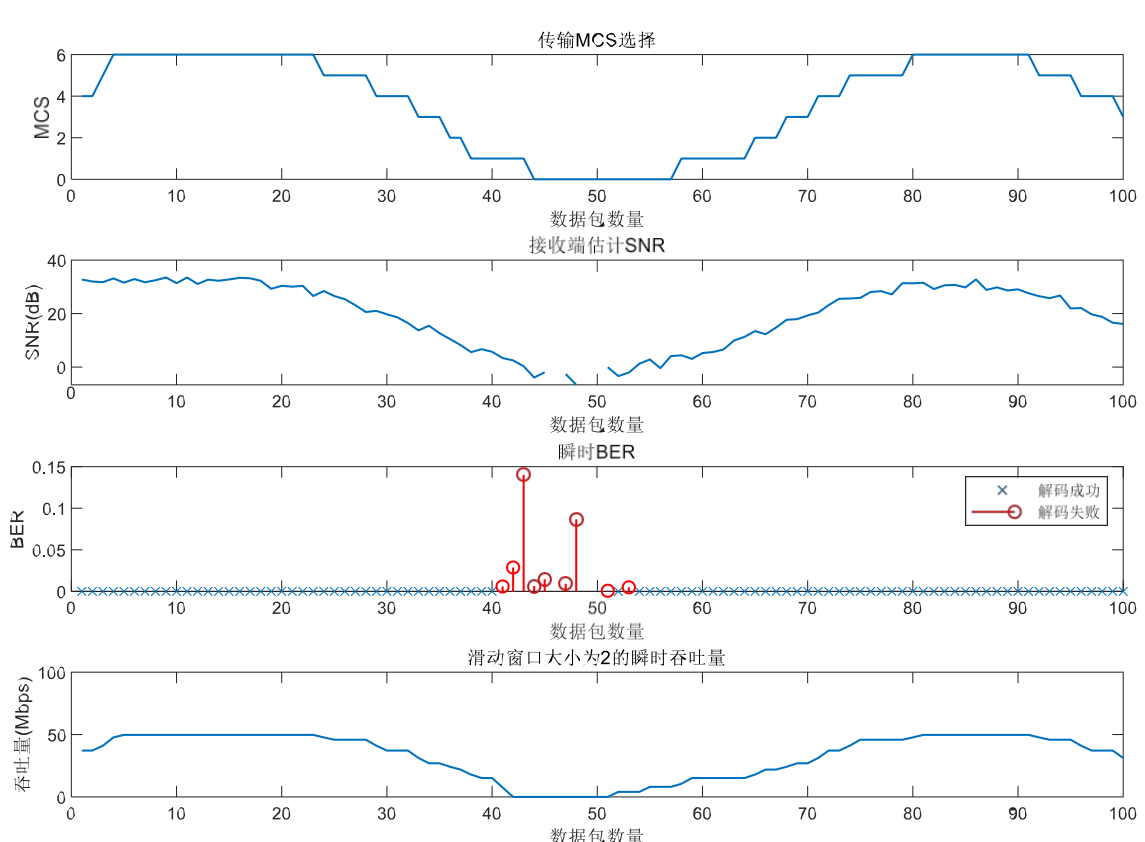


Figure 42 Statistics obtained by simulating 100 packets sent

5.2 Real-world analysis based on a software radio platform

Software Defined Radio (SDR) platforms use embedded computing programs or programmable logic to control radio hardware for radio baseband signal generation, modulation, demodulation and analysis. This section describes a real-world analysis of an avionics WLAN based on a software radio platform, including how to use the software radio platform for signal capture, signal processing, and data analysis.

5.2.1 Software radio platform parameterisation

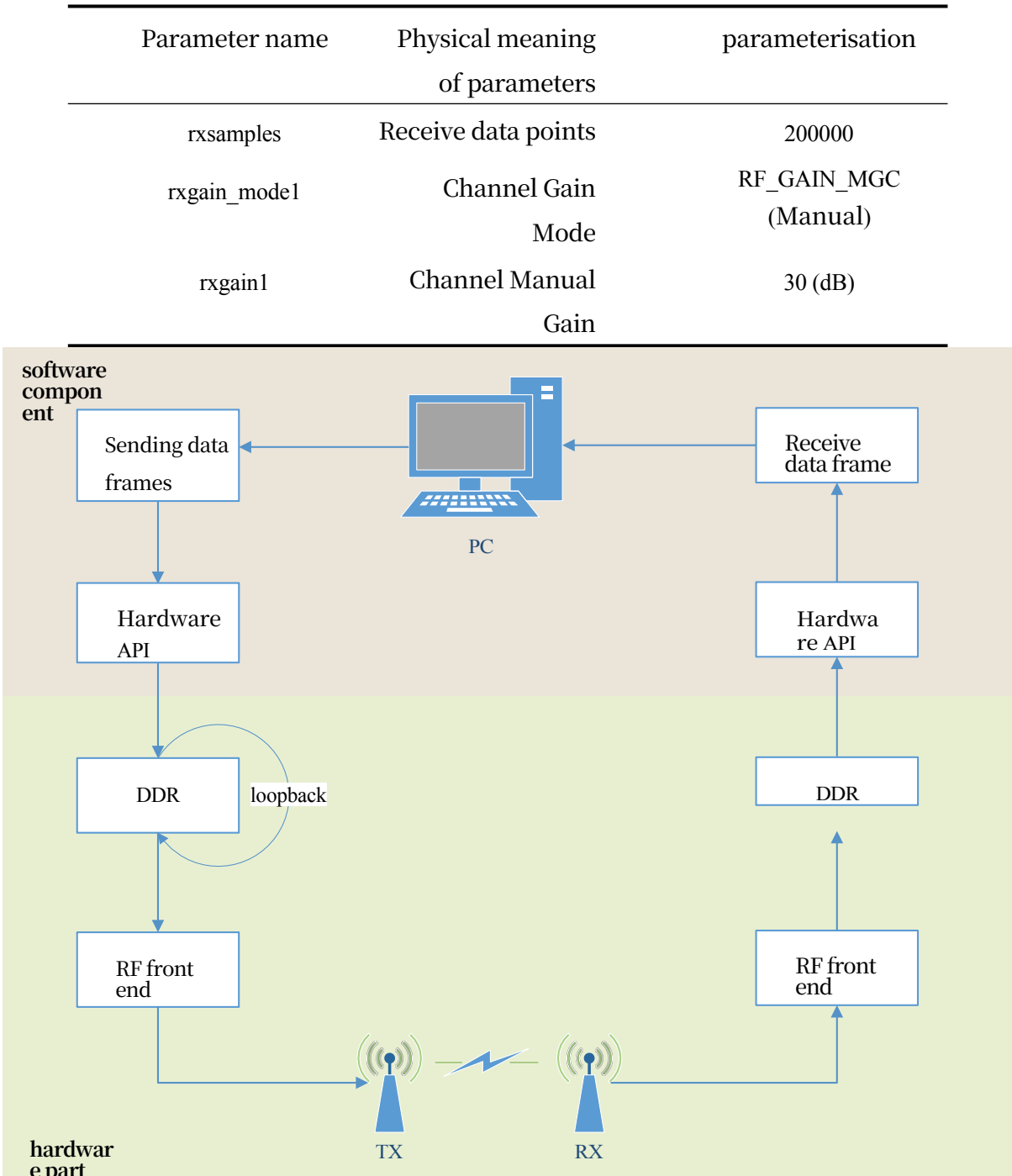
In this project, the NIVSR YunSDR Y320 platform is used for the measurement and analysis of WAIC wireless LAN technology. The platform adopts highly integrated RF shortcut transceiver AD9361, SoC architecture FPGA chip ZYNQ 7020 and ARM Cortex-A9 processor, which has excellent computational ability and processing speed, and is able to process all kinds of signals quickly and accurately. Y320 realizes a wide-band software radio system with a spectrum range of 70MHz~6GHz and an analogue bandwidth of 200KHz~56MHz. Y320 realises a wide-band software radio system with a spectrum range of 70MHz~6GHz and an analogue bandwidth of 200KHz~56MHz. The baseband processor combines the parallelism of FPGAs with the flexibility of ARM processors, and can communicate with personal computers (PCs) via Gigabit Ethernet, as well as support embedded software radio architectures running the Linux operating system independently of PCs.

In order to match the simulation environment, this experiment adopts the same parameter configuration, i.e., the communication bandwidth is 20MHz, the centre frequency is 4.3GHz, and the single signal transmission power of the Y320 platform is 15dBm. Due to the limitation of the equipment and the communication environment, the experiment adopts a pair of RF transmitter and receiver interfaces of a single Y320 board to transmit and receive signals, and the working parameters of the RF front-end are shown in Table 9 and Table 10. and Table 10, note that the table 1dB = 0.001dB.

Table 9 Y320 transmitter RF front-end operating parameter settings

Parameter name	Physical meaning of	parameterisation
	13 9	

parameters		
ipaddr	Device IP Address	192.168.0.1
samp	sampling rate	40MHz
bw	transmission bandwidth	20MHz
freq	RF frequency	4300MHz
tx_att1	Transmit Channel Attenuation	10mdB
fdd_tdd	Launch Mode Selection	FDD
tx_chan	Transmit Channel Selection	TX1_CHANNEL
txgap	transmission interval	0 (ns)

Table 10 Y320 Receiver RF Front End Operating Parameter Settings**Fig. 43 Schematic diagram of the signal processing process in PC mode of Y320 card**

As shown in Fig. 43, the operating mode of the Y320 is PC software control of the radio hardware, control the operating parameters of the RF front-end through the MATLAB API, and control the SDR to send and receive wireless signals. The PC is connected to the Y320 card through Gigabit Ethernet, and the SDR receives the data frames sent by the PC and stores the data in the internal memory DDR, and then configures the Direct Memory

Access (DMA) operating mode of the SDR to enter the loopback mode. The SDR receives the data frames from the PC, stores the data in the internal memory DDR, and then configures the SDR's Direct Memory Access (DMA) operating mode to enter loopback.

(In the loopback mode, the DMA repeatedly reads this frame of data from the DDR and sends it out through the RF front-end. After the receiver receives the data, the SDR moves the received data to the DDR and sends it back to the PC for processing through the Gigabit Ethernet via a socket, thus forming a wireless communication test system. According to the above test system

architecture, the physical construction of the software radio is shown in Figure 44.



Figure 44: Physical diagram of a software radio

5.2.2 Confined Environment Communication Measurement and Analysis

As it is not possible to test in the actual aircraft environment, in order to simulate the avionics cabin metal bulkhead environment and confined communication conditions, this experiment in the lift to send and receive wireless signals, the channel is measured and analysed, a measured data and system parameter settings are outputted to the command line, and the results are shown in Figure 45.

-----通信系统参数-----
 MCS: 5, 调制方式: 64QAM, 码率: 2/3
 传输速率: 46.5116Mbps
 接收端估计SNR: 23.8835dB
 当前接收数据帧的BER: 0
 接收数据星座图的EVM: -20.6611dB

Figure 45 System Parameter Settings and Measured Data

In this experiment, the MCS of the transmitter is set to 5, i.e., the modulation mode is 64QAM, the code rate is 2/3, and the straight line distance between the two antennas is 90 cm, and it can be seen that the BER of the

receiver is 0, which can correctly decode the signal, and the transmission rate can satisfy the requirement of the maximum instantaneous communication rate of WAIC. Fig. 46 shows the time-domain waveform of the received signal and the constellation diagram of the data domain after equalisation, and Fig. 47 shows the power spectral density of the received signal and the channel response value obtained by HE-LTF estimation, which shows that the wireless channel under the confined environment has a certain degree of frequency selectivity, which is reflected in the power spectra of the received signal, with different gains at different frequency points, but after channel equalisation, the receiving end can recover the original signal very well.

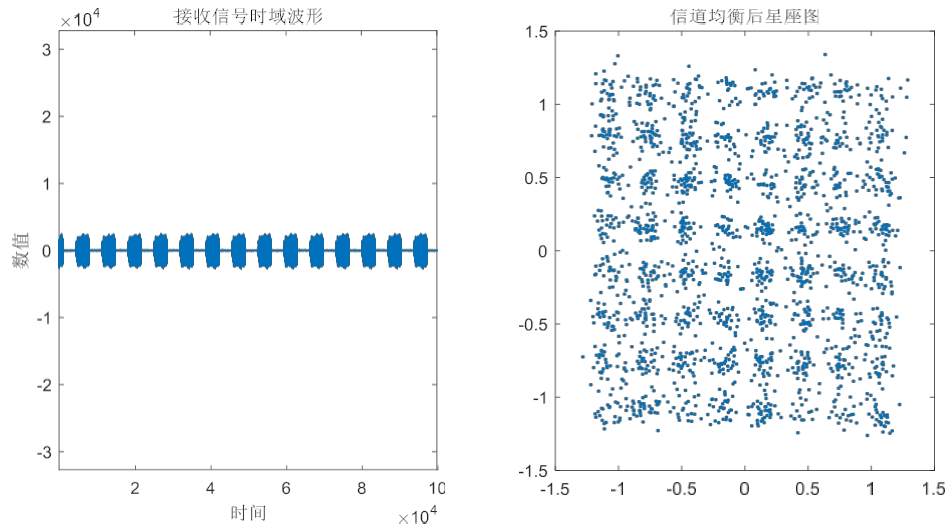


Fig. 46 Constellation diagram of the received signal waveform in the time domain and after channel equalisation in the data domain

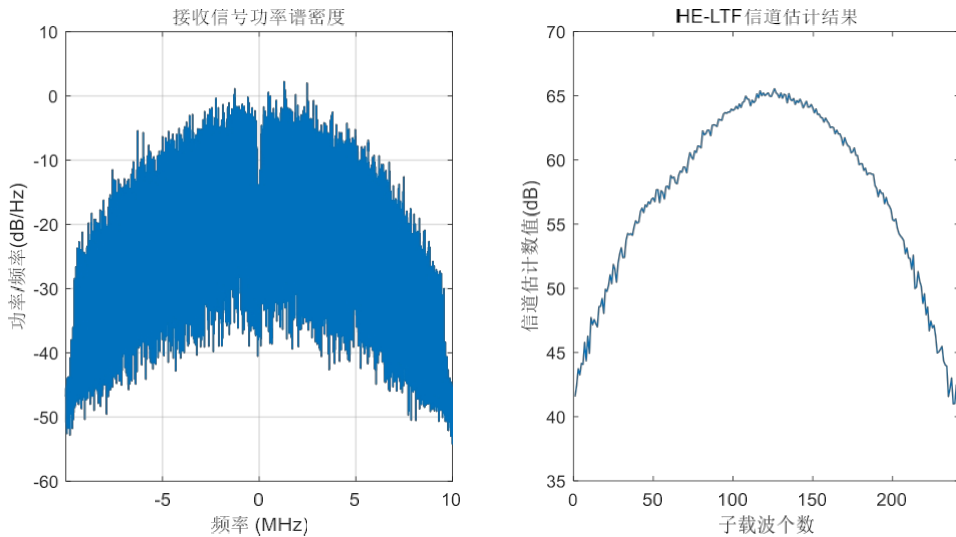


Fig. 47 Received signal power spectral density and channel estimation results

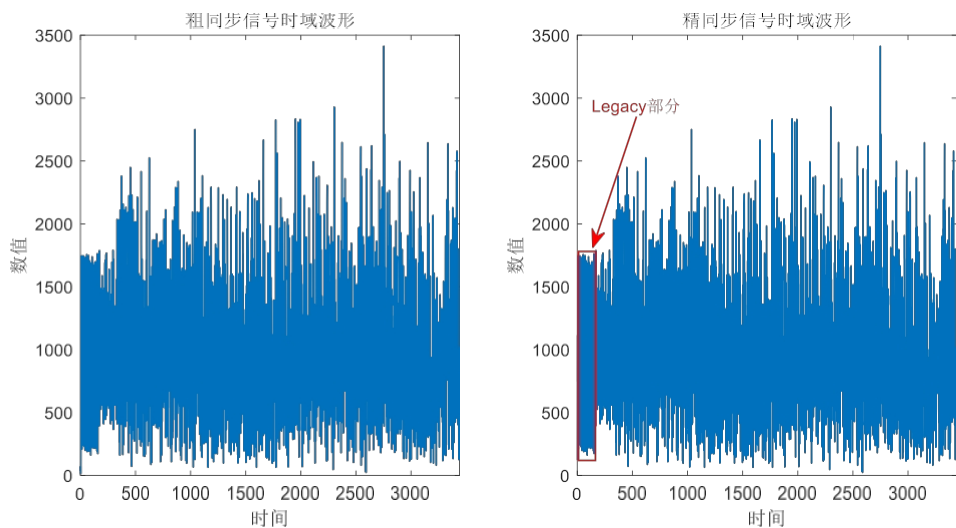


Fig. 48 Coarse and fine synchronisation time domain signal waveforms

Figure 48 shows the time-domain waveform obtained by synchronising the L-STF with the L-LTF, and the part marked by the red box on the left side of the figure is the Legacy domain signal. The demo interface obtained by integrating the above modules is shown in Fig. 49.

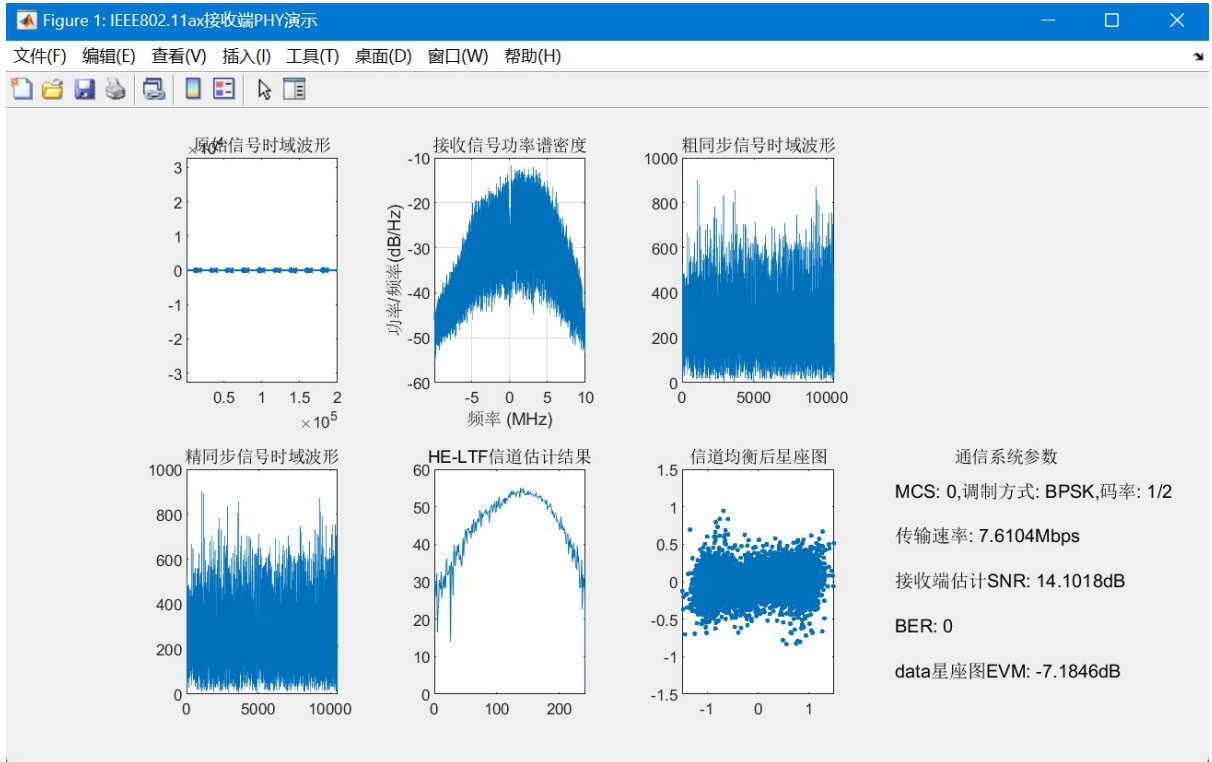


Figure 49 IEEE802.11ax Receiver PHY Demo Simulation Interface

5.2.3 Rate adaptive algorithm empirical analysis

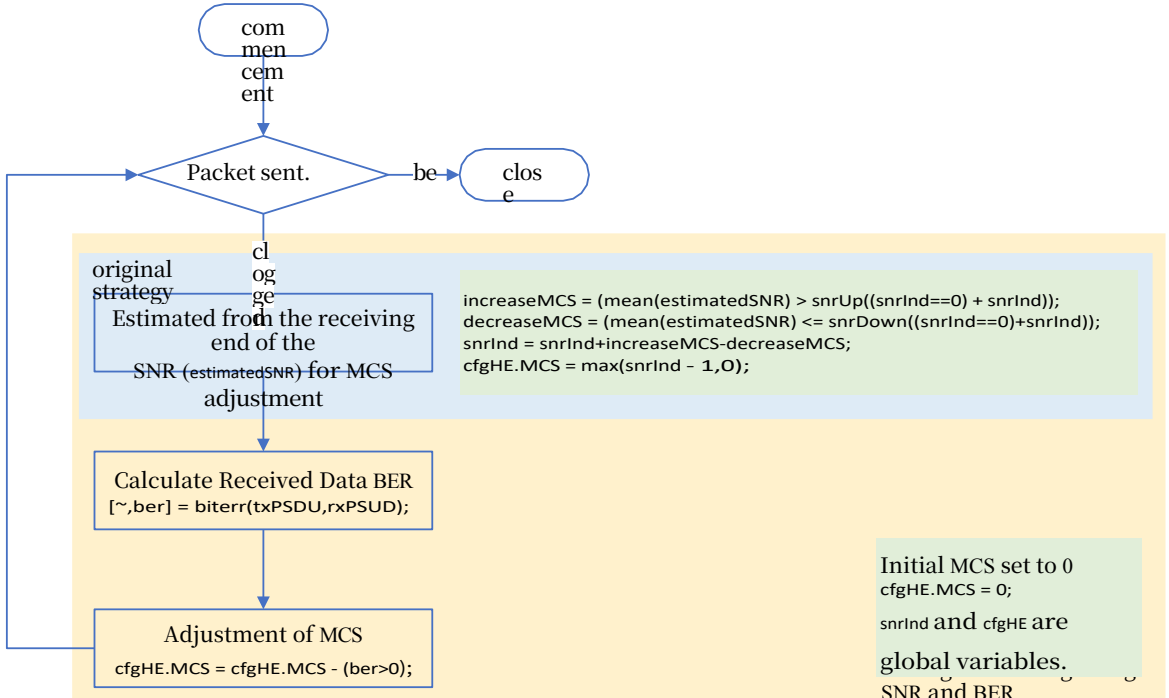
In order to meet the potential fast changing communication environment in WAIC and to maximise the transmission rate, the rate adaptive control technique is introduced. According to the rate adjustment method in Subsection 2.3.2, the initial MCS is set to 0, rcaAttack=0, rcaRelease=1 as the original strategy. In the actual measurement process, there are sources of errors that do not exist in the simulation. In order to attenuate the effect of the estimation error of the SNR at the receiver side, the following improvement strategy is considered:

When the BER of the current data frame is not 0, in order to adapt to the current channel state change more conservatively, the transmitter will subtract one from the MCS adjusted by the original strategy, and then send the next data frame until no BER occurs, the flow of the algorithm is shown in Fig. 50.

In order to simulate the scenario of continuous change of SNR, the SNR can be affected by changing the distance between the transmitting antenna and the receiving antenna or using objects to block the transmission path in the actual measurement process. The measured results of the above two strategies are shown in Figures 51 and 52.

In Fig. 51, it can be observed that the SNR of packet 24 decreases drastically during transmission and the BER value reaches around 0.5. In addition, there are successive decoding failures for packets 23 and 24, 32 and 33, and 48 and 49. It is concluded that when the SNR changes smoothly, the transmitter can follow the changes in the communication environment well and change the coding strategy. However, when the SNR value changes rapidly, the original algorithm cannot adapt well to this kind of situation, and even continuous decoding may occur.

The case of error. This is due to the fact that the original policy of the rate-adaptive algorithm is continuous with respect to changes in the MCS and



cannot adapt to sudden types of changes.

Fig. 50 Flow of rate adaptation algorithm

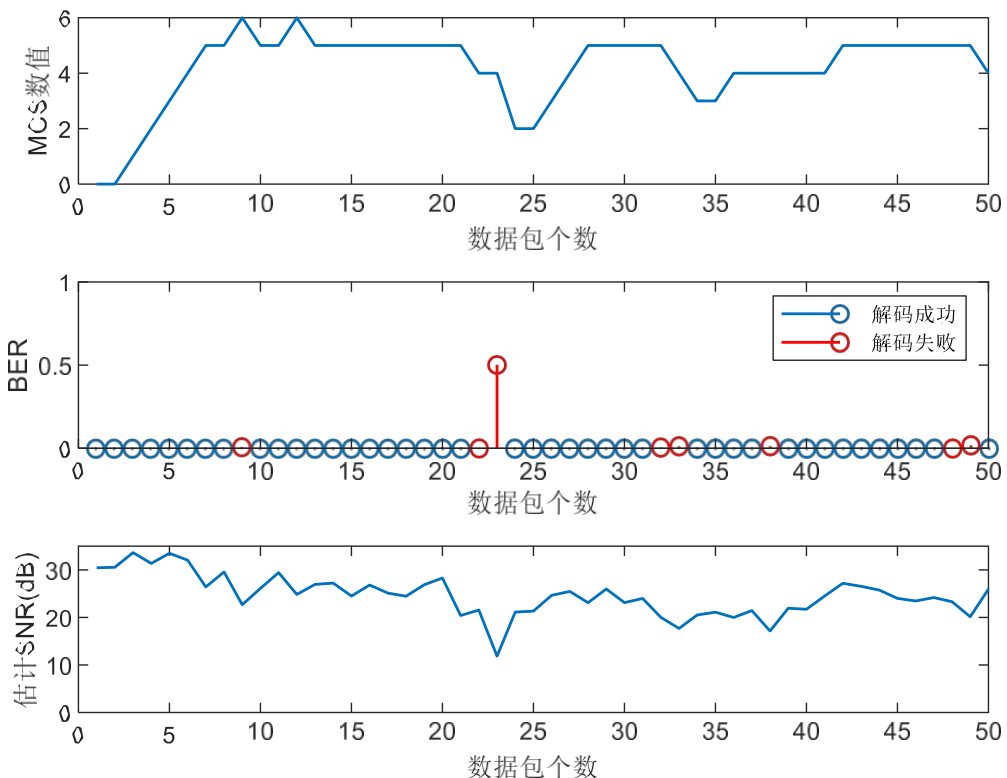


Fig. 51 Results of the adaptive algorithm for the measured rate of the original policy

Figure 52 shows the results of the rate adaptation algorithm for the

improved strategy, where packet 18 is in the presence of an error code.

The MCS rapidly decreases by two values, which is more adaptable to the rapid change of SNR. Compared with the measured results of the original strategy, the probability of successive decoding failure events of the packet decreases significantly, and the BER value does not fluctuate less, so the improved strategy is better adapted.

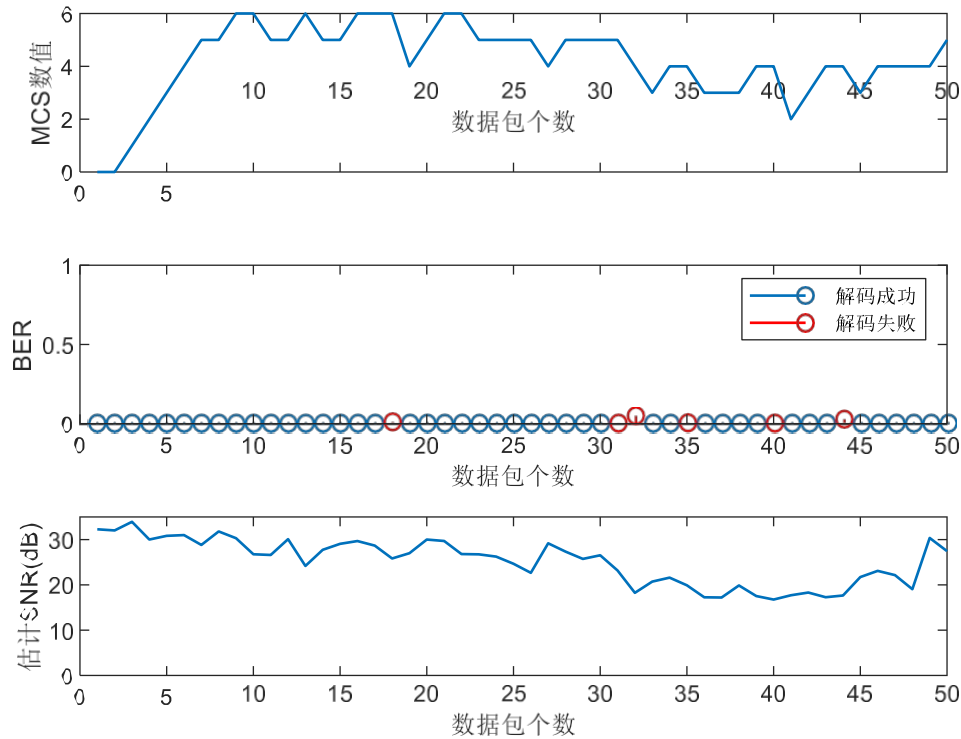


Fig. 52 Improved strategy measured rate adaptive algorithm results

5.3 Summary of the chapter

In this chapter, WAIC WLAN technologies are analysed in simulation and field measurements, and evaluated for different technologies. To address the reliability and validity concerns of WAIC, an avionics bay channel model is constructed in the software simulation, and field measurements are made in a confined metal environment to analyse the respective channel characteristics and physical layer QoS metrics such as BER, PER and throughput. Based on the IEEE 802.11ax protocol, a complete simulation platform and a real-time analysis interface are constructed from the transmitter to the receiver, which can monitor the channel characteristics of the transmitted packets and the QoS metrics at the receiver in real time. The analysis results show that compared with the

software simulation modelling, the actual measurement of the communication environment is more severe, but the signal processing techniques used in the software simulation can still be better adapted to the changes in the actual communication environment.

Summary and outlook

With the development of wireless avionics in-flight communication (WAIC) technology, adaptive modification using commercial shelf technology has become one of the current development directions. Compared with the traditional wired communication, the random communication characteristic of the air interface of WAIC makes it lack of deterministic support, which cannot guarantee the communication quality and QoS demand. In order to meet the demand of avionics for communication effectiveness and reliability, this study is based on the physical layer technology of IEEE 802.11 protocol for applicability modification, introduces the effective capacity model and relay cooperative communication system, and analyses the communication system's ability to support the QoS and throughput size under the probability guarantee. Finally, the technical optimisation and development direction of the WAIC system are proposed through software simulation and hardware measurement analysis. This study aims to provide a useful reference for the application and development of WAIC technology in the field of aviation, and to provide a theoretical basis for related researchers and manufacturers.

The main work of this paper is as follows:

(1) In this paper, based on the physical layer transmission technology of IEEE 802.11 protocol, we carry out the applicability simulation analysis, analyse the mechanism of obtaining channel state information, measure the reference threshold of SNR switching, simulate the adaptive rate control algorithm, and validate the feasibility of the technical scheme;

(2) In this paper, the channel environment of the avionics bay is constructed by 3D modelling software, and a multipath channel model is built using a ray tracing algorithm to fit the channel fading optimal obeying Rice distribution. By introducing the effective capacity model, the queuing delay of the transmitter buffer queue under flat fading and frequency selective fading channels is analysed, and the feasibility of

the communication scheme is simulated and verified under the WAIC delay constraint;

(3) In this paper, by studying the AF and DF relay collaborative communication techniques in WAIC, we simulate and analyse the optimal power allocation strategy of the nodes under the QoS constraints, maximize the effective capacity of the system under the constraint of constant total power, and verify the feasibility of the relay collaborative communication scheme;

(4) In this paper, a WAIC end-to-end communication simulation platform based on the physical layer of IEEE 802.11 protocol has been built to observe the whole process of signal transmission and reception, and physical testing and technical verification have been carried out by software radio.

The paper also suffers from the following shortcomings:

(1) The applicable technology analysis of IEEE 802.11 protocol proposed in this paper is the physical layer signal simulation processing on the software platform without actual hardware code development, and lacks the simulation analysis of IEEE 802.11 data link layer protocol, which can be further developed on the actual hardware to consider the analysis of the competition and scheduling of the air ports between multiple nodes;

(2) Due to research time constraints, the relay communication model in this paper is a relatively simple three-node communication collaboration, in the effective capacity analysis of the system as a whole for end-to-end capacity analysis, and does not consider more detailed relay node receive buffer queue state, is a relatively simplified analysis model, subsequent research can consider more complex relay

Impact of communication protocols and CSI feedback on latency.

(3) Due to practical constraints, no real-world testing was conducted in the specific scenario of the avionics bay. The narrow environment of the lift is the closest environment to the confinement characteristics of the avionics bay and the metal parts contained therein. However, there are no equipment racks in the lift room, and the physical environment differs from that of a real avionics cabin, and the generality of the conclusion that the measured channel is frequency selective needs to be further evaluated with more experiments.

bibliography

- [1] He Feng. Fundamentals of airborne network technology [M]. Beijing: National Defence Industry Press, 2018: 171-172.
- [2] LI Shining,FAN Xianghui,LIU Zhouzhou,CHEN Changsheng,CHEN Tao. Current status and analysis of wireless avionics internal communication network protocol[J]. Journal of Beijing University of Posts and Telecommunications,2021,44(03):1-8.
- [3] Samano-Robles R , Tovar E , Cintra J , et al. Wireless avionics intra-communications: current trends and design issues[C]// 2016 Eleventh International Conference on Digital Information Management (ICDIM). IEEE, 2016.
- [4] Park P, Di Marco P, Nah J, et al. Wireless avionics intracommunications: a survey of benefits, challenges, and solutions[J]. IEEE Internet of Things journal, 2020, 8(10): 7745- 7767.
- [5] FAN Xianghui,CHEN Changsheng,SHI Yan,YANG Jianxi. A review of wireless avionics internal communication network technology for civil aircraft[J]. Aeronautical Engineering Progress in Engineering, 2021, 12(01):129-135.
- [6] Technical Characteristics and Spectrum Requirements of Wireless Avionics Intra-Communications Systems to Support Their Safe Operation (ITU-R). Report M. 2283-0)[J]. 2013.
- [7] Reji P, Natarajan K, Shobha K R. Performance evaluation of wireless protocols for avionics wireless network[J]. Journal of Aerospace Information Systems, 2020, 17(3): 160-170.
- [8] Baltaci A, Zoppi S, Kellerer W, et al. Evaluation of cellular technologies for high data rate WAIC applications[C]//ICC 2019-2019 IEEE International Conference on Communications (ICC). ieee, 2019: 1-6.
- [9] Zhang C, Xiao J, Zhao L. Wireless Asynchronous Transfer Mode based fly-by-wireless avionics network[C]//2013 IEEE/AIAA 32nd Digital Avionics Systems Conference (DASC). IEEE, 2013: 4C5-1-4C5-9.
- [10] Zhang C, Yu J, Pang K. Multiple access points deployment optimization in cabin

wireless communications[J]. IEEE Antennas and Wireless Propagation Letters, 2013, 12: 1220- 1223.

- [11] Wu D, Negi R. Effective capacity: a wireless link model for support of quality of service[J]. IEEE Transactions on wireless communications, 2003, 2(4): 630-643.
- [12] Chang C S, Zajic T. Effective bandwidths of departure processes from queues with time

- varying capacities[C]//Proceedings of INFOCOM'95. IEEE, 1995, 3: 1001-1009.
- [13] Guo X, Dong L, Li Y, et al. Effective capacity of MIMO MRC system with constant and variable power loading[C]//2013 13th Canadian Workshop on Information Theory. IEEE, 2013: 117-121.
- [14] Angrishi K, Killat U. Analysis of a real-time network using statistical network calculus with effective bandwidth and effective capacity[C]//14th GI/ITG Conference-Measurement and Modelling and Evaluation of Computer and Communication Systems. ITG Conference- Measurement, Modelling and Evalutation of Computer and Communication Systems. VDE, 2008: 1-15.
- [15] Angrishi K. An end-to-end stochastic network calculus with effective bandwidth and effective capacity[J]. Computer Networks, 2013, 57(1): 78-84.
- [16] Hammouda M, Akin S, Peissig J. Effective capacity in multiple access channels with arbitrary inputs[C]//2015 IEEE 11th International Conference on Wireless and Mobile Computing, Networking and Communications (WiMob). ieee, 2015: 406-413.
- [17] Wang C, Urgaonkar B, Gupta A, et al. Effective Capacity Modulation as an Explicit Control Knob for Public Cloud Profitability[C]//2016 IEEE International Conference on Autonomic Computing (ICAC). IEEE, 2016: 95-104.
- [18] Feng Z, Wen G, Chen C W. Multiuser effective capacity analysis for queue length based rate maximum wireless scheduling[C]//2012 1st IEEE International Conference on Communications in China (ICCC). IEEE, 2012: 438-442.
- [19] Ji Z, Dong C, Wang Y, et al. On the analysis of effective capacity over generalised fading channels[C]//2014 IEEE International Conference on Communications (ICC). IEEE, 2014: 1977-1983.
- [20] Davy A, Meskill B, Domingo-Pascual J. An empirical study of effective capacity throughputs in 802.11 wireless networks[C]//2012 IEEE global communications conference (GLOBECOM). IEEE, 2012: 1770-1775.
- [21] Tang J, Zhang X. Quality-of-service driven power and rate adaptation over wireless links[J]. IEEE Transactions on wireless Communications, 2007, 6(8): 3058-3068.
- [22] Tang J, Zhang X. Cross-layer resource allocation over wireless relay networks for quality of service provisioning[J]. IEEE Journal on selected areas in Communications, 2007,

25(4): 645-656.

- [23] Laneman J N, Tse D N C, Wornell G W. Cooperative diversity in wireless networks: efficient protocols and outage behaviour[J]. IEEE Transactions on Information theory, 2004, 50(12): 3062-3080.
- [24] Wang Z, Chen W. Relay beamforming design with SIC detection for MIMO multirelay networks with imperfect CSI[J]. IEEE transactions on vehicular technology, 2013, 62(8): 3774-3785.
- [25] Toding A, Khandaker M R A, Rong Y. Optimal joint source and relay beamforming for parallel MIMO relay networks[C]//2010 6th International Conference on Wireless Communications Networking and Mobile Computing (WiCOM). IEEE, 2010: 1-4.
- [26] Su Junxu. Research on precoding algorithm based on incomplete channel state information in MIMO relay system [D]. Nanjing Aerospace Air and Space University, 2017.
- [27] CHEN Xiaomin,FANG Zhu,HU Xujun,ZHU Qiuming,CHEN Bing. Pre-coding algorithm for multi-user MIMO relay system based on incomplete channel state information[J]. Data Acquisition and Processing,2019,34(02):252-261.
- [28] Rui Xiongli. Research on MAC layer collaboration mode and optimisation in wireless communication networks[D]. Nanjing University of Posts and Telecommunications,2019.
- [29] Jiang, X.S.. Research on buffer-assisted link selection technique for relay system[D]. University of Electronic Science and Technology,2014.
- [30] Ren S, Letaief K B. Maximising the effective capacity for wireless cooperative relay networks with QoS guarantees[J]. IEEE transactions on communications, 2009, 57(7): 2148-2159.
- [31] Peppas K P, Mathiopoulos P T, Yang J. On the effective capacity of amplify-and-forward multihop transmission over arbitrary and correlated fading channels[J]. IEEE Wireless Communications Letters, 2016, 5(3): 248-251.
- [32] Phan K T, Le-Ngoc T. Effective capacity of dual-hop networks with a concurrent buffer-aided relaying protocol[C]//2014 IEEE International Conference on Communications (ICC). ieee, 2014: 1048-1052.
- [33] Ellanti M N, Gorshe S S, Raman L G, et al. Next generation transport networks: data,

- management, and control planes[M]. Springer Science & Business Media, 2005.
- [34] Proakis J G, Salehi M. Digital communications[M]. New York: McGraw-hill, 2001.
- [35] Paul T, Ogunfunmi T. Wireless LAN comes of age: Understanding the IEEE 802.11 n amendment[J]. IEEE Circuits and systems magazine, 2008, 8(1): 28-54.
- [36] Lin C H, Chang R C H, Lin K H, et al. Implementation of channel estimation for MIMO-

- OFDM systems[C]//2010 International SoC Design Conference. IEEE, 2010: 99-102.
- [37] Kumar K, Grover A. Pilot Channel Estimation: a Performance Analysis of OFDM[J]. International Journal of Scientific & Engineering Research, 2013, 4(1): 774-777.
- [38] Kim S G, Yoon D, Park S K, et al. Performance analysis of the MIMO zero-forcing receiver over continuous flat fading channels[C]//The 3rd International Conference on Information Sciences and Interaction Sciences. IEEE, 2010: 324-327.
- [39] Perahia E, Stacey R. Next generation wireless LANs: 802.11 n and 802.11 ac[M]. Cambridge university press, 2013.
- [40] Yin W, Hu P, Indulska J, et al. MAC-layer rate control for 802.11 networks: a survey[J]. Wireless Networks, 2020, 26: 3793-3830.
- [41] Kamerman A, Monteban L. WaveLAN®-II: a high-performance wireless LAN for the unlicensed band[J]. Bell Labs technical journal, 1997, 2(3): 118-133.
- [42] Lacage M, Manshaei M H, Turletti T. IEEE 802.11 rate adaptation: a practical approach[C]//Proceedings of the 7th ACM international symposium on Modeling, analysis and simulation of wireless and mobile systems. 2004: 126-134.
- [43] Bicket J. Bit-Rate Selection in Wireless Networks. master's thesis, Massachusetts Institute of Technology[J]. Dept. of Electrical Engineering and Computer Science, 2005.
- [44] Wong S H Y, Yang H, Lu S, et al. Robust rate adaptation for 802.11 wireless networks[C]//Proceedings of the 12th annual international conference on Mobile computing and networking. 2006: 146-157.
- [45] Diaz N R, Achilli C. Cabin channel characterization for personal communications via satellite[C]//21 st AIAA International Communications Satellite Systems Conference (ICSSC) and Exhibit. 2003.
- [46] ZUO Yuanjun,LI Cliff,XIONG Huagang,LU Guangshan. Analysis and Simulation of Avionics MB-OFDM-UWB Wireless Interconnection Channel [J]. Journal of Aviation,2019,40(07):176-185.
- [47] WU Qing, WANG Tong, TU Xiaojie, LIU Xiaomin. Parameter simulation of ultra-wideband wireless channel inside the cabin[J]. Computer Simulation,2014,31(12):49-53+58.
- [48] JIANG Yule, XIONG Huagang, CHA Zhenyu. Modelling of ultra-wideband deterministic channel in the cabin[J]. Journal of Aviation,2010,31(01):158-

164.

[49] Saghir H, Nerguzian C, Laurin J J, et al. In-cabin wideband channel characterization for

- WAIC systems[J]. IEEE Transactions on Aerospace and Electronic Systems, 2014, 50(1): 516-529.
- [50] Moraitis N, Panagopoulos A D. In-cabin aircraft channel temporal variations due to moving human bodies: measurements and channel characterisation[C]. //2013 7th European Conference on Antennas and Propagation (EuCAP). IEEE, 2013: 2606-2610.
- [51] Chuang J, Xin N, Huang H, et al. UWB radiowave propagation within the passenger cabin of a Boeing 737-200 aircraft[C]//2007 IEEE 65th Vehicular Technology Conference- VTC2007-Spring. ieee, 2007: 496-500.
- [52] NATO-STANAG4626(DRAFT 1)-Modular and open avionics architectures, PART IV [M]: Packaging. Military Agency for Standardization, 2005.
- [53] HUANG Zilin, LU Zhengren. Research on LRM Module and its Application in Avionics System[C]//Aeronautical Society of China, China Aviation Society. Air Force Research Institute. Proceedings of the Sixth International Forum on Civil Aircraft Avionics. Aviation Industry Press, 2017: 4.
- [54] Chen Y, Darwazeh I. An accurate approximation of delay with Nakagami-m channels and exponential arrivals[C]//2015 IEEE Global Communications Conference (GLOBECOM). IEEE, 2015: 1-6.
- [55] Wu D, Negi R. Effective capacity channel model for frequency-selective fading channels[J]. Wireless Networks, 2007, 13: 299-310.
- [56] Chen Y, Darwazeh I. An accurate approximation of delay with Nakagami-m channels and exponential arrivals[C]//2015 IEEE Global Communications Conference (GLOBECOM). IEEE, 2015: 1-6.
- [57] Abdi A, Tepedelenlioglu C, Kaveh M, et al. On the estimation of the K parameter for the rice fading distribution[J]. IEEE Communications letters, 2001, 5(3): 92-94.
- [58] Sijbers J, den Dekker A J, Scheunders P, et al. Maximum-likelihood estimation of Rician distribution parameters[J]. IEEE Transactions on Medical Imaging, 1998, 17(3): 357-361.
- [59] Matthaiou M, Alexandropoulos G C, Ngo H Q, et al. Analytic framework for the effective rate of MISO fading channels[J]. IEEE Transactions on communications, 2012, 60(6): 1741-1751.
- [60] Kolbig K S, Prudnikov A P, Bryckov Y A. Integrals and series: more special functions[J]. Math. Comput. 1985, 44(170): 573.

[61] Laneman J N, Tse D N C, Wornell G W. Cooperative diversity in wireless networks.

- Efficient protocols and outage behaviour[J]. IEEE Transactions on Information theory, 2004, 50(12): 3062-3080.
- [62] Host-Madsen A, Zhang J. Capacity bounds and power allocation for wireless relay channels[J]. IEEE transactions on Information Theory, 2005, 51(6): 2020-2040.
- [63] Hong Y W P, Huang W J, Kuo C C J. Cooperative communications and networking: technologies and system design[M]. Springer Science & Business Media, 2010.
- [64] Gunduz D, Erkip E. Opportunistic cooperation by dynamic resource allocation[J]. IEEE Transactions on Wireless Communications, 2007, 6(4): 1446-1454.
- [65] Kurt S, Tavli B. Path-Loss Modelling for Wireless Sensor Networks: a review of models and comparative evaluations[J]. IEEE Antennas and Propagation Magazine, 2017, 59(1): 18-37.

appendice

A. Derivation of the effective capacity formula

Considering the communication scenario of a single transmitter and single receiver communication system within a flat fading channel in the avionics equipment bay, the channel gain $x = h^2$ obeys the Rice distribution with the same transmit power of the different subcarriers, with the following PDF equation:

$$p(x) = \frac{(1+K)e^{-K}}{\Omega} \exp\left(-\frac{(1+K)x}{\Omega}\right) {}_{10}I_0\left(2\sqrt{\frac{K(1+K)x}{\Omega}}\right) \quad (\text{A1})$$

where the first type of zero-order modified Bessel function is expanded as:

$${}_{10}I_0(z) = \sum_{k=0}^{\infty} \frac{1}{k! \Gamma(k+1)} \left(\frac{z}{2}\right)^{2k} \quad (\text{A2})$$

which, when

taken into equation (A1),

yields

$$p(x) = \frac{(1+K)e^{-K}}{\Omega} \exp\left(-\frac{(1+K)x}{\Omega}\right) \sum_{n=0}^{\infty} \frac{n! \Gamma(n+1)}{\Omega} \quad (\text{A3})$$

From the defining

equation of the effective capacity

$$\alpha^{(c)}(\rho, \theta) = \frac{1}{\Omega} \log_2 \left(\frac{\Gamma(1+\rho x)}{\beta} \right)$$

$$\begin{aligned} &= \frac{1}{\Omega} \log_2 \left(\int_0^{\infty} (1+\rho x)^{-\beta} p(x) dx \right) \quad (\text{A4}) \end{aligned}$$

where $\beta = \theta T_f B / \ln 2$, and ρ is the average SNR.

For the integrals in Eq. (A4) a further derivation can be carried out by exchanging the order of integration and summation:

$$\begin{aligned}
& \int_0^\infty (1+\rho x)^{-\beta} p(x) dx \\
&= \int_0^\infty (1+\rho x)^{-\beta} (1+K) e^{-K} \exp \left[-\frac{(1+K)x}{\Omega} \right] \frac{K^n}{n!} \binom{(1+K)x}{n} dx \\
&= \sum_{n=0}^{\infty} \frac{n! \Gamma(n+1)}{(1+\rho x)^{\beta}} \exp \left[-\frac{(1+K)x}{\Omega} \right] \binom{(1+K)x}{n} \frac{K^n}{n!} \binom{(1+K)x}{n} dx
\end{aligned} \tag{A5}$$

The permutation $t = \frac{(1+K)}{\Omega} x$, it can be deduced that equation (A5) is equal to the following equation

$$\sum_{n=0}^{\infty} \frac{n! \Gamma(n+1)}{(1+\rho t)^{\beta}} \frac{t^{\beta}}{\Gamma(1+K)} {}_0F_K \left(\frac{t}{1+K}; \frac{t}{\Omega} \right) dt \tag{A6}$$

According to the defining equation of the merging hypergeometric function:

$$\int_0^\infty (1+ax)^{-v} e^{-px} x^{q-1} dx = \frac{\Gamma(q)}{a} {}_U\mathcal{F}_q \left(\begin{matrix} q; q+1-v \\ -a \end{matrix} \right) \quad (A7)$$

The above integrals can be

nearly simplified

$$\int_0^\infty (1+\rho x)^{-\beta} p(x) dx = \sum_{n=0}^{\infty} \frac{n! \Gamma(n+1)}{\Omega\rho} {}_U\mathcal{F}_q \left(\begin{matrix} n+1; n+2-\beta \\ 1+K \end{matrix} \right) \quad (A8)$$

Then transformed

by Kummer:

$$U(a; b; x) = x^{1-b} \left(a \cdot b + 1; 2 \cdot b \right) \quad (A9)$$

Equation (A8) can be

further simplified:

$$\begin{aligned} & \sum_{n=0}^{\infty} \frac{n! \Gamma(n+1)}{\Omega\rho} {}_U\mathcal{F}_q \left(\begin{matrix} n+1; n+2-\beta \\ 1+K \end{matrix} \right) \\ &= \sum_{n=0}^{\infty} \frac{n!}{\Gamma(n+1)} \left(\frac{1+K}{\Omega\rho} \right)^{n+1} \left(\frac{1+K}{\Omega\rho} \right)^{\beta-n-1} \Psi \left(\begin{matrix} \beta; \beta+n; 1+K \\ \Omega\rho \end{matrix} \right) \\ &= \left[\sum_{n=0}^{\infty} \frac{1}{n!} \left(\frac{1+K}{\Omega\rho} \right)^n \right] \left(\frac{1+K}{\Omega\rho} \right) \end{aligned} \quad (A10)$$

In summary, it is possible to introduce a formula for the effective capacity equation expressed in terms of the merging hypergeometric function:

$$\alpha^{(c)}(\rho, \theta) = \frac{K}{\beta \ln 2} + \log_2 \left(\frac{1}{1+K} \right) \left(\frac{\Omega\rho}{\beta} \right)^{\log_2 \left(\frac{K}{1+K} \right)} \sum_{n=0}^{\infty} \frac{1}{\Gamma(n+1)} \left(\frac{1+K}{\Omega\rho} \right)^n \quad (A11)$$

In order to derive more general closure expressions, the merging hypergeometric function can be replaced by the more general Meijer's G-function or Fox's H-function:

$$= \frac{U \left(\begin{matrix} \beta; \beta+n; 1+K \\ \Omega\rho \end{matrix} \right)}{\Gamma(n+1) \Gamma(\beta-1, 1, 2)} \frac{1}{\Omega\rho} {}_{G_{2,1}} \left(\begin{matrix} 1+ & 1-\beta \\ 0, n+1-\beta & \end{matrix} \right) \quad (A12)$$

$$\frac{1}{K} \frac{\Gamma(n+1)\Gamma(\beta - 1,2)}{\Gamma(\Omega\rho)} \left| \frac{1 \otimes \beta}{\Omega\rho} \right|_{(0,1), (n+1 \otimes \beta, 1)} = H^{2,1} \left(1+ \begin{matrix} 1 \\ \{0,1 \otimes \beta\} \end{matrix} \middle| \frac{\Omega\rho}{(0,1), (n+1 \otimes \beta, 1)} \right) \quad (\text{A13})$$

In this case, the expression for Meijer's G function is as follows:

$$G_{p,q}^{m,n} \left| \begin{matrix} a, \dots, a \\ b^1, \dots, b^p \end{matrix} \right|_z = \frac{1}{2\pi i} \int \frac{\prod_{j=1}^m \Gamma(b_j + s)}{\prod_{j=m+1}^q \Gamma(1 \otimes b_j + s)} \frac{\prod_{j=1}^n \Gamma(1 \otimes a_j + s)}{\prod_{j=n+1}^p \Gamma(a_j + s)} ds \quad (\text{A14})$$

Academic achievements during the master's degree programme

Academic Achievements:

- [1] **Wu J**, Li Q, Zhuo Y. Analysis of WAIC QoS Guarantees Using Wireless LAN Technology[C]//2022 21st International Symposium on Communications and Information Technologies (ISCIT). IEEE, 2022: 76-81.

The main work completed at the Master's level:

1. Participated in the simulation and analysis of wireless LAN technology applicability modifications in the wireless avionics in-flight communications longitudinal study.
2. Participated in a collaborative project with an avionics research institute to complete the development of a time-triggered network configuration management toolset, which mainly realises the generation of hardware-loaded binary files and is responsible for the maintenance of the software at a later stage.
3. Participated in an aeronautical radio research institute cooperation project, completed the network protocol stack development package part of the underlying function call relationship requirements analysis and documentation.